



AN ABSTRACT OF THE THESIS OF

Jason R. Casey for the degree of Master of Science in Nuclear Engineering presented on December 19, 2012.

Title: High Pressure Condensation Heat Transfer in the Evacuated Containment of a Small Modular Reactor

Abstract approved:

---

Qiao Wu

At Oregon State University the Multi-Application Small Light Water Reactor (MASLWR) integral effects testing facility is being prepared for safety analysis matrix testing in support of the NuScale Power Inc. (NSP) design certification progress. The facility will be used to simulate design basis accident performance of the reactor's safety systems. The design includes an initially evacuated, high pressure capable containment system simulated by a 5 meter tall pressure vessel. The convection-condensation process that occurs during use of the Emergency Core Cooling System has been characterized during two experimental continuous blowdown events. Experimental data has been used to calculate an average heat transfer coefficient for the containment system. The capability of the containment system has been analytically proven to be a conservative estimate of the full scale reactor system.

© Copyright by Jason R. Casey

December 19, 2012

All Rights Reserved

High Pressure Condensation Heat Transfer in the Evacuated Containment of a Small  
Modular Reactor

By

Jason R. Casey

A THESIS

submitted to

Oregon State University

in partial fulfillment of  
the requirements for the  
degree of

Master of Science

Presented December 19, 2012

Commencement June 2013

Master of Science thesis of Jason R. Casey presented on December 19, 2012.

APPROVED:

---

Major Professor, representing Nuclear Engineering

---

Head of the Department of Nuclear Engineering and Radiation Health Physics

---

Dean of the Graduate School

I understand that my thesis will become part of the permanent collection of Oregon State University libraries. My signature below authorizes release of my thesis to any reader upon request.

---

Jason R. Casey, Author

## ACKNOWLEDGEMENTS

The author expresses sincere appreciation for those that have assisted in this research. It would not have been possible without the guidance and leadership of Dr. Qiao Wu throughout the course of the past several years.

The engineers and safety analysis team at NuScale Power Inc. deserve recognition for making this study possible.

The fellow members of the MASLWR research team, namely Garret Ascherl, Bradyn Wuth and Jacob Owen, have lent their time and thoughts to the author on countless occasions and have picked up the slack left in times of great concentration.

The author would also like to thank his parents, all four of them, for their continued support throughout the term of his education. Their writing suggestions, their support (both financial and therapeutic) and their guidance have been immeasurably important to the completion of this work.

# TABLE OF CONTENTS

	<u>Page</u>
1 Introduction.....	1
2 Research Background.....	7
2.1 Condensation Heat Transfer .....	7
2.2 Reactor Containment Characterization .....	8
2.3 Integral Test Facility Scaling.....	10
2.4 Contribution to the Body of Knowledge.....	11
3 Test Facility Description .....	12
3.1 Reactor Pressure Vessel.....	14
3.2 High Pressure Containment.....	16
3.3 Containment Cooling Pool .....	19
3.4 Heat Transfer Plate .....	19
3.5 Data Acquisition and Control System .....	21
4 Facility Instrumentation and Error .....	28
4.1 Thermocouples .....	29
4.2 Pressure Transmitters.....	33
4.3 Level Indicators.....	35
4.4 Input/Output Modules .....	36

TABLES OF CONTENTS (CONTINUED)

	<u>Page</u>
4.5 Experimental Error Quantification.....	37
5 Methods and Experimental Data .....	39
5.1 Analysis Methods.....	40
5.2 Procedures and Experimental Results .....	44
6 Data Analysis .....	62
6.1 Heat Transfer Characterization.....	63
6.2 Condensation Scaling Analysis.....	77
7 Conclusions and Future Work .....	85
7.1 Research Conclusions .....	85
7.2 Future Work.....	87
Bibliography .....	88
Appendix.....	92

## LIST OF FIGURES

<u>Figure</u>	<u>Page</u>
1.0-1: MASLWR reactor concept illustration. ....	2
1.0-2: MASLWR test facility construction diagram. ....	4
3.0-1: First level view of the MASLWR Test Facility. ....	13
3.1-1: Reactor pressure vessel cross-sectional view. ....	15
3.1-2: ADS line flow restriction nozzle schematics. ....	16
3.2-1: OSU MASLWR Test Facility Containment and Cooling Pool Vessels without insulation. ....	18
3.4-1: Plot of the thermal conductivity SS316L data (35). ....	20
3.5-1: MASLWR test facility data acquisition system physical layout. ....	22
3.5-2: MASLWR instrumentation panel 1 of 4. ....	23
3.5-2: MASLWR test facility data acquisition and control system with overhead display. ....	24
3.5-3: MASLWR test facility main control screen of the DACS. ....	25
3.5-3: MASLWR test facility secondary control screen of the DACS. ....	26
3.5-4: MASLWR Facility Master Piping and Instrument Diagram. ....	27
4.1-1: Watlow K-type thermocouple. ....	29
4.2-1: Rosemount pressure transmitter, Model 1151. ....	34
5.1-1: Heat transfer plate energy transport diagram. ....	40
5.1-2: Heat transfer plate thermocouple spacing diagram. ....	42

5.1-3: Heat transfer plate thermocouple extension diagram.....	42
5.2-1: Test case 1 containment pressure (absolute) response with error bounding. ....	47
5.2-2: Containment level measurement during experiment 1 (error shown).....	48
5.2-3: Plot of the thermocouple data from 4.1 (m) above the bottom of the HPC indicating the initial superheating of the incoming vapor and the wall heating beyond saturation. ....	49
5.2-4: Example plot of one of the thermocouple rakes across the HTP, 5.1 (m), for test case 1 that illustrates the conduction transient across the steel plate (Error bars included). ....	50
5.2-5: HTP thermocouple rake measurements at a height of 2.5 (m) for test case 1 (error bars omitted). ....	52
5.2-6: HTP thermocouple rake measurements at a height of 3.19 (m) for test case 1 (error bars omitted). ....	53
5.2-7: HTP thermocouple rake measurements at a height of 4.1 (m) for test case 1 (error bars omitted). ....	54
5.2-8: Calculated saturation temperature data from test case 1 for the HTC calculation. ....	56
5.2-9: Containment pressure from test case 2. ....	57
5.2-10: Wall heating condition plot for test case 2. ....	58
5.2-11: Test case 2 condensate level measurement.....	59
5.2-12: Thermocouple rake across the HTP for test case 2 at 2.5 (m). ....	60
5.2-13: Thermocouple rake across the HTP for test case 2 at 3.19 (m). ....	60
5.2-14: Thermocouple rake across the HTP for test case 2 at 4.1 (m). ....	61

5.2-15: Thermocouple rake across the HTP for test case 2 at 5.1 (m). .....	61
5.2-16: Saturation temperature in the HPC for test case 2. ....	62
6.1-1: Conduction heat rate data from experimental data set. 63	
6.1-2: Conduction heat rate data from the second experimental data set.....	65
6.1-3: Containment level measurement and fit function for test case 1. ....	67
6.1-4: Containment level measurement and fit function for test case 2. (Time span adjusted to fit the blowdown).....	67
6.1-5: Condensation heat rate for the first test case. The three regions are the initial blowdown phase, the over-heated wall transition, and the extended condensation region. ....	69
6.1-6: Conduction-convection heat flow comparison for test case 1.....	70
6.1-7: Condensation heat transfer coefficient calculated from test case 1 experimental data. ....	71
6.1-8: Condensation heat transfer coefficient vs. temperature difference for test case 1. ....	72
6.1-9: Comparison of the calculated condensation HTC to the formulated correlation, eq. 2.2 (18) and the Uchida model, (25). ....	73
6.1-10: Calculated condensation heat rate from the second experimental data set.....	75
6.1-11: Calculated condensation HTC for the second test case. ....	75
6.1-12: Condensation HTC for test case 2 vs. temperature difference. ....	76
6.2-1: Condensate mass transfer diagram displaying film heat transfer. ....	80
6.2-2: Calculated film heat transfer coefficient scaling ratio.....	85

## LIST OF TABLES

<u>Table</u>	<u>Page</u>
3.4-1: Tabulated values of thermal conductivity SS16L data (35). .....	20
3.4-2: Specific parameters used in the calculation of HTP conduction heat flux.....	21
4.1-1: Table of thermocouple specifications, Part 1. ....	30
4.1-2: Table of thermocouple specifications, Part 2.....	31
4.2-3: Thermocouple instrument ranges, size and accuracy. ....	33
4.2-1: Pressure transmitter instrument specifications. ....	35
4.2-2: Pressure instrument calibration and accuracy data (values shown are gauge values).....	35
4.3-1: Level differential pressure transmitter instrument specifications. ....	36
4.3-2: Level differential pressure transmitter calibration data. ....	36
4.5-1: Error sources in the MASLWR test facility containment. ....	38
4.5-2: Combined maximum error in MASLWR test facility containment. ....	38
5.2-1: Experimental initial conditions. ....	46
6.2-1: Summary of MASLWR test facility geometric parameters.....	79
6.2-2: Summary of parameter scaling ratios.....	79
6.2-3: Condensate film Reynolds number observations, predictions and plotted region.....	84

## NOMENCLATURE

MASLWR	Multi-Application Small Light Water Reactor
HPC	High Pressure Containment
RPV	Reactor Pressure Vessel
CPV	Cooling Pool Vessel
HTP	Heat Transfer Plate
NSP	NuScale Power Incorporated
NRC	Nuclear Regulatory Commission
SMR	Small Modular Reactor
NSSS	Nuclear Steam Supply System
LOCA	Loss of Coolant Accident
ADS	Automatic Depressurization System
PLC	Programmable Logic Controller
DACS	Data Acquisition and Control System
ATHRL	Advanced Thermal Hydraulics Research Laboratory

# **High Pressure Condensation Heat Transfer in the Containment of a Small Modular Reactor**

## **1 Introduction**

Many natural systems and industrial processes rely on the enthalpy change of evaporation to remove or generate energy for practical applications. The planet's water cycle employs this effect to moderate the climate and provide temperate regions suitable for life. The advent of refrigeration technology relied on the immense heat removal capability of boiling highly volatile fluids. In fact many kinds of heat exchangers depend on this principle in conjunction with convection to absorb or transmit heat. The research performed as part of this thesis examines the rate steam is cooled inside of a highly pressurized reactor containment vessel and subsequently applies the results to formulate an empirical definition of the condensation heat transfer from the working fluid to the walls of the vessel.

The industry is researching new approaches to safety mechanisms, core coolant supply methods and fuel materials as well as rethinking the reactors' size and scale. The Multi-Application Small Light Water Reactor (MASLWR) research concept has progressed into a design concept as the NuScale Power Inc. (NSP) reactor. The integral reactor test facility currently in operation at Oregon State University is designed to authenticate safety analysis efforts in the certification process of the NSP reactor.

The primary containment structure of a modern nuclear reactor serves not only as a barrier between radioactive materials and the environment, but as a heat exchanger that dissipates energy during an accident scenario. Natural circulation systems have been developed to enhance the wall cooling properties of this structure while utilizing both evaporation and condensation, most notably as a part of Westinghouse's AP1000 design. In an emergency, the working fluids of the reactor can vent out into the steel enclosure of the containment, rise and come into contact with the conductive surfaces. The working fluids condense on the steel surface and circulate back toward the reactor. The exterior of the enclosure is both convection air cooled and sprayed with a reserve of water which subsequently evaporates, removing heat in the process. It is essential to accurately understand the capability of systems like these to prepare for the worst possibilities.

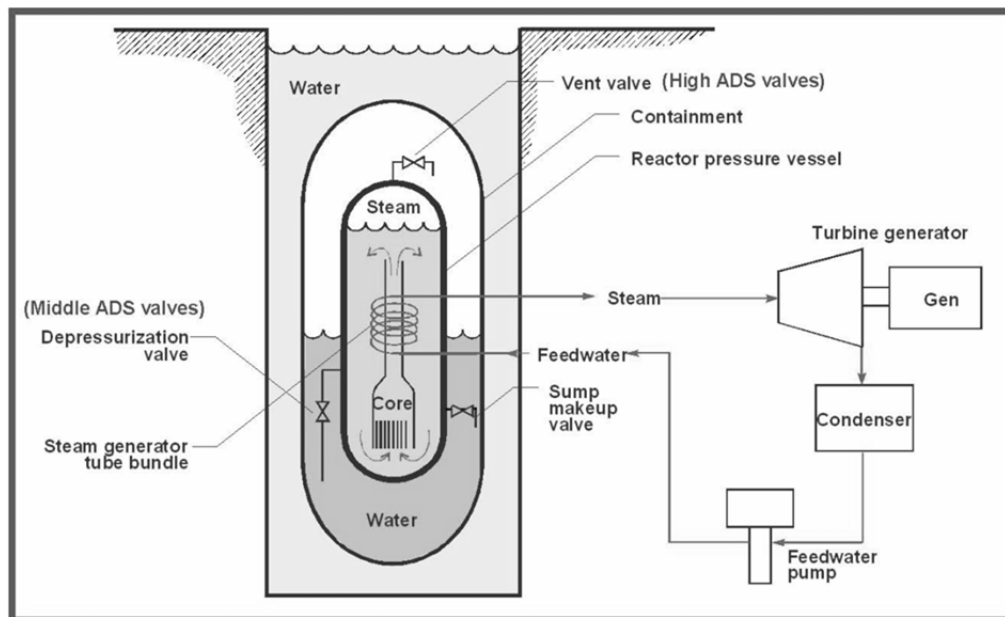


Figure 2.0-1: MASLWR reactor concept illustration.

Much in the same way that the afore mentioned containment serves as a macroscopic heat exchanger, the MASLWR containment vessel does so on a smaller scale at a greater pressure. In an accident, the working fluid is released from the primary reactor vessel and fills the High-Pressure Containment (HPC) where it condenses onto the interior surface and collects at the bottom of the vessel. Recirculation valves open in the lower portion of the reactor vessel to allow a natural circulation loop to begin flow through the reactor-containment loop.

To simulate this effect the MASLWR test facility utilizes three pressure vessels to model the reactor pressure vessel (RPV), the containment vessel and the cooling pool vessel (CPV) respectively. The RPV is connected to the containment by four depressurization lines which are controlled by pneumatic valves and limited by restrictive flow nozzles. The containment consists of a semi-cylindrical vessel standing 5.75 meters tall which may be pump-evacuated and externally heated. This external heating covers the exterior of the HPC that is not in contact with the CPV by way of the heat transfer plate (HTP) to ensure all heat is transferred to the CPV and condensation takes place on the plate surface.

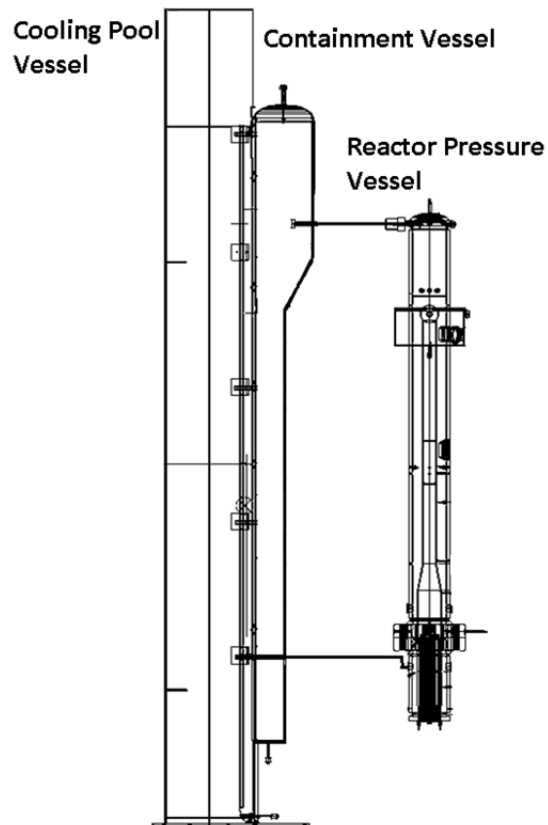


Figure 1.0-2: MASLWR test facility construction diagram.

While other containment structures are designed to withstand upwards of 70 psi, the MASLWR containment can withstand 300 psi and is being redesigned to reach higher pressures. Numerous studies have been performed to evaluate the heat removal capabilities of reactor containment structures at low pressure; however the MASLWR containment has not been through such rigorous analysis. The higher pressure's effect on condensation shifts the equilibrium saturation temperature higher and forces the phase change to take place at this temperature and to transfer heat more rapidly to the thermally stable CPV.

This thesis is intended to measure the performance of the containment structure and generalize the condensation process by formulating a condensation heat transfer coefficient (HTC) based on experimental results. This parameter can be used to predict the system's performance during accident scenarios and to benchmark computer simulation code analyses as a point of reference. In addition to the benefit afforded by this research to the MASLWR design this work will also supplement the many investigations into condensation heat transfer and its role in reactor safety.

A number of assumptions were necessary to evaluate the heat transfer coefficient from experimental data. Temperature profiles across the heat transfer plate were skewed by transients as the thermal mass heated up during the blowdown events. After a given period these temperatures were assumed to be linear such that an estimation of the conduction heat rate could be made. Additionally, the HPC is covered by 10.2 cm of Thermo-12 hydrous calcium silicate insulation which directs nearly all of the energy of the steam to the heat transfer plate though not all. This and other thermal losses from the facility are assumed to be negligible and are not addressed here. The effects of radiative heat transfer are also assumed to be of no consequence in this analysis. Internally the working fluid undoubtedly transfers a portion of its heat to the heat transfer plate which is impregnated with temperature measurement instrumentation. The instrumentation presence within the heat transfer medium is assumed to have little effect on the thermal conductivity of the material and is not accounted for.

The work conducted in this study is not a perfect evaluation of the containment system and it contains several inherent limitations. Since this method uses

entirely experimental data to describe the condensation heat transfer a significant portion of the potential analysis is neglected. The fluid dynamic properties of the working fluid are not explored entirely and the surface conditions of the fluid boundary layer are not characterized. The structure itself does not accurately portray the intended containment design for the NuScale reactor and these experiments will be repeated for the newly designed system in the future. In addition, the proper instrumentation was not installed to measure bulk vapor temperature inside of containment during the tests. In this case an assumption was made equating the critical insulated wall temperature to the system vapor temperature. This assumption will be explained further in the analysis section. Regardless, the specific scenario tested in this thesis will provide a useful reference point for the next iteration of containment evaluation. Finally, the heat transfer through the condensate film was not evaluated. It presents a resistance to the heat flow and lowers the final resulting heat transfer. While this may seem conservative, it neglects the true nature of the heat removal process.

The following sections will present and discuss the results of the research to evaluate the containment condensation heat transfer. Chapter 2 will discuss the literary background to this study and review the previous work relevant to this investigation. Chapter 3 will discuss the experiment procedures and the analysis methods for determining the heat transfer coefficient. Chapter 4 will describe the test facility and data acquisition system that was used in these experiments. Chapter 5 will discuss the instrumentation that was used in these experiments and their associated calibration error. Chapter 6 will present the data analysis of the experimental results. Chapter 7 will conclude this thesis with a discussion of observations and results as well as the potential areas for future work.

## 2 Research Background

The object of this thesis is to characterize a specific system under a controlled set of parameters. The work completed in that effort is not directly applicable in a general sense to all systems of similar design yet the methods employed within are universal. What conclusions that have been found have been built off of the methods of others and their work should be recognized. This section will outline the applicability and pertinence of each of the referenced documents.

### 2.1 *Condensation Heat Transfer*

At the heart of this research is an evaluation of the energy removal capability of a specialized heat exchanger. In this respect the heat transfer mechanism of importance is the combined convection-condensation process that is undertaken during a depressurization event in the facility. These individual processes, condensation and convection, have been studied extensively since the preliminary work presented by Nusselt (1). This work has been expanded upon for the effect of a subcooled condensate film (2) and cases with high Reynolds numbers (3). The work of Sparrow and Gregg (4) explored the boundary layer analysis of condensate films to account for momentum changes. Research has been conducted evaluating condensation heat transfer under the conditions of free convection (5) (6) (7), forced convection (8), with the added suction effect of downward flowing condensate (9), and convection condensation effects in horizontal configurations (10) (11).

Analysis of the condensate-vapor boundary suggests that the most prominent factor influencing the condensation rate is the presence of non-condensable gas. This gas builds resistance to the mass-energy transfer rate near the boundary

layer. Numerous experimental studies have been conducted on the subject under low pressure conditions (12) (13) (14) (15), as well as high pressure conditions (16) (17). All of which have either varied the air/steam mass ratio to observe the effect of non-condensable gases or have changed the orientation of the condensation surface to affect the boundary layer behavior. However these studies have not addressed the specific region the MASLWR facility will operate under given low air/vapor mass fractions and high pressure condensation conditions. A more detailed analysis of the operating region is warranted.

A comprehensive experiment by Dehbi et al. (18) has produced a working correlation for high pressure steam condensation in free convection/condensation processes. This work has produced a correlation that predicts an average HTC for steam condensation in a sealed volume. The limits of applicability of the correlation are not entirely consistent with the parameters of this experiment however the condensate cooling conditions and range of pressure are consistent making it the most relevant work.

## ***2.2 Reactor Containment Characterization***

The construction of nuclear reactor systems requires a robust and exhausting analysis that addresses every conceivable failure through an evaluation of the design's ability to prevent radioactive material release (19). The final barrier to the release of radioactive material into the environment is the iconic dome-shaped reactor containment building. The outer most shell of MASLWR reactor design serves the same purpose of the containment building (20). Evaluation of the structure's mechanical capability is only a fraction of the research that is conducted prior to construction. The containment's material and configuration is also capable of mitigating an accident through the removal of thermal energy

released from the reactor pressure vessel. This phenomena has been studied in great detail in reference to currently operating nuclear reactors that employ large scale containment facilities (21) (22) (23) (24). These studies and the containment analysis codes used through the last generation of reactor construction cite and employ the results of two primary source containment condensation reports from the 1960's. Those being the safety analysis reports of Uchida et al. (25) and Tagami (26). It is important to note that Peterson (27) does identify a non-conservative error that propagates in the Uchida methods at pressures greater than 1 atm.

These two primary sources generated the methods employed to evaluate reactor containment systems for over 30 years. These methods have been proven to produce conservative estimations of containment system heat transfer and condensation by Dehbi (18). That work produced a correlation for the condensation HTC for given pressure, geometry and air/steam mass ratios that were marked against the work of Uchida and Tagami and will be used as reference in this study. The correlation developed is given below:

$$\bar{h}_L = \frac{L^{0.05}[(3.7+28.7P)-(2438+458.3P)\text{Log}_{10}(W)]}{(\bar{T}_\infty - \bar{T}_W)^{0.25}} \quad (\text{eq. 2.1})$$

Where  $L$  is the length of the condensation surface,

$P$  is the volume pressure and,

$W$  is the air/steam mass ratio of the volume.

Herranz et al. (28) produced a diffusion layer model for steam condensation that builds upon the work of both primary sources and verifies the correlation of Dehbi et al. These investigations are each based upon large scale reactor containments which are assumed filled with air prior to an accident event. In the small modular reactor containment this is not the case and much lower regions of air/steam mass concentrations are of importance. The MASLWR design containment is also designed to withstand pressures of much greater magnitude than those currently evaluated.

### **2.3 Integral Test Facility Scaling**

The final contribution of this study will be to improve the scaling evaluation of the MASLWR test facility containment structure accident mitigation performance. The condensate film that develops during testing procedures reaches turbulent conditions ( $Re_{\delta} > 1800$ ) even during low pressure blowdown scenarios ( $P_{max} < 700$  kPa). A more robust containment modeling system is being designed at the time that will allow for greater maximum pressures ( $P_{max} < 2.5$  MPa) during blow down events. Full scale experimentation of the currently designed containment will show that the turbulent region is in fact the primary operating region of the condensation process. Furthermore, it is currently assumed that the containment structure currently in place will over approximate the containment HTC in the full scale reactor design.

An evaluation of the MASLWR facility dimensional scaling analysis (29) (30) combined with a modified Nusselt analysis has indicated that the condensation heat transfer is in fact conservatively estimated by the integral test facility. The modified Nusselt analysis will employ correlations from the work of Kutateladze (31) and Labuntsov (32) to evaluate the heat transfer during turbulent

condensate flow and during transition condensate flow. These methods have been verified experimentally by Gregorig et al. (33). The conceptual foundation of that analysis was outlined by the text, *Fundamentals of Heat and Mass Transfer* by Incropera et al. (34).

#### **2.4 Contribution to the Body of Knowledge**

The concentration of this study relates to a well-defined area of research that many detailed investigations have explored. Despite this aspect the specific features of the operating region of the test facility containment warrants a greater analysis of the condensation heat transfer. The unique nature of the integral effects facility also permits a more comprehensive evaluation of the physical processes that occur in a small modular reactor design. Additionally the evaluation of the accident scenario testing that will be undertaken by Oregon State University and NuScale Power Inc. will greatly benefit from the scaling analysis evaluation.

### 3 Test Facility Description

At Oregon State University, a new integral reactor test facility has been prepared by NuScale for use in the Nuclear Regulatory Commission's (NRC) design certification process. The facility was constructed a decade ago to test the feasibility of a design prototype; a design which has evolved into the NuScale reactor design. The MASLWR test facility models the MASLWR conceptual design including the RPV vessel and containment structure. It is scaled at 1:3 length scale, 1:254.7 volume scale and 1:1 time scale, constructed entirely of stainless steel, and designed for full pressure (11.4 MPa) and full temperature (590 K) prototype operation. Prior to the commencement of matrix testing for the evolved NuScale design testing effort, experiments for the International Atomic Energy Agency (IAEA) and facility shakedown tests were conducted. In addition, three research oriented experiments were developed and executed as part of this study to explore the capability of the small modular reactor's (SMR) containment heat removal system.

These experiments focus on the steam cooling function of the containment design and gather data on the heat removal capability of the condensation process. The computational nuclear safety codes, GOTHIC and RELAP, are being employed independently to simulate the activity of this facility and the NuScale reactor during both normal operation and accident conditions. The ability to reference experimental data to benchmark these codes' results will provide an impartial verification in accordance with NQA-1 requirements for those studies.



Figure 3.0-1: First level view of the MASLWR Test Facility.

### **3.1 *Reactor Pressure Vessel***

The RPV is a model nuclear steam supply system (NSSS) that uses an array of 56 ceramic heater rods to simulate the heat generation of a nuclear core. The system incorporates an in-vessel pressurizer to regulate system pressure and promote primary coolant flow in a natural circulation driven loop. This allows for the emancipation of the system from coolant pumps which are capable of failure or misuse. The RPV has been designed to withstand limits of 11.4 MPa and a primary side temperature of 866 K; its core produces a full 398 kW of electric power. This energy is imparted on the primary fluid, which rises and flows across a steam generator internal to the RPV. This heat exchanger employs thirteen flow tubes in a helical structure to maximize the surface area within the limited space of the reactor volume. The energy from the primary fluid is removed with an externally fed feedwater system which traverses the exterior of the steam generator before venting to atmosphere.

The RPV is designed to release its primary system pressure into the containment in the event of a loss-of-coolant accident (LOCA). This intentional “blowdown” event reduces the primary pressure very rapidly; concurrently it removes a great deal of energy through a pair of depressurization valves located at the top of the vessel. The released steam cools in the CPV, condenses and recirculates back into the RPV through a second pair of connecting pipes. This automatic depressurization system (ADS) ensures long time cooling of the reactor through a second natural circulation loop. The ADS lines are much larger than the analogous lines in the reactor design and had to be fitted with regulation nozzles to restrict the flow rate of primary coolant. A diagram of these nozzles and the RPV can be found in Figures 3.1-1 and 3.1-2.

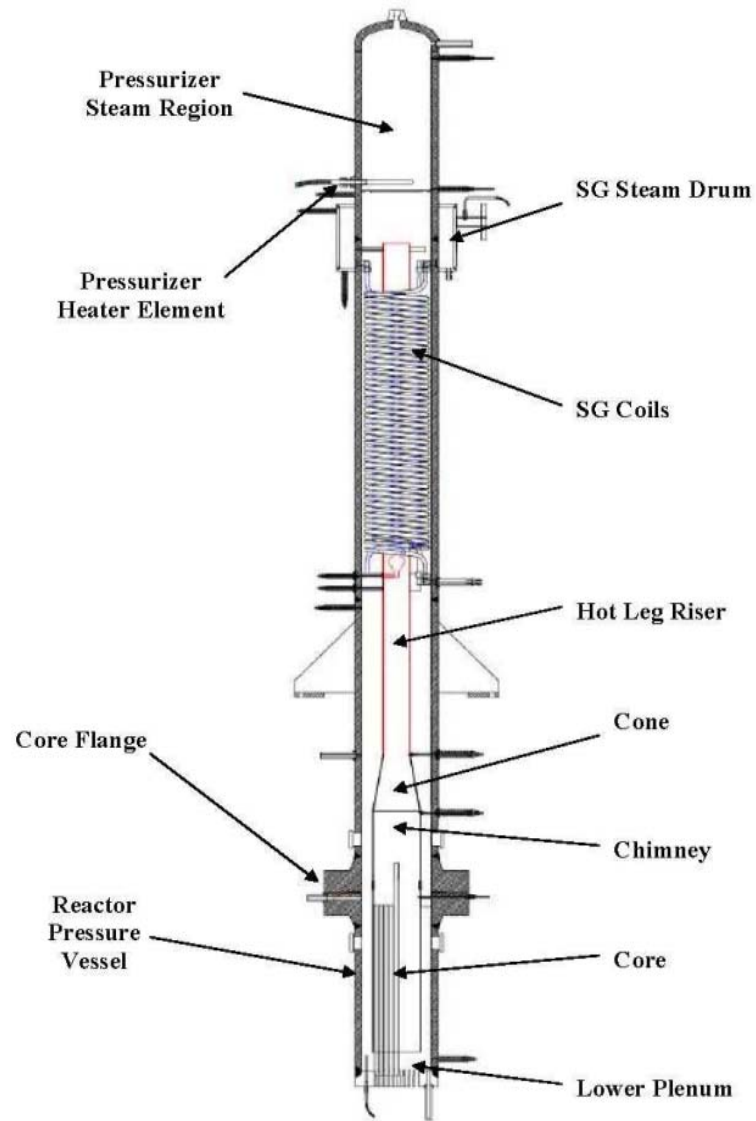


Figure 3.1-1: Reactor pressure vessel cross-sectional view.

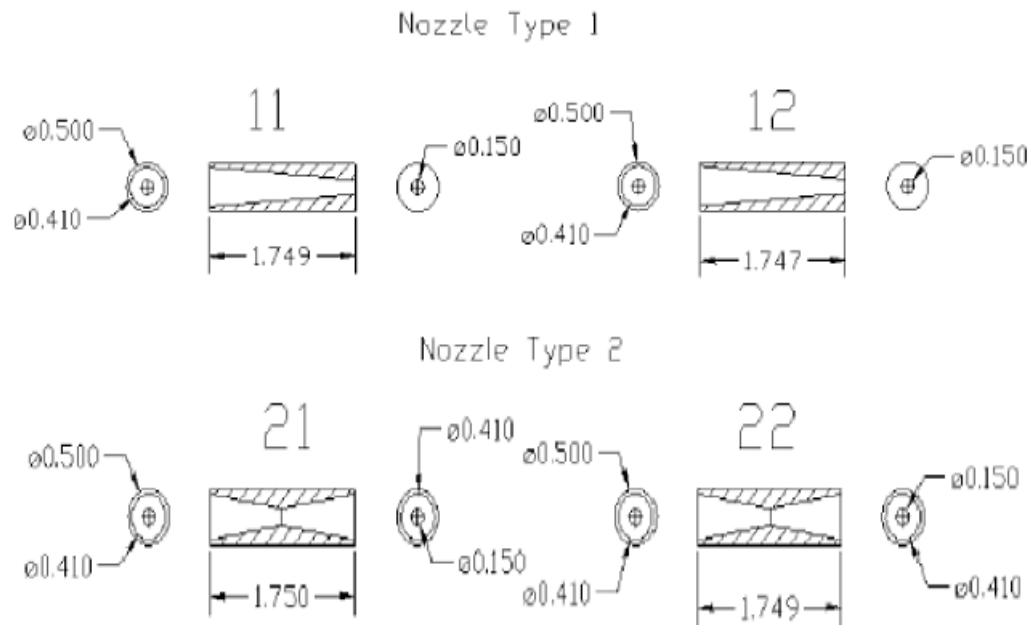


Figure 3.1-2: ADS line flow restriction nozzle schematics.

### 3.2 High Pressure Containment

The stainless steel HPC system stands 5.75 m tall and is constructed of three segments, the lower cylindrical section, the upper cylindrical section and an eccentric cone section that joins the two. A 2.54 cm flat plate covers the lower opening. The structure is capped with a 0.635 cm hemispherical head. The containment vessel is capable of prolonged operation at 2.22 MPa and 505.4 K. However, actual blowdown events in the facility from full conditions would raise the containment pressure far past this limit. As a consequence, many other tests than those performed for this work require cycling of the ADS valves to allow for condensation to lower containment pressure before continuing the blowdown event. A containment redesign is currently underway.

Strip heaters are attached to the exterior of the upper region of the structure and are used to raise wall temperature to or near the saturation temperature of the incoming steam; this process ensures that the containment walls do not cool the bulk fluid steam. In addition, the entire structure is covered with a fiberglass insulation blanket to prevent thermal losses to the environment.

Experiments have been conducted using the wall heaters however in this study it was found that the incoming steam sufficiently heated the insulated walls in less time than required to bring the HPC to CPV medium up to thermal linearity required for the energy balance evaluation method. The HPC is also equipped with a positive-displacement vacuum pump to remove non-condensable gases from the vessel prior to testing procedures. The cylindrical shape of the HPC is intersected by the HPC to CPV medium. This medium is the heat transfer plate used to direct energy to the ultimate heat sink of the cooling pool. A photograph of the containment and cooling pool modeling structure can be found in Figure 3.2-1.



Figure 3.2-1: OSU MASLWR Test Facility Containment and Cooling Pool Vessels without insulation.

### **3.3 Containment Cooling Pool**

The stainless steel CPV is a 7.37 m tall right cylindrical tank made from 76.2 cm OD, 0.635 cm wall thickness pipe. The CPV is covered by a 5.08 cm thick blanket of fiberglass insulation. The vessel is filled with deionized water past the upper most point of contact with the containment vessel. This structure serves as the ultimate heat sink for the energy imparted from the RPV into the HPC and through the heat transfer plate. The system contains no cooling mechanism though; CPV temperature changes during tests are minimal.

### **3.4 Heat Transfer Plate**

The HTP is a 3.81 cm thick type 316L stainless steel plate which intersects both the HPC and the CPV. The plate is welded into contact with the two volumes, intersecting the circumference of both vessels to form a conduction pathway. The plate extends the entire length of the HPC, less the hemispherical cap, of 5.59 m. The plate is 16.8 cm wide. This plate, in conjunction with sufficient instrumentation, allows for the quantification of the conduction heat flux passing between the two pressure vessels. Having known property data and accurate thermal measurements during testing for the steel plate are essential to the methods in this work. The instrumentation scheme is discussed in detail in chapter 5.

As for the property data of type 316L stainless steel, the thermal conductivity was a pertinent factor. It was found that this property was significantly variable over the range of temperatures addressed in these experiments. And for each experiment a linear interpolation was fit to the available data and an average thermal conductivity was calculated to suit the range of temperature. A table

and plot of the thermal conductivity's variance can be found in Table 3.4-1 and Figure 3.4-1. The specific parameters used for each experiment are tabulated in Table 3.4-2.

Table 3.4-1: Tabulated values of thermal conductivity SS16L data (35).

Temperature (K)	Thermal Conductivity (W/m*K)
300	13.5
400	15.2
500	16.9
600	18.4
700	19.9
800	21.4
900	22.7
1000	24.1

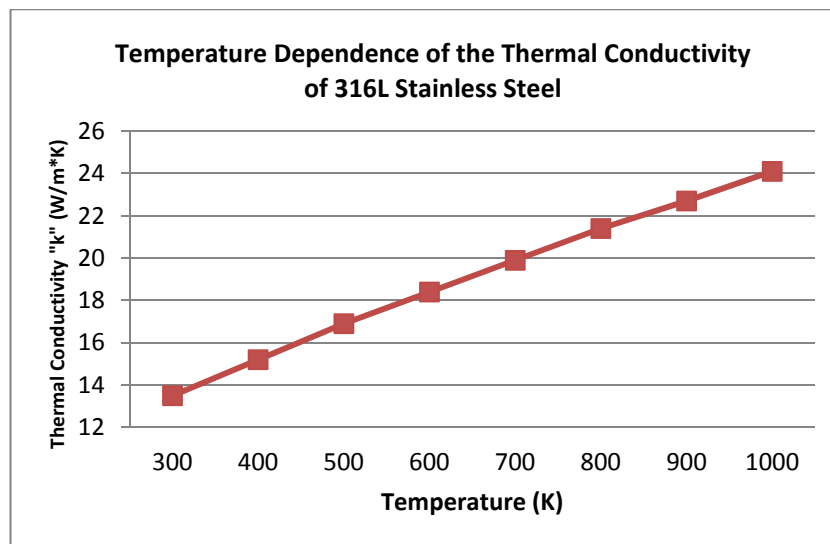


Figure 3.4-1: Plot of the thermal conductivity SS316L data (35).

Table 3.4-2: Specific parameters used in the calculation of HTP conduction heat flux.

	Thermal Conductivity (W/m*K)
1	16.441
2	16.526

### 3.5 *Data Acquisition and Control System*

The test facility instrumentation and control devices are all wired to a central programmable logic controller (PLC) through an Ethernet network of modules, base controllers and an Ethernet switch. The control signals are relayed to the PLC where relay positions and control device values are channeled. Instrument measurement signals are directed to IO modules and transmitted along the Ethernet pathway via the IO base controllers. An emergency stop button is wired straight to the PLC that immediately shuts down the heaters and pumps. The data values are sent through another Ethernet switch and recorded by a PC, the Data Acquisition and Control System (DACS). The DACS runs a custom developed control program as a part of Entivity Studio, a data control software application capable of data acquisition and control signal management. A flow chart of the control system and data network can be found in Figure 3.5-1.

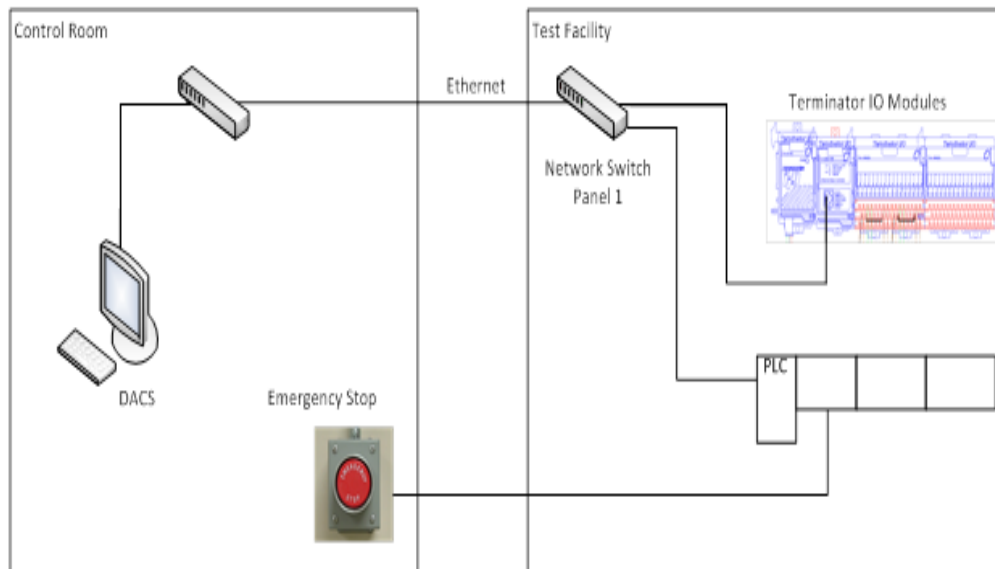


Figure 3.5-1: MASLWR test facility data acquisition system physical layout.

The facility wiring is carefully mapped out and directed into 1 of 4 main electrical boxes. These boxes contain the Ethernet base controllers and device IO modules. Each rack of instrument terminations has its own power supply and controller which transforms the data signals into network packets and transmits the data to the data acquisition software. A picture of Panel 1 instrumentation wiring that includes the PLC, Instrument Base 3, the pneumatic air supply control relays and their power supply can be found in Figure 3.5-2. The instrument rack can be seen in the lower portion of the image colored in blue.

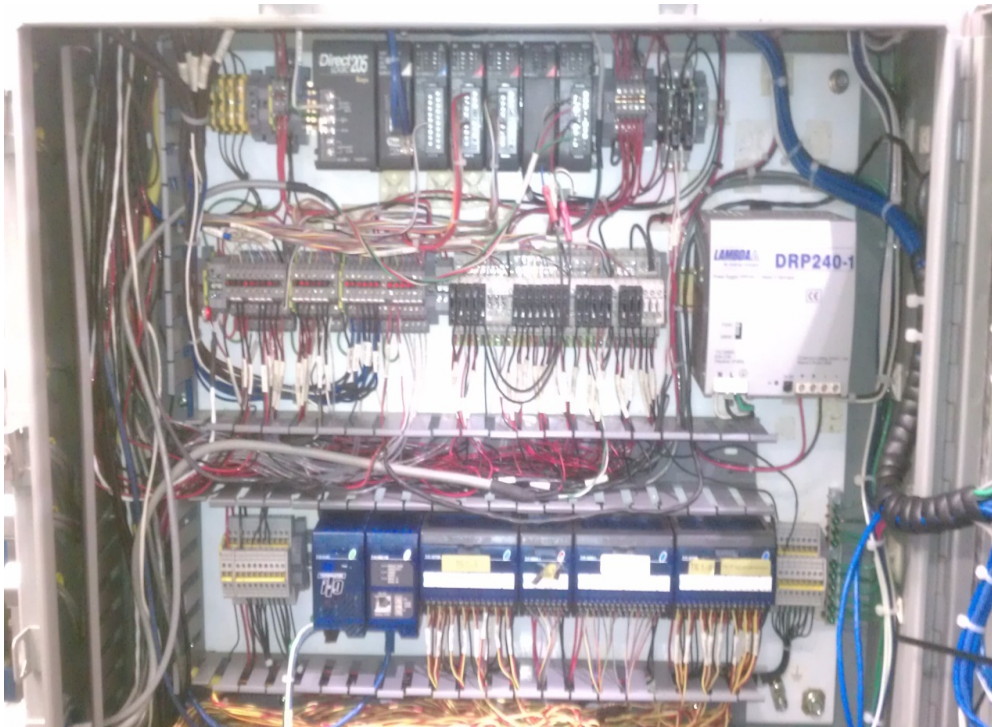


Figure 3.5-2: MASLWR instrumentation panel 1 of 4.

The DACS can be seen in Figure 3.5-2. Screen views can be found in Figure 3.5-3 and Figure 3.5-4. Controls for every system on the facility have been programmed and arranged to fit on one dual-monitor display. Pertinent measurements for system operation during steady state are the most prevalent on the control screen which allows for rapid responses to system fluctuations. The development screen plots out any chosen instrument on the screen to the left for careful observation and can be readily tailored to any experiment. A system of safety alarms has been programmed into the control software that monitors given parameters and has the full capability to trip reactor systems. A display showing warnings and trips is on the far right hand side. From these two

controls screens, data from every instrument and system can be monitored directly. Piping and instrument diagrams can be found in Figure 3.5-4.

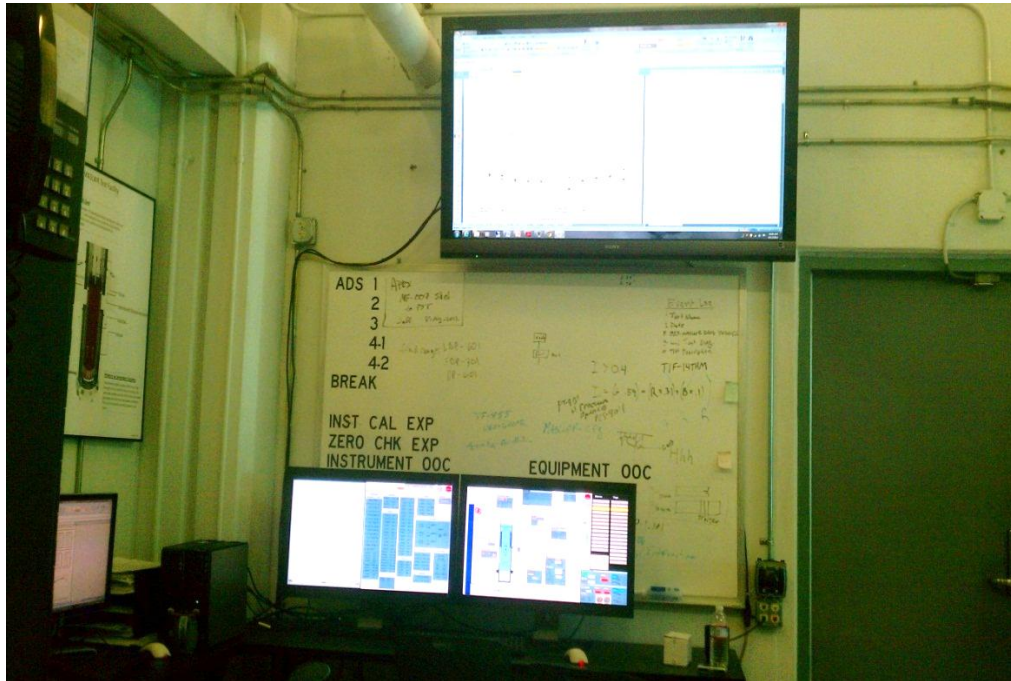


Figure 3.5-2: MASLWR test facility data acquisition and control system with overhead display.



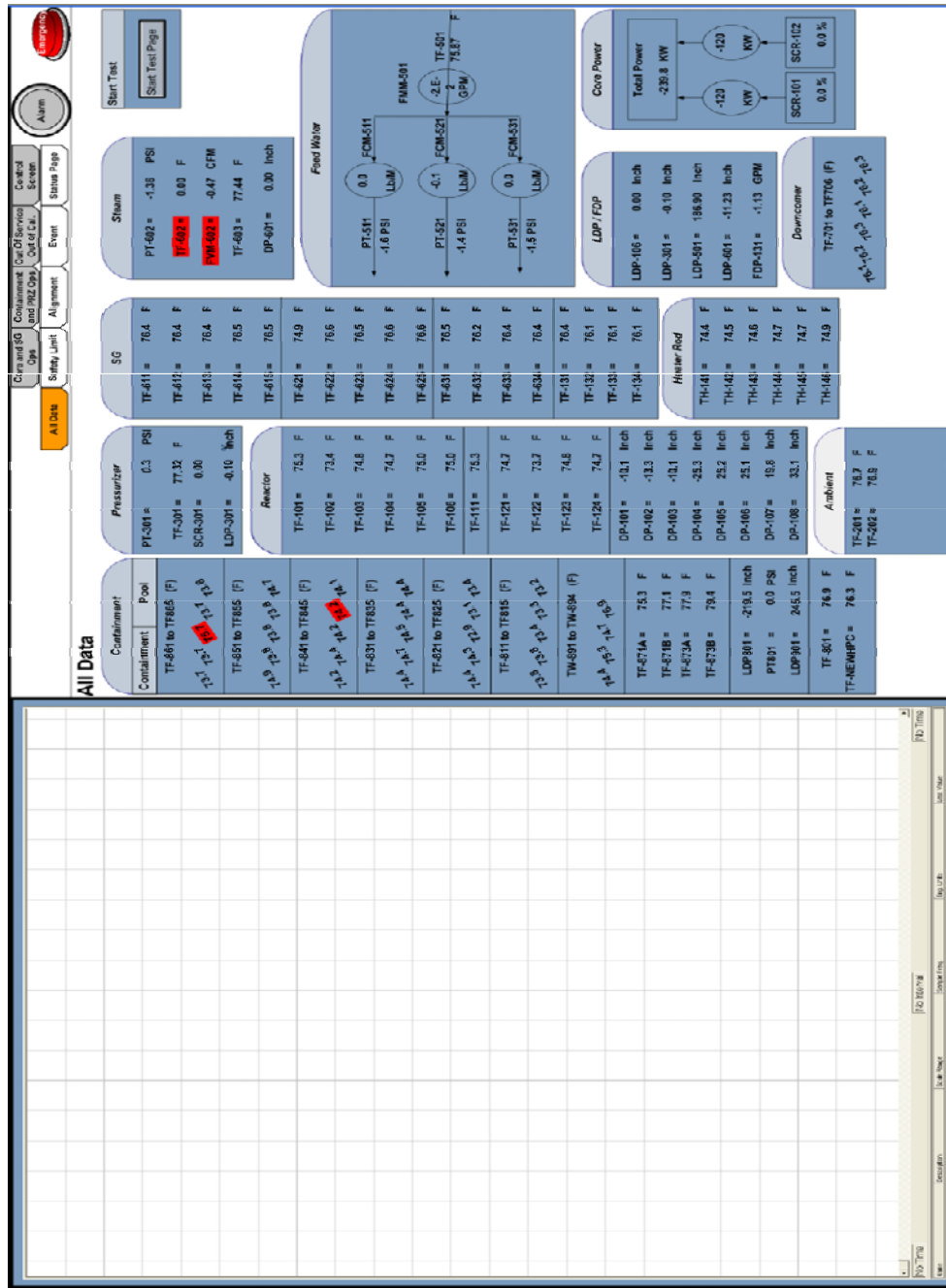


Figure 3.5-3: MASLWR test facility secondary control screen of the DACS.

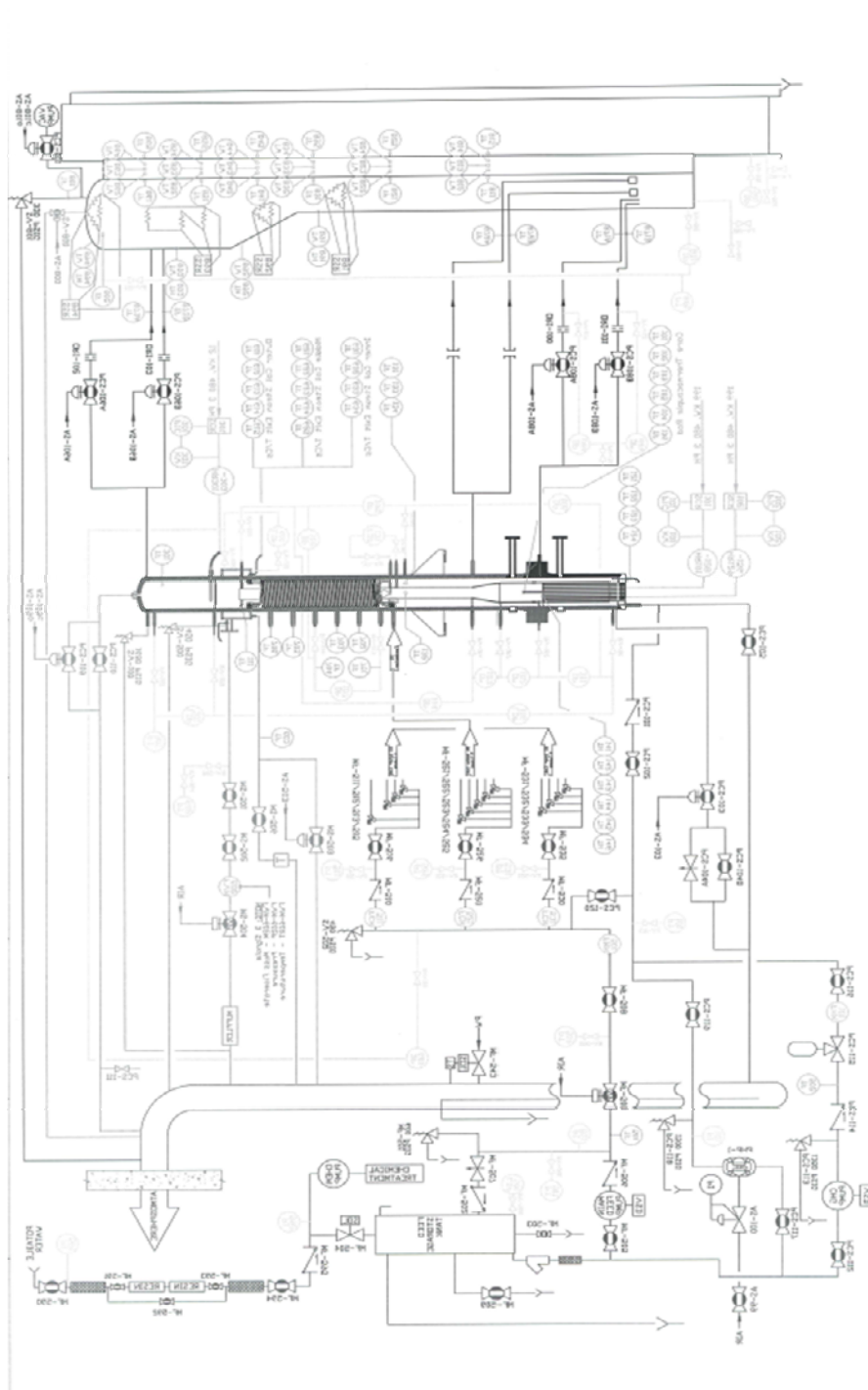


Figure 3.5-4: MASLWR Facility Master Piping and Instrument Diagram. (42)

## **4 Facility Instrumentation and Error**

To collect quality experimental data for the analysis of the containment system the facility is fitted with instrumentation specifically placed to measure the physical processes occurring within the volume during a test. The thermal processes that occur in this volume rely greatly on temperature gradients, mass transport and system pressure. These topics will be discussed in this chapter and the instrumentation used to collect measurements of these parameters will be described. This section focuses on the instrumentation required to collect data in the containment and cooling pool only as the entire facility contains many unrelated instruments to this work.

The data collection system is comprised of forty two thermocouples, 2 pressure transducers, 3 differential pressure transducer level indicators, 1 thermocouple module, 1 instrumentation module, 1 Ethernet base controller and a desktop computer. Error in data reading stems from both the instrument measurement mechanism and the analog to digital conversion process which is conducted in the IO modules. Both sources of data will be quantified in this chapter. The data acquisition layout has already been presented but may be found in Figure 3.5-1 for reference.

#### 4.1 *Thermocouples*

The forty-two Watlow K-type thermocouples are capable of measuring temperature data over a range of 0 to 1200°C. This range is more than capable of meeting the requirements for this experimentation. The thermocouples have been calibrated down from this to a range of 10 to 315°C. The original calibration of the HTP thermocouples was conducted upon construction and the instruments were subsequently sealed there. It should be noted that for nuclear quality assurance purposes these thermocouples are not sufficiently verified since construction was completed nearly a decade ago. The thermocouple have however been checked against properly calibrated thermocouples under similar conditions yet further verification procedures are ongoing at the time of this work. All of the k-type thermocouples have been wired using small gauge wires and ungrounded sheaths to combat the signals' susceptibility to electromagnetic interference. Table 4.1-1 and 4.1-2 provide information of each instrument's model number and function in the process. The construction of the thermocouple can also be observed in Figure 4.1-1 below.



Figure 4.1-1: Watlow K-type thermocouple.

Table 4.1-1: Table of thermocouple specifications, Part 1.

Call Name	Make	Model	Serial #	Function
TF-301	Watlow	AFJK0FA120U4040	N/A	PZR Temp
TF-801	Watlow	AFGJ0FA040U4030	N/A	Safety Valve Temp
TF-802	Watlow	AFGJ0FA080U4030	N/A	HPC top Bulk Temp
TF-811	Watlow	AFEK0FA090G4030	N/A	Plate Temp: HPC side film
TW-812	Watlow	AFEK0FA090G4030	N/A	Plate Temp: HPC side
TW-813	Watlow	AFEK0FA090G4031	N/A	Plate Temp: Center
TW-814	Watlow	AFEK0FA090G4032	N/A	Plate Temp: CPV side
TF-815	Watlow	AFEK0FA090G4030	N/A	Plate Temp: CPV side film
TF-821	Watlow	AFEK0FA090G4030	N/A	Plate Temp: HPC side film
TW-822	Watlow	AFEK0FA090G4030	N/A	Plate Temp: HPC side
TW-823	Watlow	AFEK0FA090G4031	N/A	Plate Temp: Center
TW-824	Watlow	AFEK0FA090G4032	N/A	Plate Temp: CPV side
TF-825	Watlow	AFEK0FA090G4030	N/A	Plate Temp: CPV side film
TF-831	Watlow	AFEK0FA090G4030	N/A	Plate Temp: HPC side film
TW-832	Watlow	AFEK0FA090G4030	N/A	Plate Temp: HPC side
TW-833	Watlow	AFEK0FA090G4031	N/A	Plate Temp: Center
TW-834	Watlow	AFEK0FA090G4032	N/A	Plate Temp: CPV side
TF-835	Watlow	AFEK0FA090G4030	N/A	Plate Temp: CPV side film
TF-841	Watlow	AFEK0FA090G4030	N/A	Plate Temp: HPC side film
TW-842	Watlow	AFEK0FA090G4030	N/A	Plate Temp: HPC side
TW-843	Watlow	AFEK0FA090G4031	N/A	Plate Temp: Center

Table 4.1-2: Table of thermocouple specifications, Part 2.

Call Name	Make	Model	Serial #	Function
TW-844	Watlow	AFEK0FA090G4032	N/A	Plate Temp: CPV side
TF-845	Watlow	AFEK0FA090G4030	N/A	Plate Temp: CPV side film
TF-851	Watlow	AFEK0FA090G4030	N/A	Plate Temp: HPC side film
TW-852	Watlow	AFEK0FA090G4030	N/A	Plate Temp: HPC side
TW-853	Watlow	AFEK0FA090G4031	N/A	Plate Temp: Center
TW-854	Watlow	AFEK0FA090G4032	N/A	Plate Temp: CPV side
TF-855	Watlow	AFEK0FA090G4030	N/A	Plate Temp: CPV side film
TF-861	Watlow	AFEK0FA090G4030	N/A	Plate Temp: HPC side film
TW-862	Watlow	AFEK0FA090G4030	N/A	Plate Temp: HPC side
TW-863	Watlow	AFEK0FA090G4031	N/A	Plate Temp: Center
TW-864	Watlow	AFEK0FA090G4032	N/A	Plate Temp: CPV side
TF-865	Watlow	AFEK0FA090G4030	N/A	Plate Temp: CPV side film
TF-873A	Watlow	AFGJ0FA040U4050	N/A	ADS Line Temp
TW-891	Watlow	AFGM0TA120U4080	N/A	Cont Wall Temp
TW-892	Watlow	AFGM0TA120U4080	N/A	Cont Wall Temp
TW-893	Watlow	AFGM0TA120U4080	N/A	Cont Wall Temp
TW-894	Watlow	AFGM0TA120U4080	N/A	Cont Wall Temp
TH-891	Watlow	N/A	N/A	Cont Heater Temp
TH-892	Watlow	N/A	N/A	Cont Heater Temp
TH-893	Watlow	N/A	N/A	Cont Heater Temp
TH-894	Watlow	N/A	N/A	Cont Heater Temp

Six sets of five thermocouples are implanted into the HTP at elevations of 99.38 cm, 249.55 cm, 319.4 cm, 409.57 cm, 509.27 cm and 559.43 cm. Three of the thermocouples are inserted into the mass of the plate at the centerline position and at the two faces while two others are inserted through the plate and angled out into the containment and cooling pool volumes respectively. Direct verification of the accuracy of these thermocouples was not possible at the time of this study. Comparison was made with newly installed thermocouples in the area that supported this assumption. The physical positioning of these plate thermocouple sets will be discussed in further detail along with the analysis method in the next section.

Another set of four thermocouples are placed next to the strip heaters on the exterior of the vessel just inside the thermal insulation. These instruments ensure overheating of the heaters does not occur. Another set of four thermocouples are inserted directly into the containment vessel through four independent penetrations. These thermocouples are designed to measure the temperature near the wall directly opposite the strip heaters. However, in tests where the heaters are not used, these thermocouples accurately measure the bulk steam temperature after a given period where the wall temperature is raised to that of the bulk fluid and condensation no longer takes place in the region.

The four remaining thermocouples measure the primary reactor temperature, the temperature of the safety relief valve outlet line, pre-expansion temperature of the ADS line fluid and the bulk fluid temperature. It is important to note that the bulk fluid thermocouple was out of service during the period of testing included in this work. The heater fluid thermocouples described above were

used for this data for the bulk fluid temperature. The thermocouple accuracy in all cases is derived from the standard instrument accuracy and that of the analog to digital conversion process done by the IO modules. The standard instrument accuracy, sizing, calibration ranges and standard ranges are provided in Table 4.1-3.

Table 4.2-3: Thermocouple instrument ranges, size and accuracy.

Model	Range	Cal Range	Dimension (cm)	Max error
AFEK0FA090G4030	0-1200 C	10-315 C	0.159	1.1 C
AFEK0FA090G4031	0-1200 C	10-315 C	0.159	1.1 C
AFEK0FA090G4032	0-1200 C	10-315 C	0.159	1.1 C
AFGJ0FA040U4030	0-1200 C	10-315 C	0.318	1.1 C
AFGJ0FA040U4050	0-1200 C	10-315 C	0.318	1.1 C
AFGJ0FA080U4030	0-1200 C	10-315 C	0.318	1.1 C
AFGM0TA120U4080	0-1200 C	10-315 C	0.318	1.1 C
AFJK0FA120U4040	0-1200 C	10-315 C	0.318	1.1 C

## 4.2 Pressure Transmitters

Two pressure measurements are recorded and relevant to the performance of the containment. Pressure transmitters utilize a single reference line that penetrates the volume being measured and compares this value with an open line to atmosphere. The incoming steam pressure to the CPV, i.e. the pressure of the RPV, is measured in the pressurizer section of that vessel. The second transmitter measures the containment system pressure from an instrument reference line which penetrates the upper region of the HPC. The RPV pressure

measurement provides a reference point for the incoming steam and could be incorporated into another energy balance for the convection-condensation heat transfer process. The containment pressure is the second most influential parameter, next to temperature gradients, in the formulation of the energy balance calculations.



Figure 4.2-1: Rosemount pressure transmitter, Model 1151

The two pressure measurements are standard coplanar Rosemount pressure transmitters; Models 3051C and 1151. The primary difference is the instrument accuracy. The instrument produces a 4 to 20 mA signal that corresponds to the low and high range values respectively. Detailed information on the instruments, their calibration and their accuracy can be found in Table 4.2-1 and Table 4.2-2.

Table 4.2-1: Pressure transmitter instrument specifications.

Call Name	Make	Model	Serial #	Function
PT-301	Rosemount	3051CG5A02A1AH2Q4	1098316	PZR Pressure
PT-801	Rosemount	1151GP8S22B1	1555616	HPC Pressure

Table 4.2-2: Pressure instrument calibration and accuracy data (values shown are gauge values).

Call Name	Inst. Range	Cal Range	Dim. (cm)	Max error
PT-301	- 13.79 to 13.79 MPa	0 to 13.79 MPa	N/A	0.1% of span
PT-801	0 to 6.895 MPa	0 to 2.514 MPa	N/A	0.25% of span

### 4.3 *Level Indicators*

The level measurements in the RPV and HPC are relevant to the energy balance between the two vessels during a blowdown event. The HPC level also factors greatly into the evaluation of condensation heat transfer. These measurements are made using differential pressure transmitters which operate using two reference lines as opposed to the single line and atmosphere arrangement of the pressure transmitters. These reference lines are situated at different elevations in the pressure vessel such that they are both exposed to the system pressure and only one is exposed to the weight of the liquid level. This arrangement allows for a rapid calculation of the pressure difference and subsequently the level of water.

Level differential pressure indicators are nearly identical in form to the pressure transmitters and operate on the same principle. The reference line pressure

meets a sealed interface diaphragm that displaces in response to incoming pressure. This diaphragm's position is recorded and electronically converted to a pressure measurement. The instrument data can be found in Table 4.3-1 and Table 4.3-2.

Table 4.3-1: Level differential pressure transmitter instrument specifications.

Call Name	Make	Model	Serial #	Function
LDP-106	Rosemount	3051CD2A02A1AH2Q4	1098336	RPV Level
LDP-301	Rosemount	3051CD2A02A1AH2Q4	116905	PZR Level
LDP-801	Rosemount	3051CD2A02A1AH2DFM5B3	1799856	HCP Level

Table 4.3-2: Level differential pressure transmitter calibration data.

Call Name	Inst Range	Cal Range	Dimension	Max error
LDP-106	-635 to 635 cm	-375.285 to 0 cm	N/A	0.1% of span
LDP-301	-63.5 to 63.5 cm	-62.66to 0 cm	N/A	0.1% of span
LDP-801	-635 to 635 cm	-560.4to 0 cm	N/A	0.1% of span

#### **4.4 *Input/Output Modules***

The thermocouple input receivers of the MASLWR facility are the Automation Direct T1F-14THM IO modules. The modules are coupled to Ethernet bases which relay the signal to the PC control station. The modules are fitted with 14-channels for input reception and convert the analog signal from the instruments to a digital output. This process takes place in 100 ms and contributes a small error to the data acquisition process. The maximum bound on the error from

the modules is reported at  $\pm 3$  C which is the largest source of error in the temperature data. The instruments have an independent input receiver also manufactured by Automation Direct. The module is equipped with a 16-channel termination deck and similarly connects to a base controller which relays the signal to the PC control station. The T1H-16AD-1 introduces an error of 0.18% of the instrument reading at ambient temperature (25 C).

#### **4.5 *Experiment Error Quantification***

Prior to presenting and drawing conclusions from the data produced during experimentation it is necessary to evaluate the correctness of the measurements. The work completed in this study was not held to ASME NQA-1 requirements of the nuclear industry but the facility will be held to those standards in the upcoming battery of testing. As such many of the guidelines and requirements have been followed in the experimental process. This allows for a relatively direct estimation of error to be conducted here.

It is important to present the findings of this research in a way that can be utilized in the future operation of this integral test facility and appreciated by other investigations of small modular reactor containment systems. To that end the calculated error will be presented along with the results from both experiment runs. While the experimental conditions may be recreated independently from this research, the facility itself will be demolished in the coming year. The current containment will be replaced with a pressure vessel capable of simulating the necessary conditions for NSP testing. This point makes it important to annotate this research with the exact conditions of the experiments performed.

After quantifying the individual components of calibration, manufacturing and acquisition error it is possible to estimate the degree of accuracy of the findings in this work. In the previous sections of this chapter the error contribution of each instrument and data acquisition system component was reported. The cumulative sources of error in the instrumentation system are displayed in Table 4.5-1.

Table 4.5-1: Error sources in the MASLWR test facility containment.

Error Source	Quantity
Thermocouple	1.38% of reading
Thermocouple Module	3.75% of reading
Pressure Inst.	0.25% of span
Level Inst.	0.1% of span
Instrument Module	0.18% of span

The experimental data will incorporate the effective combined error for all sources using equation 4.1.

$$\epsilon_{combined} = \sqrt{(\epsilon_{component})^2 + (\epsilon_{instrument})^2} \quad (\text{eq. 4.1})$$

Applying the above equation yields total error quantities for all measured data which is shown in Table 4.5-2. The pressure instruments error has been calculated to be less than 1.5% of the reading for the entire range.

Table 4.5-2: Combined maximum error in MASLWR test facility containment.

Error Source	Quantity
Thermocouples	4% of reading
Pressure Inst.	1.5% of reading
Level Inst.	1.5% of reading

The experimental error in data acquisition is not the only manner of error analysis necessary for this work. The uncertainty's effect on the calculated parameters of heat rate and heat transfer coefficient must also be taken into account. To properly evaluate the error in these calculated properties the method of the root of the sum of the squares (RSS) was employed to accurately gauge not the maximum error but a reasonable approximation.

The RSS approximation produced exceptionally high error bounds for the final value of the HTC. These values approached 25-30% of the value of the parameter. However, these limits must be accepted due to the inherent error that arises from the complexity of the quantity calculation. The RSS method is shown below for clarity.

For any data set that is a function of any number of variables,  $x_1, x_2, \dots, x_n$ ,

$$Y = f(x_1, x_2, \dots, x_n) \quad (\text{eq. 4.2})$$

$$\rho Y = \rho x_1 \frac{\delta Y}{\delta x_1} + \rho x_2 \frac{\delta Y}{\delta x_2} + \dots + \rho x_n \frac{\delta Y}{\delta x_n} \quad (\text{eq. 4.3})$$

For a maximum estimate of the uncertainty in Y, the absolute value of the sum of this series would be taken. However, the method employed in this work takes the root of the sum of the squares.

$$\varepsilon_Y = \left( \sum_{i=1}^n \left[ \varepsilon_{x_i} \frac{\delta Y}{\delta x_i} \right]^2 \right)^{1/2} \quad (\text{eq. 4.4})$$

## 5 Methods and Experimental Data

The objective of this study can be approached in a number of different ways as the literature has shown. The physical processes that occur at the fluid-vapor boundary are complex and affect the mass-energy transfer directly. The fluid layer itself and how it traverses the heat transfer surface has an important role in both the convection and condensation heat transfer quantities. The gaseous composition has other effects as well which inhibit the condensation of the working fluid. While these factors are immensely influential in the operation of the containment system, the work conducted in this thesis takes advantage of the exceptionally well characterized integral test facility at the Advanced Thermal Hydraulics Research Laboratory (ATHRL).

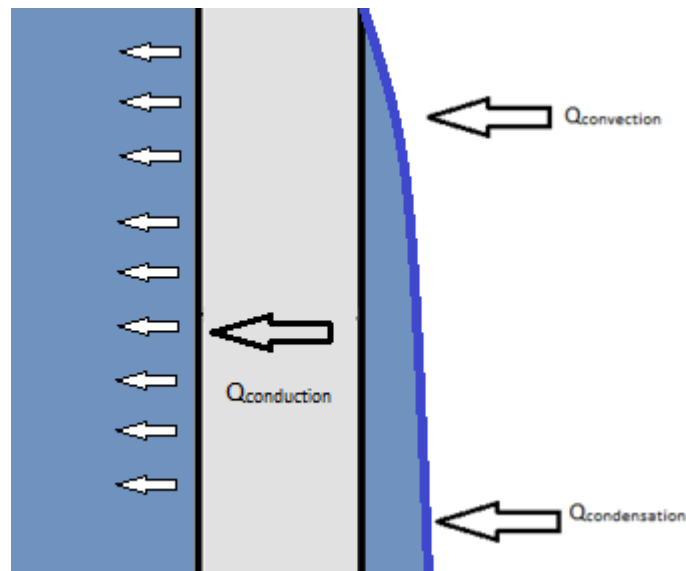


Figure 5.1-1: Heat transfer plate energy transport diagram

## **5.1 *Analysis Method***

The physical aspects of the MASLWR facility will be discussed in detail in the next section. This chapter will address the process of data collection and the method used to quantify the final heat transfer coefficient. Two experiments were run at the ATHRL location to characterize the condensation-convection cooling function of the containment structure. Each test case was begun from different starting pressures in the RPV at full operating temperature. In this work a 1-dimensional approach is taken to quantify the conduction energy transfer during an accident simulation. This data is then used to evaluate the convection-condensation heat transfer that takes place in the HPC.

The basis of this research hinges on the measurement of the conduction heat transfer that is traversing the medium between the HPC and the CPV. In fact this boundary has been specifically designed and instrumented for this purpose. Thermocouples have been inserted into the mass of the HTP: one on the centerline, one at each face and one raised from the surface so as to measure the fluid layer temperature. Drawings of the thermocouple placement inside the HTP are shown in Figure 5.1-2 and Figure 5.1-3.

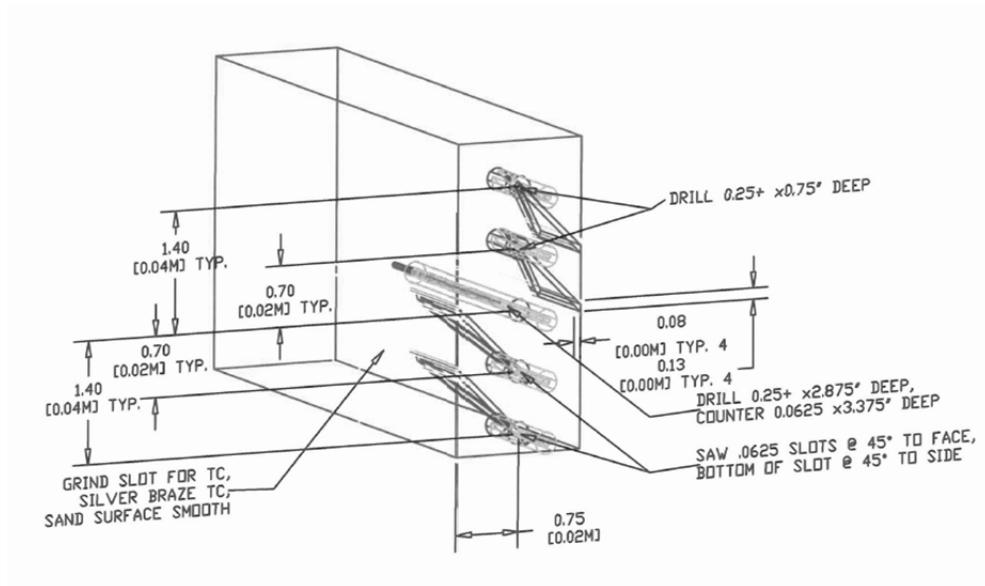


Figure 5.1-2: Heat transfer plate thermocouple spacing diagram.

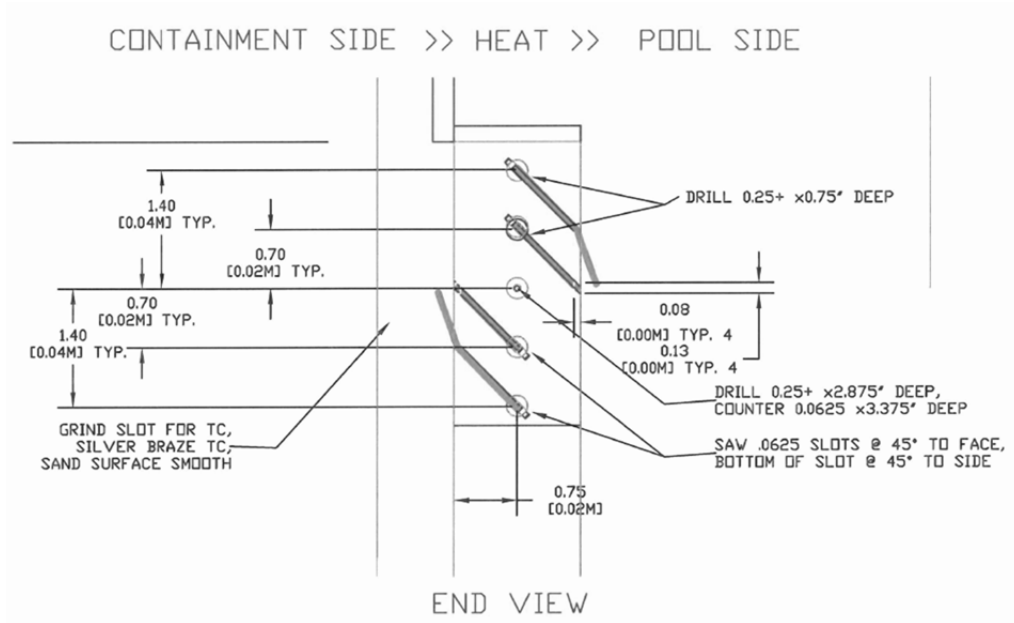


Figure 5.1-3: Heat transfer plate thermocouple extension diagram.

As the figures show the HTP instrumentation allows for the quantification of the conduction heat rate through the plate based on the temperature profile. The three thermocouples are equally spaced through a known material with known dimensions. Two temperatures are all that are needed to establish a temperature gradient but the third allows for the observation of transient conditions. As the plate is exposed to heat the mass requires a heating period to achieve linearity. The conduction calculation assumes this linearity and is as follows:

$$q_{conduction} = -k A \frac{dT}{dx} \quad (\text{eq. 5.1})$$

And,

$$\frac{dT}{dx} = \frac{T_{f2} - T_{f1}}{w} \quad (\text{eq. 5.2})$$

Where  $T_{f2}$  is the CPV side thermocouple reading,  $T_{f1}$  is the HPC side thermocouple reading,  $A$  is the HTP area, and  $w$  is the thickness of the HTP. This heat rate is equal to the energy entering the CPV from the reactor volume less the heat losses through the insulation. These losses are assumed to be negligible. Thus, the heat rate becomes a measure of the total heat removal rate of the containment. Ignoring radiative heat transfer as well as losses from the vessel, convection and condensation become the only modes of energy transfer interior to the containment volume.

$$q_{convection} = h_{cv} A (T_{vapor} - T_{fluid}) \quad (\text{eq. 5.3})$$

$$q_{condensation} = h_{condensation} A (T_{vapor} - T_{fluid}) \quad (\text{eq. 5.4})$$

And,

$$q_{conduction} = q_{convection} + q_{condensation} \quad (\text{eq. 5.5})$$

This evaluation is not complete however as we have not characterized either convection or condensation at this point. The condensation heat transfer rate can be measured directly through the rate at which liquid collects in the containment vessel. Instrumentation is present to collect data on the level inside the HPC throughout all experiments. Additionally, since it is known that condensation heat transfer occurs at a constant temperature for a given pressure, i.e. the saturation temperature, the density and the enthalpy of evaporation for this fluid can be determined. It is from these parameters that we may quantify the heat removed through the phase change of the fluid.

$$q_{condensation} = \dot{m} \cdot \Delta h_{fg} = \rho \cdot A \cdot \frac{dH}{dt} \cdot \Delta h_{fg} \quad (\text{eq. 5.6})$$

Where  $A$  is the cross-sectional area of the condensate collecting in the bottom of the containment vessel. Rearranging eq. 5, this definition and can be combined with equations 1 and 2 to define the convection heat transfer, and subsequently the convection heat transfer coefficient.

$$q_{convection} = -k A \frac{T_{f2} - T_{f1}}{w} - \rho A \frac{dH}{dt} \cdot \Delta h_{fg} \quad (\text{eq. 5.7})$$

$$h_{cv} = \frac{-k A \frac{T_{f2} - T_{f1}}{w} - \rho A \frac{dH}{dt} \cdot \Delta h_{fg}}{A(T_{vapor} - T_{fluid})} \quad (\text{eq. 5.8})$$

In the same respect, the condensation heat transfer coefficient may be obtained:

$$h_{condensation} = \frac{\rho A \frac{dH}{dt} \cdot \Delta h_{fg}}{A(T_{vapor} - T_{wall})} \quad (\text{eq. 5.9})$$

Where  $T_{vapor}$  is the saturation temperature,

$T_{wall}$  is the average wall temperature.

## **5.2 Procedure and Experimental Results**

This evaluation of the convection and condensation heat transfer relies heavily on the collection of quality data. Specific test procedures were developed for this effort as a part of this work and are included as an appendix to this document. However, for the sake of transparency these procedures will be discussed in brief. The goal of each experiment was to raise primary temperature and pressure inside the primary vessel to a given pressure and approximately 13.89 °C subcooled margin to prevent boiling of the coolant in the core region.

The RPV is pressurized using the core heaters and pressurizer heaters in concert to initially raise primary temperature to boiling at atmospheric pressure. Given an appropriate time period to vent all gases through the RPV vent line, the vessel is sealed and the climb to pressure is begun. At the same time primary temperature is raised and secondary coolant is provided through the steam generator. Natural circulation cycling of the primary coolant begins almost immediately ensuring the entire volume is heated.

Pressurization can take up to 2 hours when standard operating pressure is desired. However the tests that were conducted in this work required a continual blowdown event and a full pressure test would exceed the limits on the HPC pressure. Graduated pressure set points were outlined and the primary was brought to those set points. Once the RPV is primed the conditions in the HPC are verified.

For the first test a vacuum was drawn inside the containment vessel of -94.5 kPa (gauge). This step was included to remove non-condensable gases from the

containment vessel and to ensure a purely steam-water condensation process. The second set of experimental data is from a containment analysis test which was aborted prior to completion. This experiment was intended to reach a much greater pressure in the primary vessel but had to be aborted due to a discovered leak. The containment was not evacuated or heated in this experiment. Further testing was impeded by Initial conditions for both of these tests are tabulated below.

Table 5.2-1: Experimental initial conditions.

Test Case	Initial Primary Pressure (MPa gauge)	Initial Primary Temperature (°C )	Containment Vacuum Condition
1	3.103	218.333	Yes
2	6.129	287.78	No

A blowdown event is initiated by actuating the primary pneumatic ADS valve, PCS-106A. Only one of the two blowdown valves is opened to ensure the process is as long as possible. Built up steam pressure from the primary vessel is released through the ADS line and fills the containment vessel. The pressure response of the containment vessel is rapid initially but it peaks within the first quarter of the experiment. Following the pressure peak, the 1-dimensional conduction heat flux approaches linearity and the HTP wall temperature is below saturation allowing condensation to take place. The region after these conditions are established is the only suitable region for complete convection analysis with this method due to the transient conduction taking place within the HTP inaccurately representing the energy balance. The first test conducted produced the pressure response shown in Figure 5.2-1.

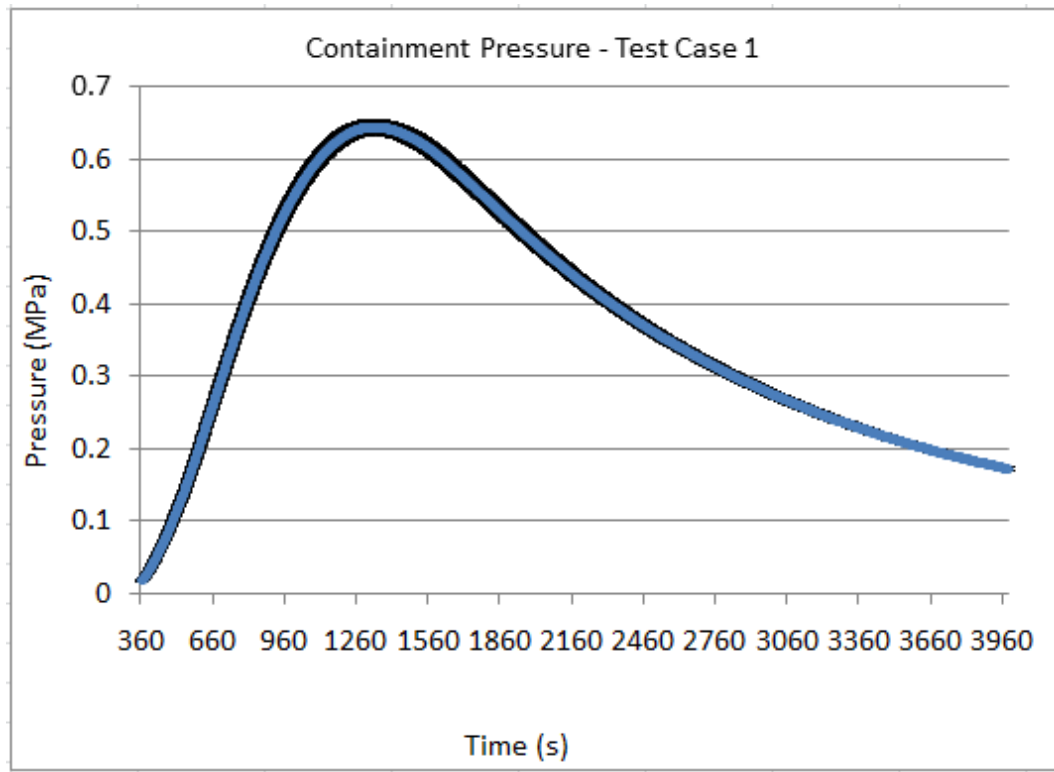


Figure 5.2-1: Test case 1 containment pressure (absolute) response with error bounding.

The depressurization of the primary vessel resulted in a rapid initial rise in the containment pressure readings. The flow through the fabricated flow nozzles was sufficient to bring the containment vessel to a maximum of 644.5 kPa. The data collected showed very little instrument noise seen here in the smooth pressure function. The tail end of the data is marked by a measure drop around the 4000 second mark which corresponds to the opening of the containment relief valve. The venting of the containment is standard at the commencement of an experiment. The pressure response of the containment is related to the condensate level measurements from the bottom of the vessel. Figure 5.2-2 shows the level measurements from test case 1.

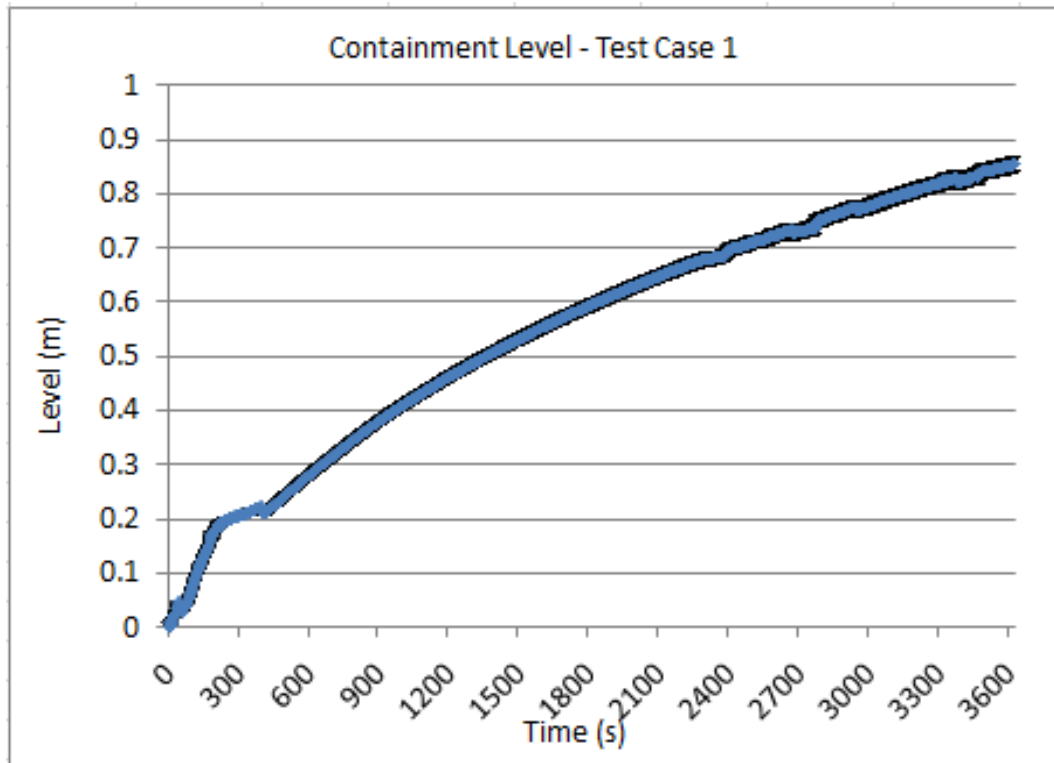


Figure 5.2-2: Containment level measurement during experiment 1 (error shown).

The initial sharp influx of steam from the primary vessel caused a preliminary surge in condensation. As the vessel was not heated at the start of the experiment, the incoming vapor was able to condense over the entire body of the vessel. This transient is reflected in the first region of the level measurements. The installed heaters on the facility are designed to mitigate this reaction through prime heating of the vessel walls and in doing so restricting the condensation to the HTP. Once the surrounding walls reached the saturation temperature the heat transfer plate became the primary condensation surface and the condensation rate dropped. In addition to this the pressure in the vessel

was not high rapid enough to facilitate condensation on the now heated walls. This effect can be seen in the temperature measurements near the HTP and at its surface when compared to the saturation temperature. This is illustrated in Figure 5.2-3 and the saturation line is clearly shown to be at or below the near wall temperature reading, TF842, and very near the wall temperature reading, TF841. These are thermocouple readings from the upper third of the HTP and represent a high average of the entire condensation surface. Error bars are excluded for clarity though the magnitude would cover the difference between the saturation line and the wall thermocouples over the initial period of rise.

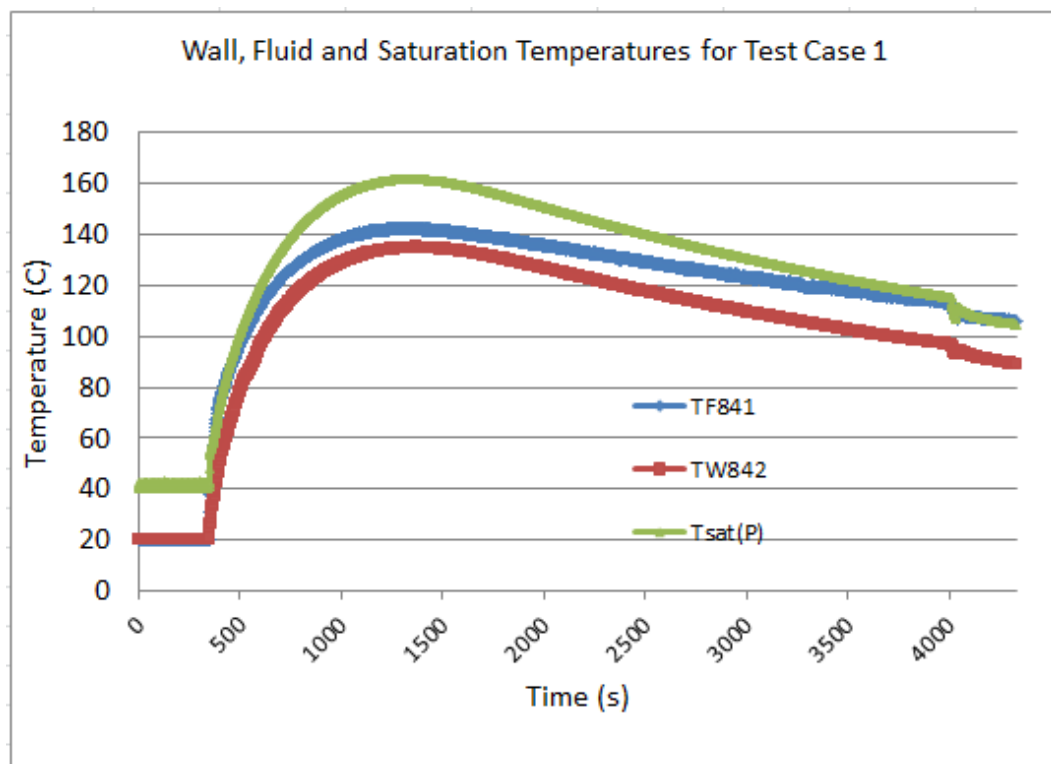


Figure 5.2-3: Plot of the thermocouple data from 4.1 (m) above the bottom of the HPC indicating the initial superheating of the incoming vapor and the wall heating beyond saturation.

The conduction data was obtained through analysis of the 6 sets of HTP thermocouples, upper region example shown in Figure 5.2-4, which span the heat transfer medium between the HPC and the CPV. The measurements taken indicate a conduction transient across the 3.81 cm plate of steel. This transient was evaluated by comparing the centerline temperature readings to the average temperature of the two face thermocouples, i.e. TW8x2 and TW8x4.

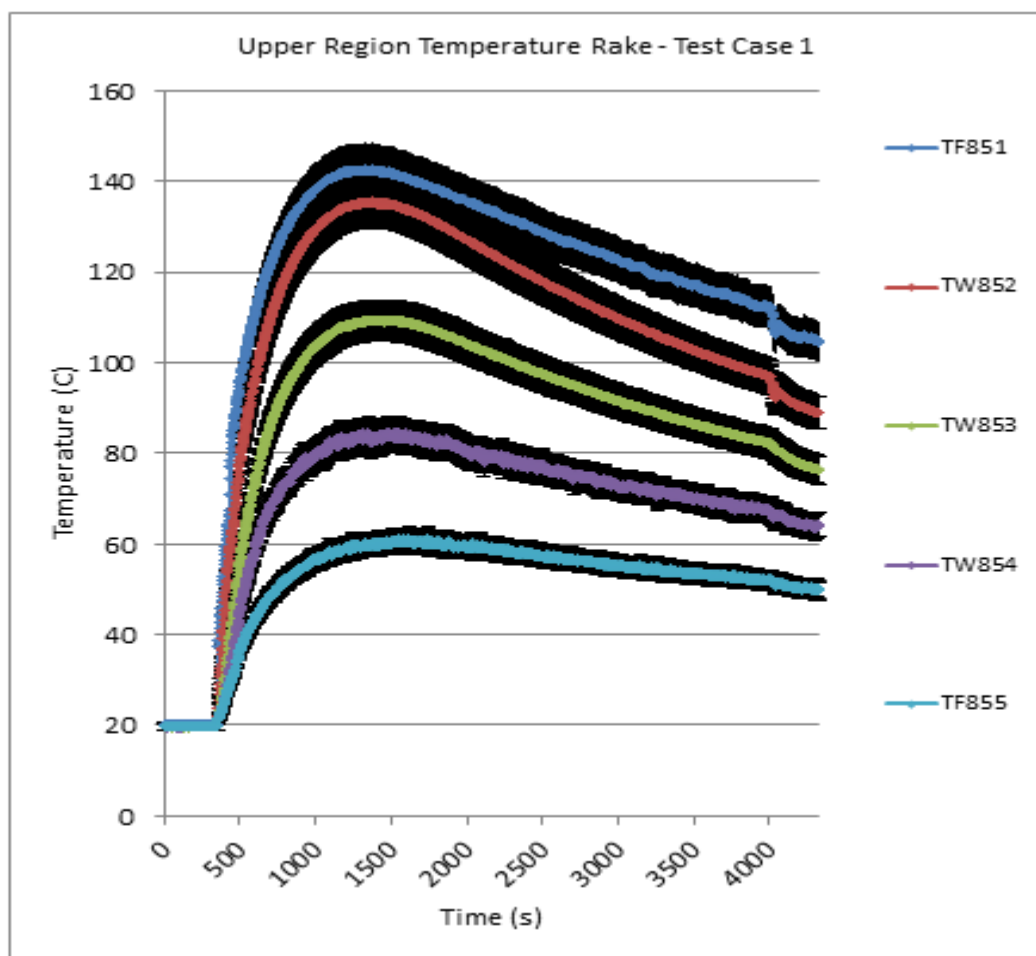


Figure 5.2-4: Example plot of one of the thermocouple rakes across the HTP, 5.1 (m), for test case 1 that illustrates the conduction transient across the steel plate (Error bars included).

The effect of the thermal transient in this analysis is that the convection evaluation performed through the calculation of both condensation and conduction heat rate is not applicable to the region prior to approximately 50% of the temperature peak. To do so would require a more in depth approach involving computed simulation and boundary layer analysis beyond the scope of this work. Ergo, the convection results will only be considered after this region.

The conduction data, discussed further in the next section, indicated the thermal transient clearly. It also showed that several of the 42 thermocouples were not functioning properly. Due to their position, welded 3.5 inches into a slab of stainless steel, they were not replaced for this thesis. The lower section also showed the highest conduction values (40% greater than mid-regions) through the first portion of the test. The effect of this rapid cooling did not appear to extend higher than the lowest region and will be neglected in the calculations. The remaining 4 sets of thermocouples were used in calculation of an average conduction heat rate over the area of the HTP. Figures 5.2-5 through 5.2-7 display the collected data for these instruments.

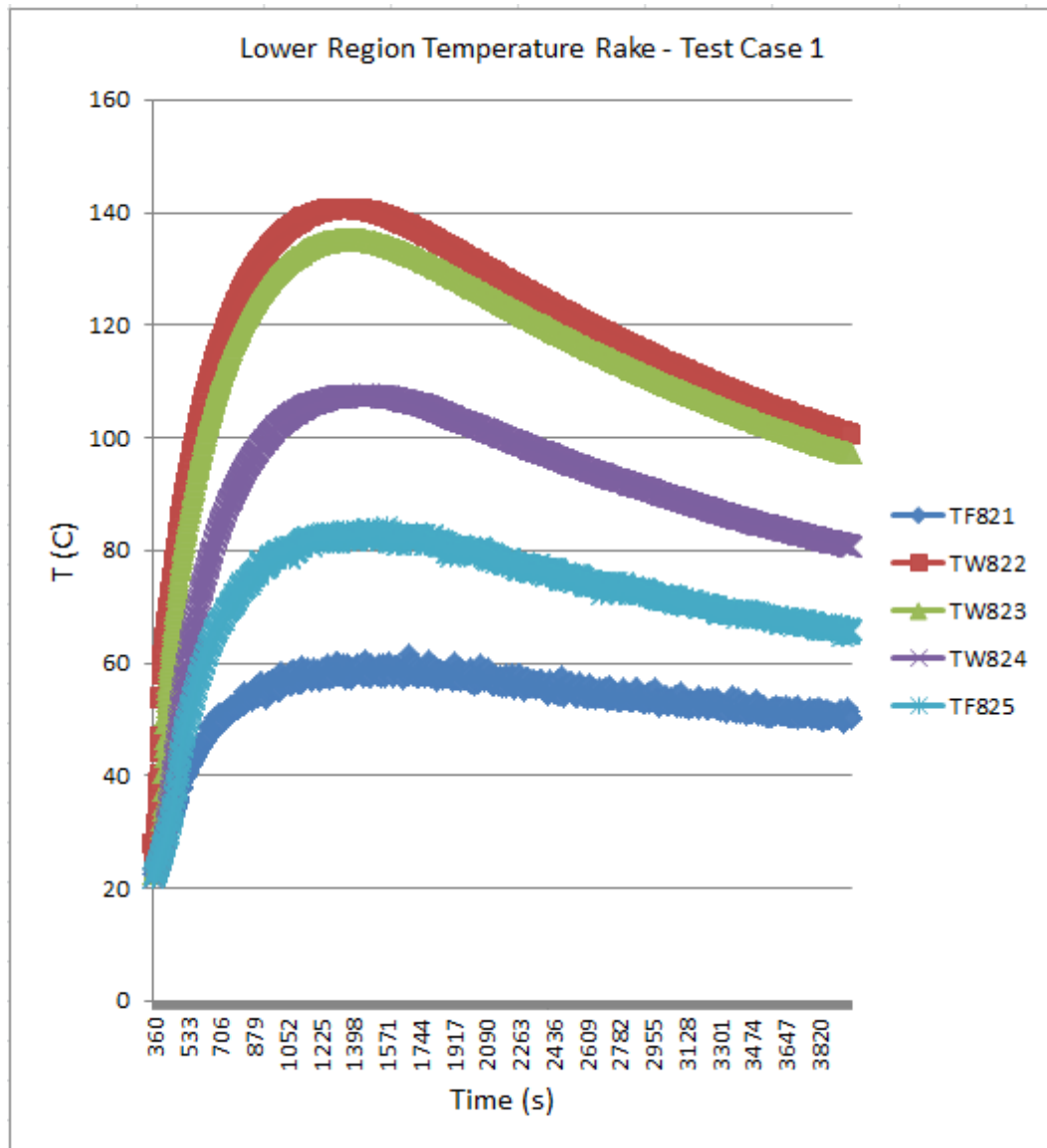


Figure 5.2-5: HTP thermocouple rake measurements at a height of 2.5 (m) for test case 1 (error bars omitted).

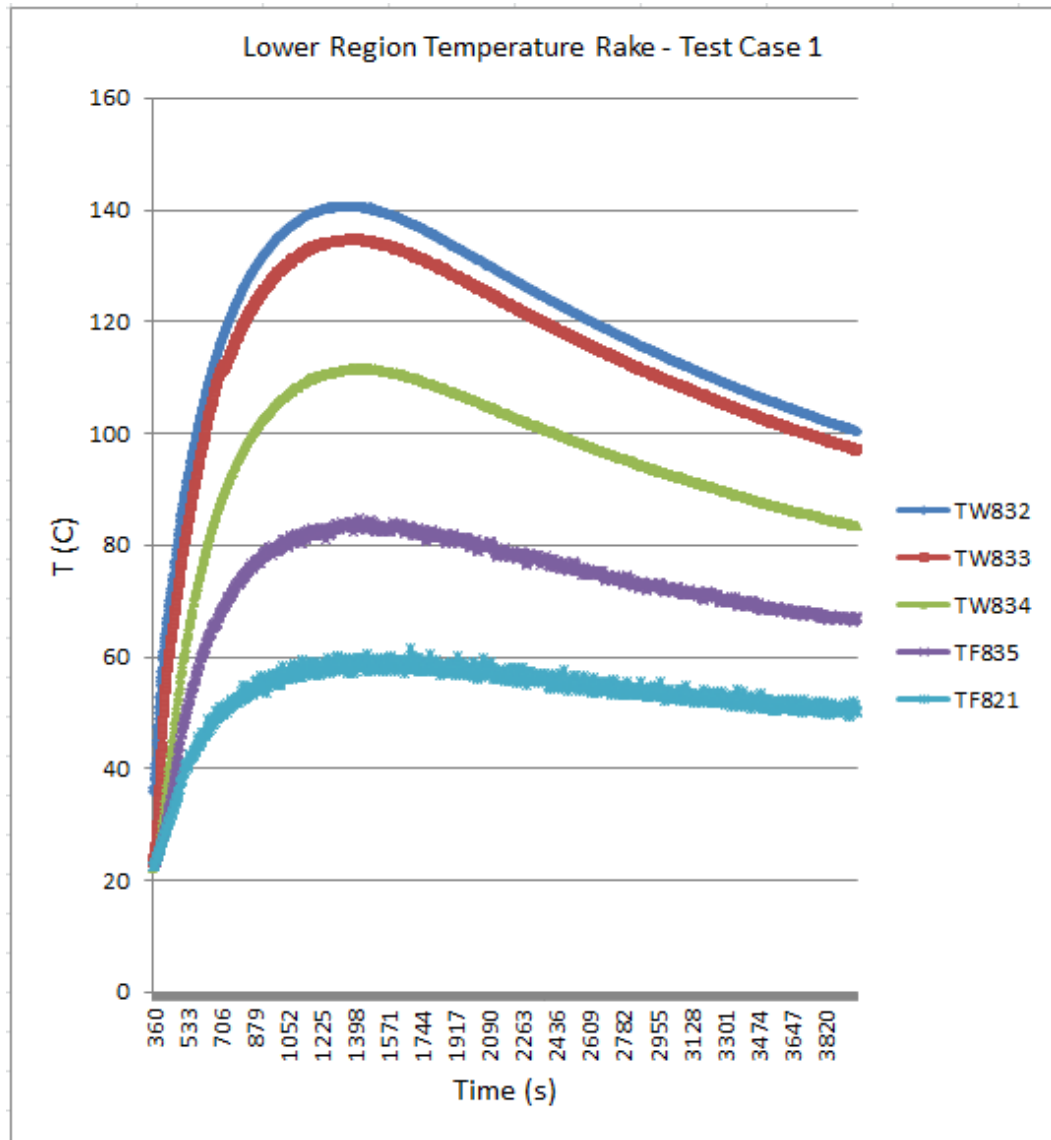


Figure 5.2-6: HTP thermocouple rake measurements at a height of 3.19 (m) for test case 1 (error bars omitted).

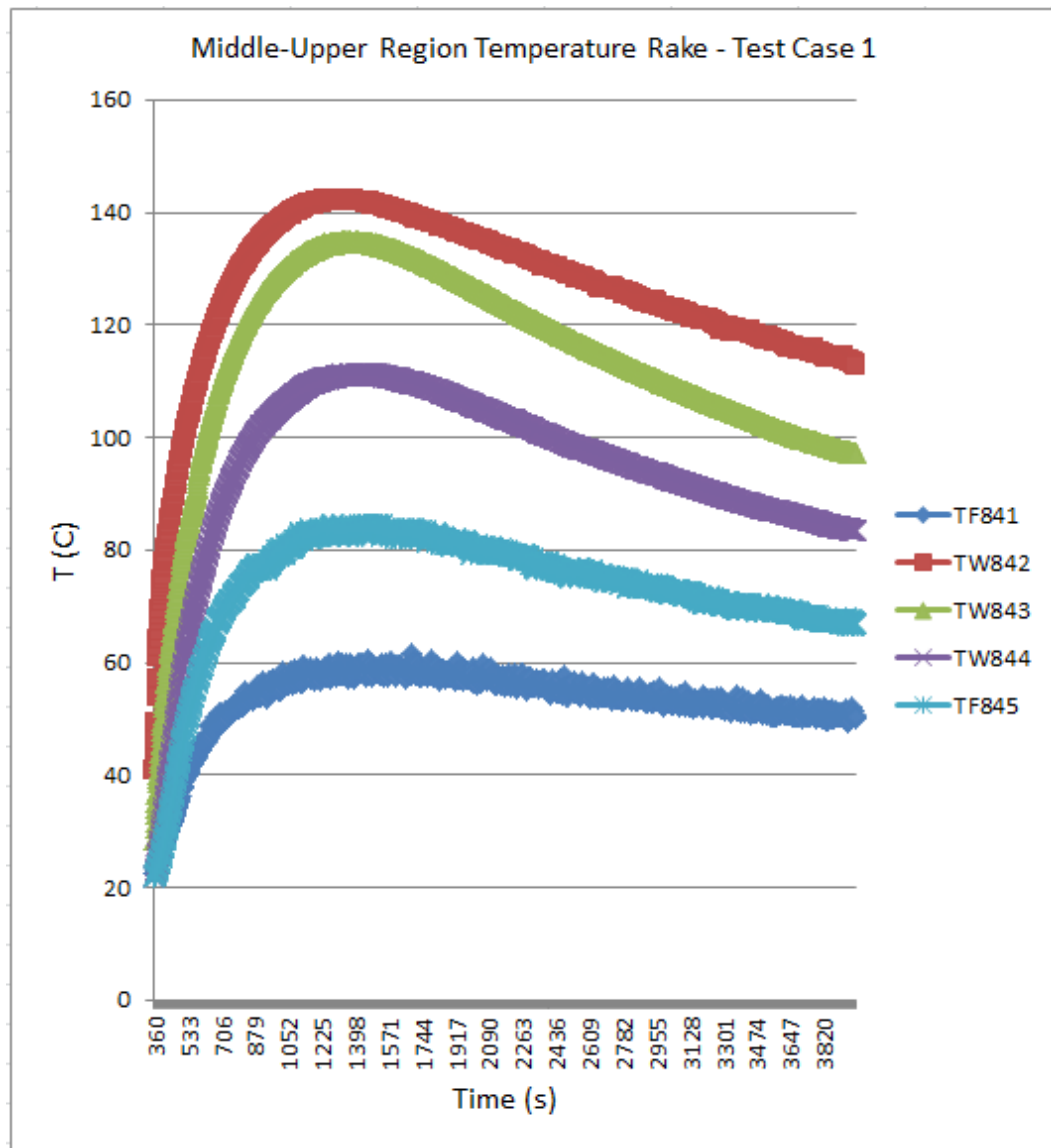


Figure 5.2-7: HTP thermocouple rake measurements at a height of 4.1 (m) for test case 1 (error bars omitted).

Apart from the wall temperature measurements and the film temperature measurements the next most significant measurement is that of the bulk fluid temperature in the containment volume. The designers of this facility neglected this point in the construction of the facility though in this work the calculated saturation temperature from pressure will be used for the bulk fluid temperature. In both experiments this approximation will be accurate as the bulk temperature is the driving force behind the convection heat transfer. It should be noted that this is not a perfect measure but since this analysis is pursuing an average heat transfer analysis for the entire system this approximation holds. This measure is also a conservative estimate of the condensation heat transfer since the phase change of vapor can only occur at the saturation temperature. The saturation data is shown in Figure 5.2-7.

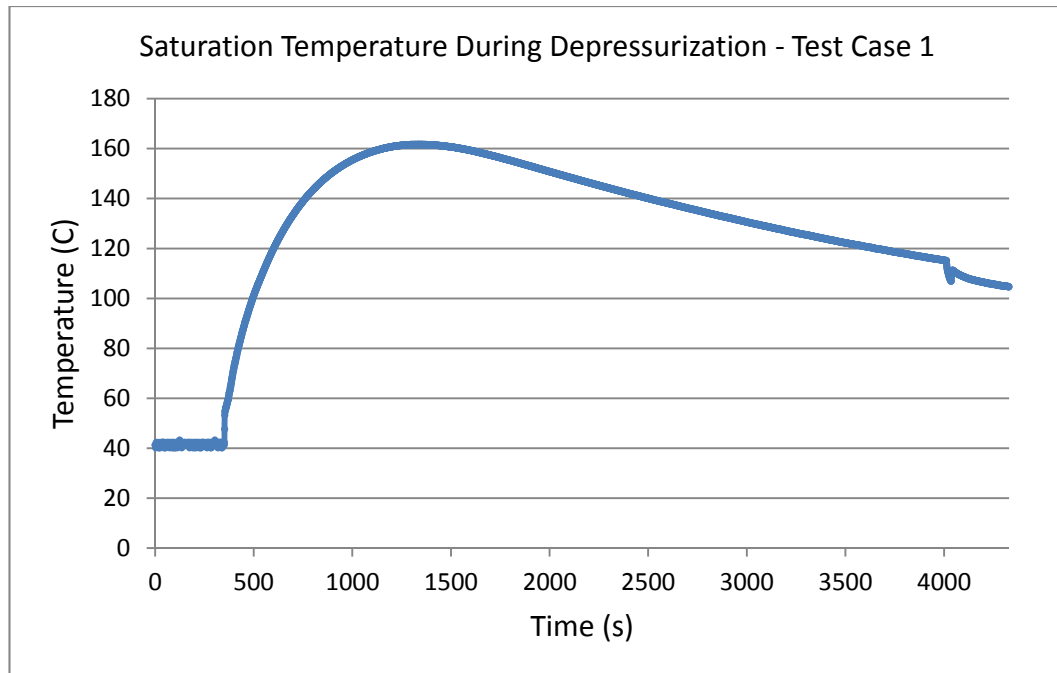


Figure 5.2-8: Calculated saturation temperature data from test case 1 for the HTC calculation.

The saturation data should be accepted as a conservative estimate of the high measurement form which heat transfer takes place as the bulk fluid is undoubtedly superheated upon entry. Conventional analyses since Nusselt's work, (37) (25) (18), have used the bulk fluid temperature as measured near the condensation surface to quantify heat transfer coefficients. In the case of forced flow condensation analyses, the bulk fluid temperature is also greater than that of saturation for a significant portion of the condensation area, (3).

The second test case acquired data on a much shorter experiment which ran with the HPC vent valve opened. This valve allowed high temperature steam to

escape through the safety line and air to enter the already air filled containment volume. Under ideal conditions comparing only the condensation in the two sets of data from shared initial conditions, the effect of this valve being opened would decrease the condensation heat transfer immensely (12). The relief of pressure under shared initial conditions would also prevent the containment from reaching the same peak pressure, further contributing to a decline in the condensation heat transfer rate. Figure 5.2-9 displays the pressure response of the containment volume in the second test case. The second peak corresponds to the opening of the second ADS line from the primary vessel signifying the end of this data.

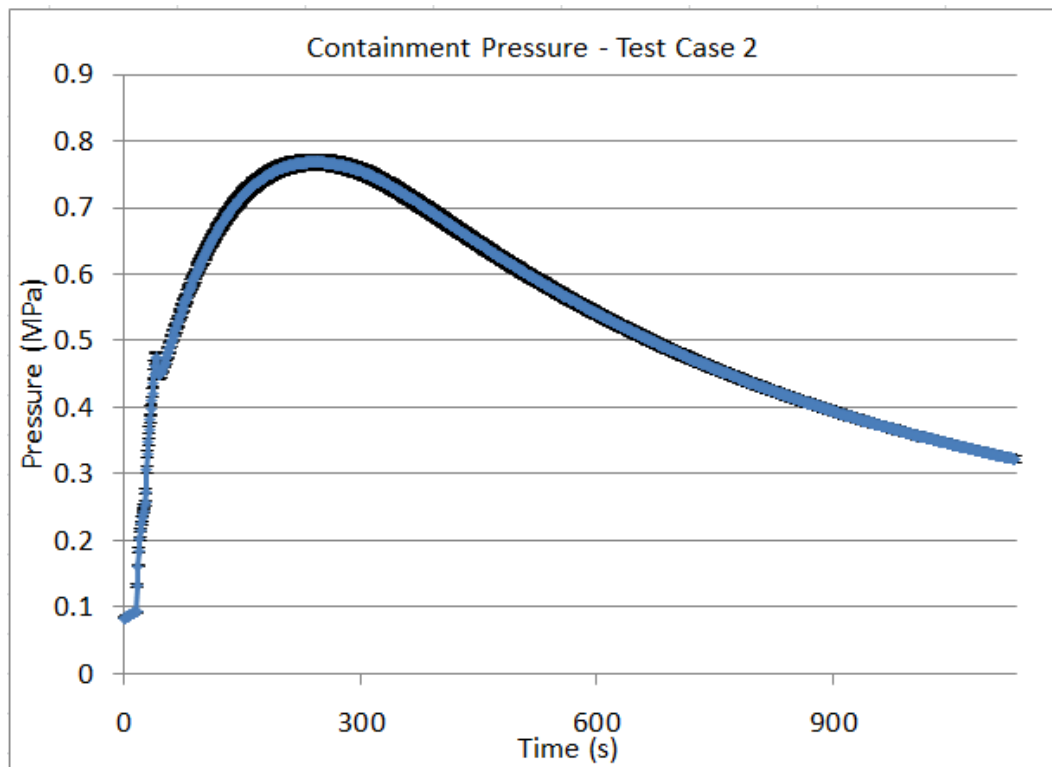


Figure 5.2-9: Containment pressure from test case 2.

Containment pressure from the second test case reached a higher maximum than that of test case 1. This is due to the substantially greater primary pressure that the experiment began from. The entire experiment ran much faster in the second case due to the larger difference between vessel pressures. The pressure response however, did have the same shape in both cases. The condensation data taken from the second case is somewhat different though in that it does not show the same drop in condensation from the walls heating past saturation. The same plot for test case 2 illustrates the difference in the two wall conditions.

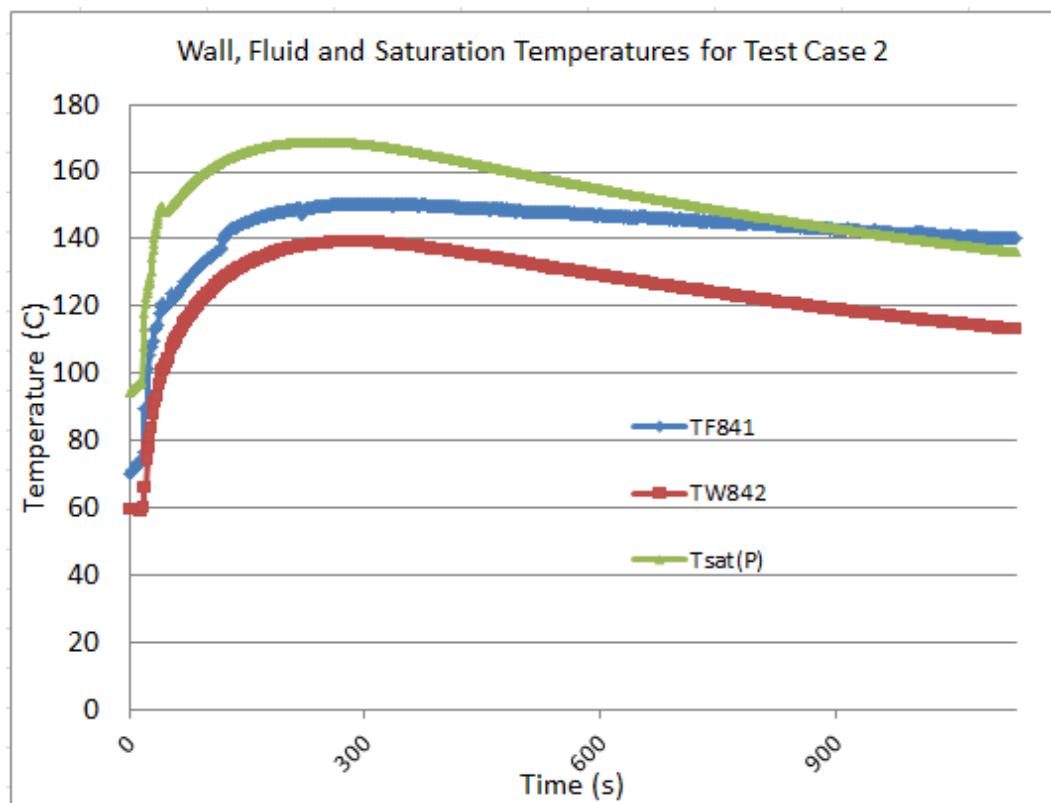


Figure 5.2-10: Wall heating condition plot for test case 2.

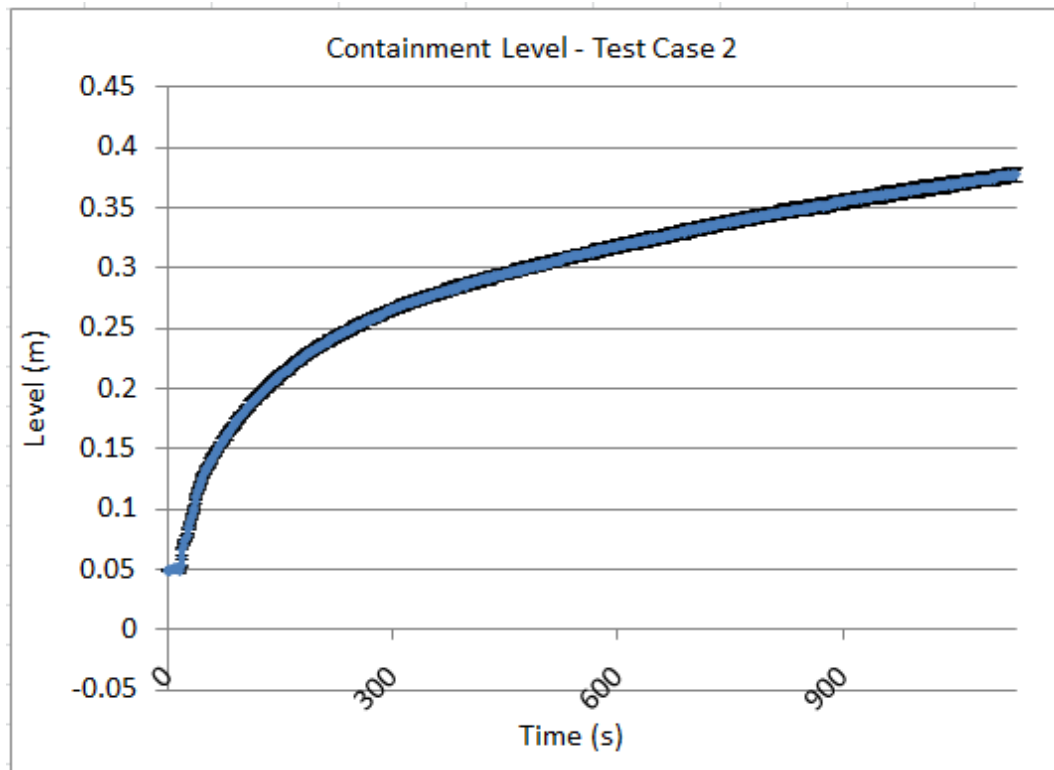


Figure 5.2-11: Test case 2 condensate level measurement.

The amount of condensate collected is similar in magnitude to that of test case one given the difference in time range. The comparison of the condensation will be presented in the next section. The wall temperature rakes for second test case are different from those of the previous case. The HPC was heated prior to this experiment making the starting conditions much higher than test case one. The same instrument failures were present during this test so the middle four temperature rakes will be presented in Figures 5.2-12 through 5.2-15.

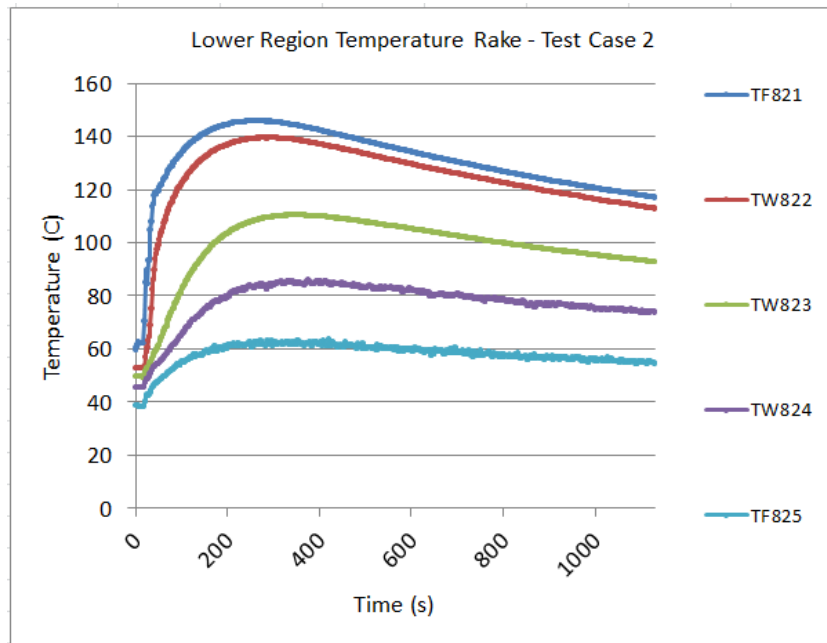


Figure 5.2-12: Thermocouple rake across the HTP for test case 2 at 2.5 (m).

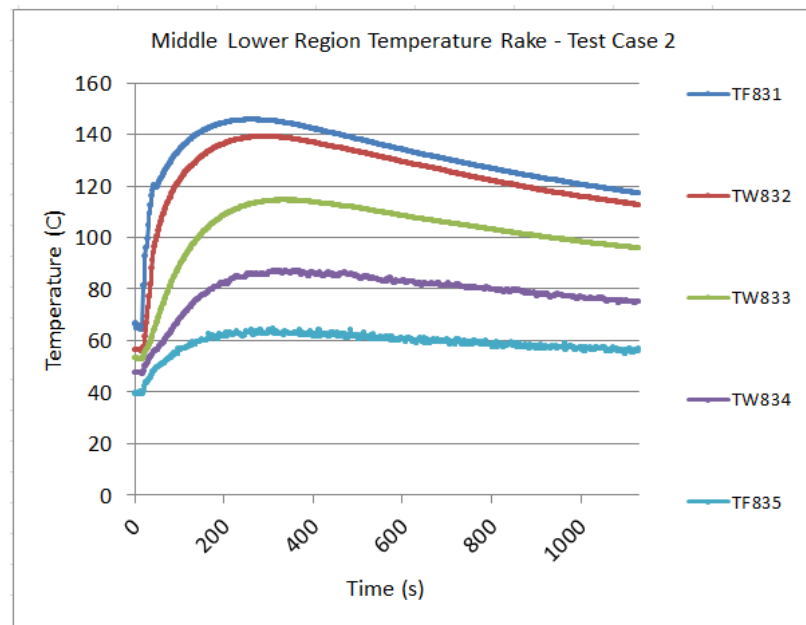


Figure 5.2-13: Thermocouple rake across the HTP for test case 2 at 3.19 (m).

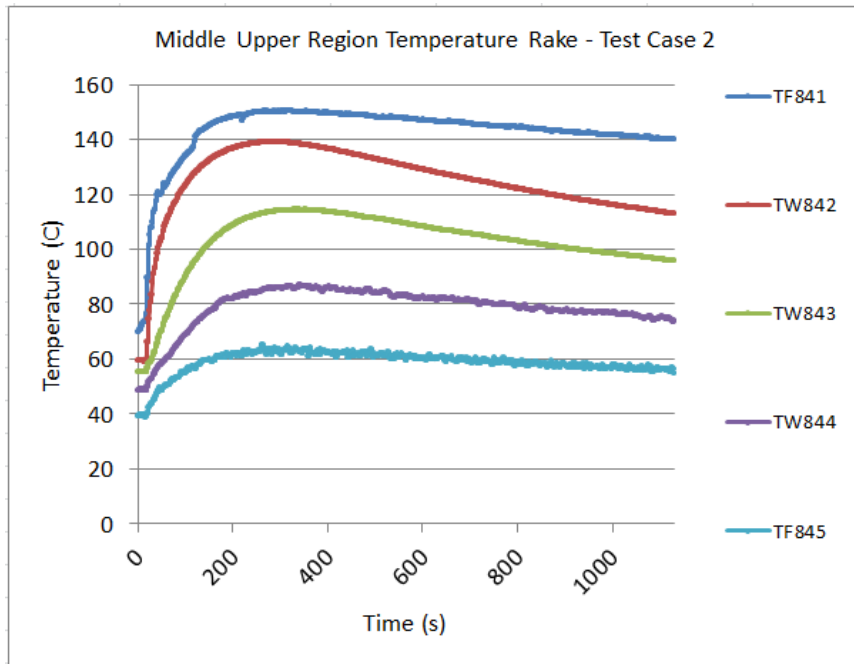


Figure 5.2-14: Thermocouple rake across the HTP for test case 2 at 4.1 (m).

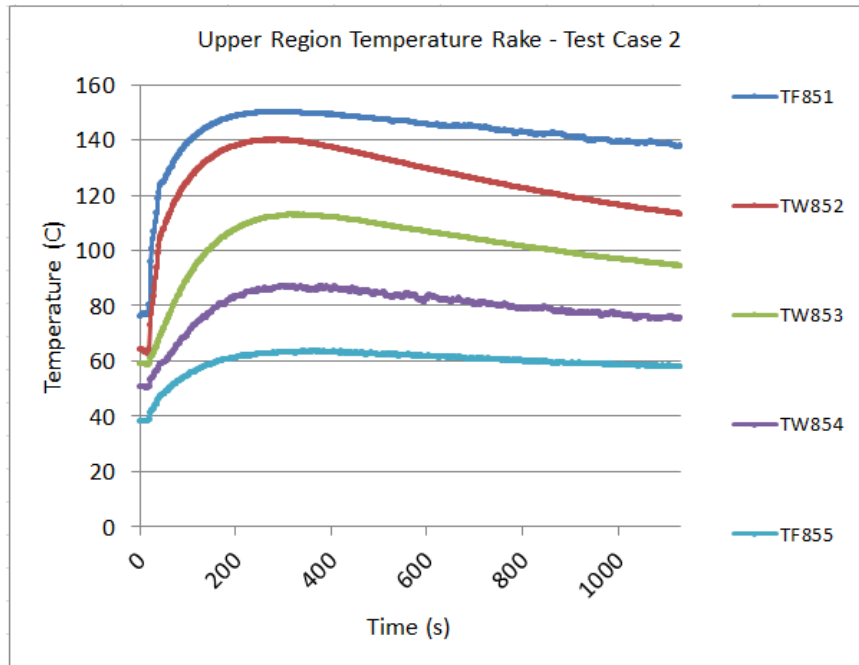


Figure 5.2-15: Thermocouple rake across the HTP for test case 2 at 5.1 (m).

The final data collected from the second test case was the saturation temperature calculated from the volume pressure.

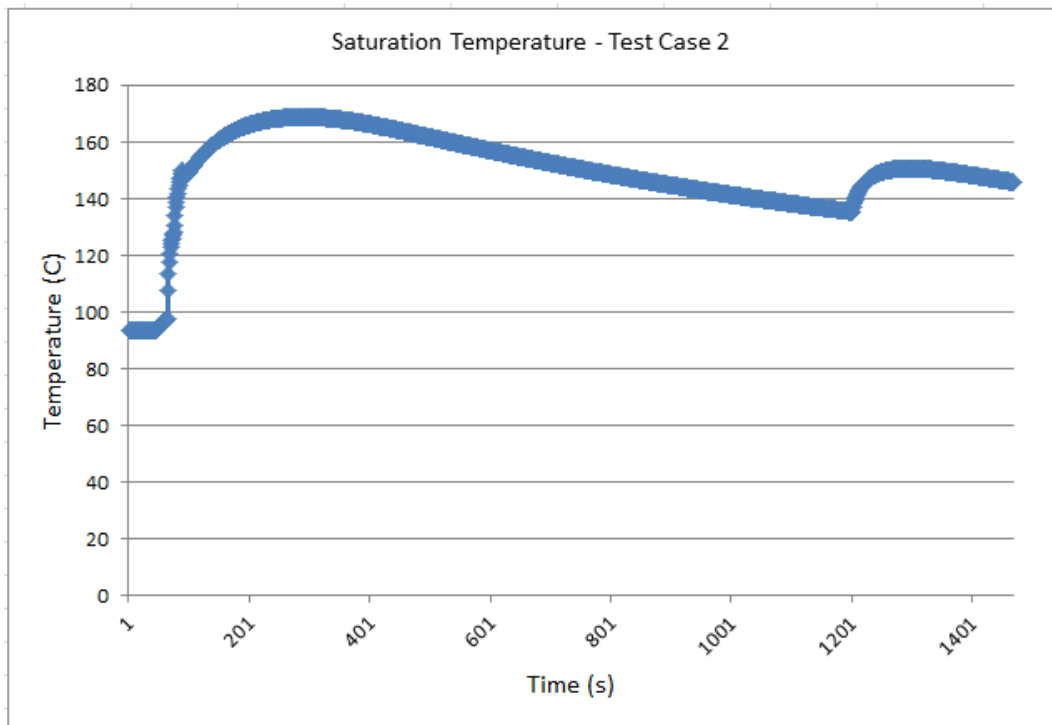


Figure 5.2-16: Saturation temperature in the HPC for test case 2.

## 6 Data Analysis

The analysis of this work as outlined in the previous section will determine the energy dissipated by the HPC vessel during a simulated accident event. To do this the conduction and condensation processes will be determined separately. The conduction heat transfer will be assessed from the transfer plate thermocouple rakes while the level measurements will determine the condensation heat transfer. The convection heat transfer contribution to the performance of the system will be evaluated from the difference of the two processes; though it has been observed to be much smaller in magnitude than the condensation process.

This study's usefulness is dependent on the relationship between the integral test facility and the full-scale reactor design. This relationship has been determined geometrically yet the comparison of the driving temperature differences and the average heat transfer coefficient are as yet quite vague. The condensation heat transfer relationship has been observed to dominate the system's heat removal capability. The condensation HTC of both systems will be reviewed in this chapter to assist in the utilization of the test facility's measurements.

## 6.1 Heat Transfer Characterization

The heat transfer through the HTP was first determined through an evaluation of the temperature gradient present during each experiment. The 1D temperature gradient was calculated from the difference of the two wall thermocouples, one in the HPC wall and one in the CPV wall. The centerline thermocouple was not used in this calculation as it was only used to check conduction linearity. The heat rate data is presented in Figure 6.1-1 and displays the initial rapid spike corresponding with the start of the blowdown event. The four sets of temperature data used are in agreement and verify that an average assessment of the wall heat transfer is possible within 7.5% error.

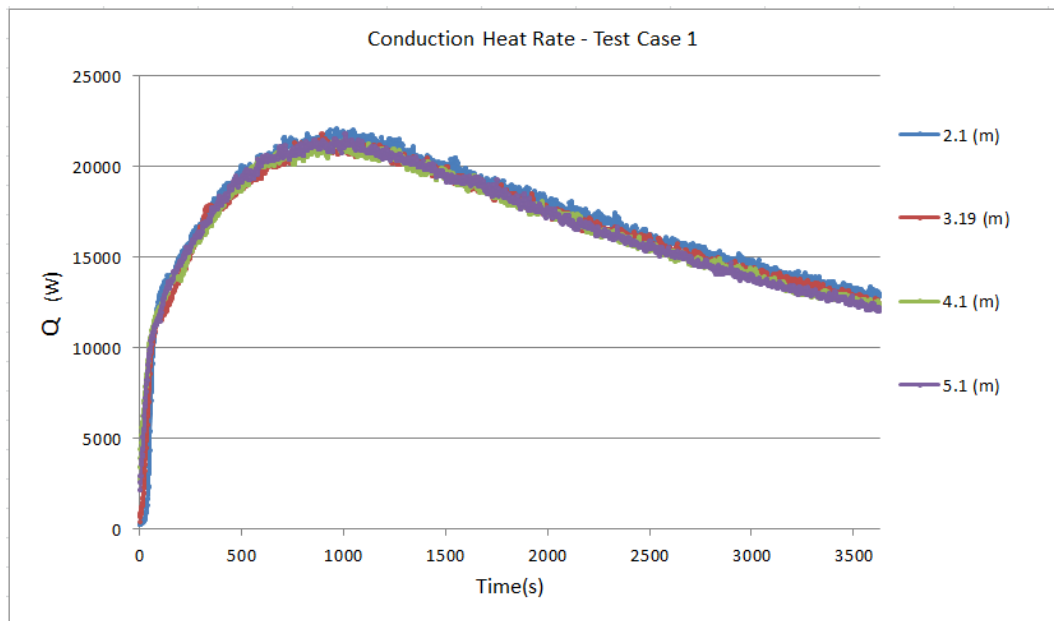


Figure 6.1-1: Conduction heat rate data from experimental data set.

The data shows a nearly linear decline in heat transfer over the course of the 45 minutes of extended cooling. This decline corresponds with the pressure curve

of the HPC system pressure and subsequently the energy addition from the primary vessel. The end of the experiment can be seen in the sudden jump near the end of the data which was due to the opening of the upper relief valve to atmosphere. The next set of data (Figure 6.1-2) shows a much different structure however due to the state of the upper relief valve remaining in the open position for the duration of the experiment. Furthermore the termination of the test is indicated by a second sharp peak corresponding to the opening of the second ADS line from the primary. The region of interest again shows a strongly linear form.

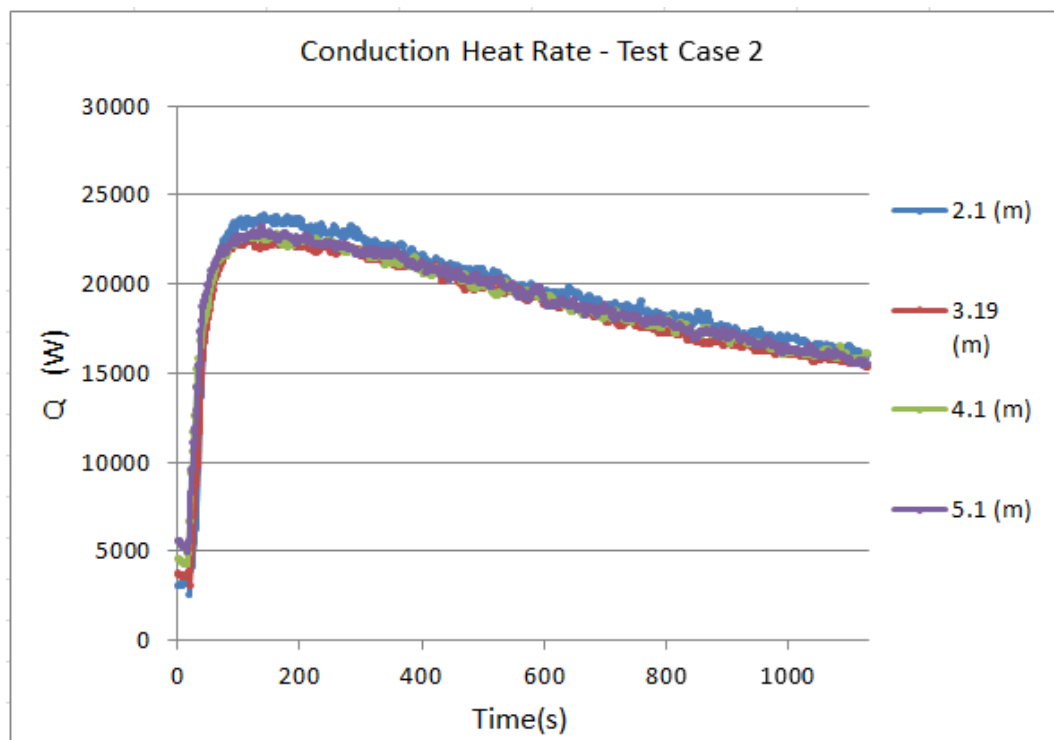


Figure 6.1-2: Conduction heat rate data from the second experimental data set.

The conduction data will provide a measure of the total heat exiting the HPC and in doing so the total heat removed from the RPV steam. The portion of that heat

removed through condensation is measurable via the level indication at the bottom of the HPC vessel as presented earlier. The condensation heat rate is proportional to the mass flow rate along the condensation surface, (HTP). This flow rate was derived from the differential change in level reading in the vessel. The experimental data was smooth over large time references but from point to point there were large discrepancies in the readings derived from system error and signal noise. A moving average would address this factor by decreasing the discontinuities between individual points but carries with it a reduction in usable data points. Additionally, the error propagation of even a three point moving average is over seven percent due to the large error introduced with the instrumentation. A numerical differentiation technique would introduce further error to the differential level values. This method was pursued and executed in this work yet the results produced error over 10 % and so inaccurately represented the mass flow rate that the method was abandoned.

To accurately obtain the mass flow rate within the limits of error already presented in this work the data was precisely fitted with both high-order polynomials and logarithmic functions which could in turn be simply differentiated. The variation between the experimental data and the fit functions was less than 1.5 % for the entire range of the data save the initial few minutes of tumultuous depressurization which is not under scrutiny here. The fit functions used to describe the experimental data are illustrated in figures 6.2-3 and 6.1-4.

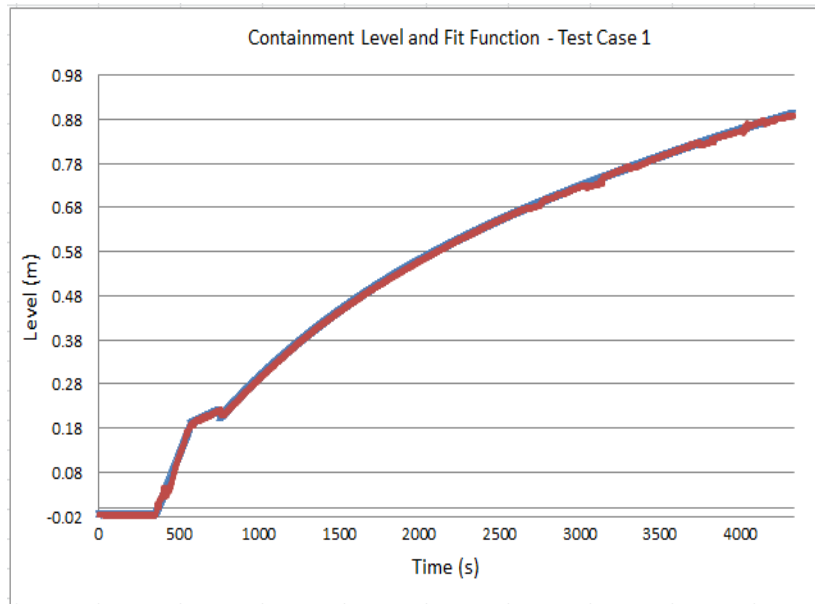


Figure 6.1-3: Containment level measurement and fit function for test case 1.

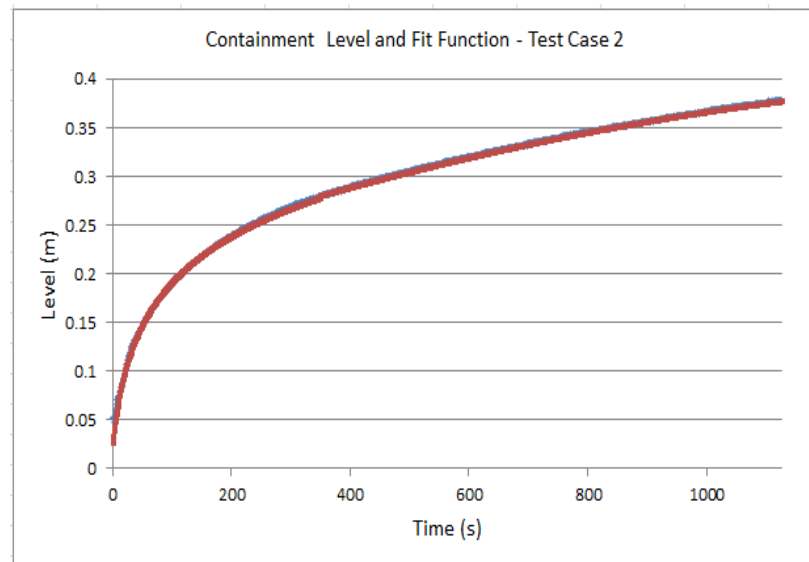


Figure 6.1-4: Containment level measurement and fit function for test case 2. (Time span adjusted to fit the blowdown)

The fit lines were analytically derived to obtain the rate of change of the condensate level. The resulting differential height of condensate was combined with a temperature dependent density as well as the cross-sectional area to calculate the mass flow rate. This mass flow rate corresponds to the mass flow of vapor changing state into fluid at the boundary layer interface. Finally, the enthalpy of evaporation was calculated from IAPWS IF-97 steam tables and used to obtain a time dependent heat rate of condensation for the incoming vapor. The condensation heat transfer produced in the first experiment was indicative of high pressure steam rapidly flashing initially into fluid across the entire volume of the HPC and concurrently condensing along the entire interior surface of the vessel. Figure 6.1-5 shows the heat rate graph for the condensation process in the first experiment.

It is important to recall that the first two regions were modeled with a form fit function prior to being derived which has greatly smoothed out the curve. The discontinuities are however representative of actual processes in the facility. The scale of the first region is 5-6 times the magnitude of the greatest conduction heat rate observed through the test which corresponds to the heating up period of the entire surface area of the vessel. The flashing process combined with unheated walls, i.e. the entire vessel surface area to condense on, removes a remarkable amount of energy initially from the RPV. The sharp increase in pressure carries with it the saturation temperature though, which rises more rapidly than the incident steam can heat the walls. The second region ceases wall condensation over nearly the entire vessel. The pressure increase slows while the walls are continually heated however, restoring wall condensation and leading to the third region.

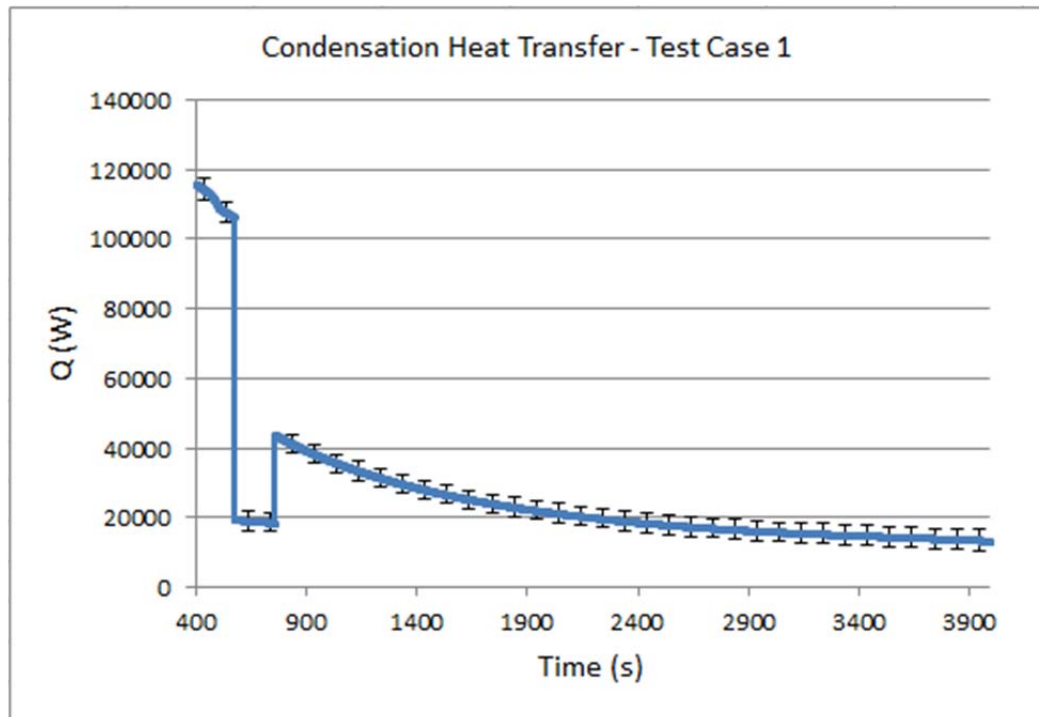


Figure 6.1-5: Condensation heat rate for the first test case. The three regions are the initial blowdown phase, the over-heated wall transition, and the extended condensation region.

The pressure peak for reference occurs at approximately 1300 (s) which corresponds with the peak temperature of the walls. What occurs after this point is of interest in this study. Once the vessel reaches its maximum temperature the heat transfer plate gradually becomes the primary mechanism for heat removal, though this process is not as rapid as originally thought. Figure 6-1.6 illustrates the condensation (red) and conduction (green) heat transfers across the span of the third region. While the pressure has not reached its maximum the condensation rate is rapidly decreasing to meet the conduction

heat rate. This calculation of the red curve attributes the condensate mass flow to only the HTP area which multiplies the actual heat rate by up to a factor of 5.

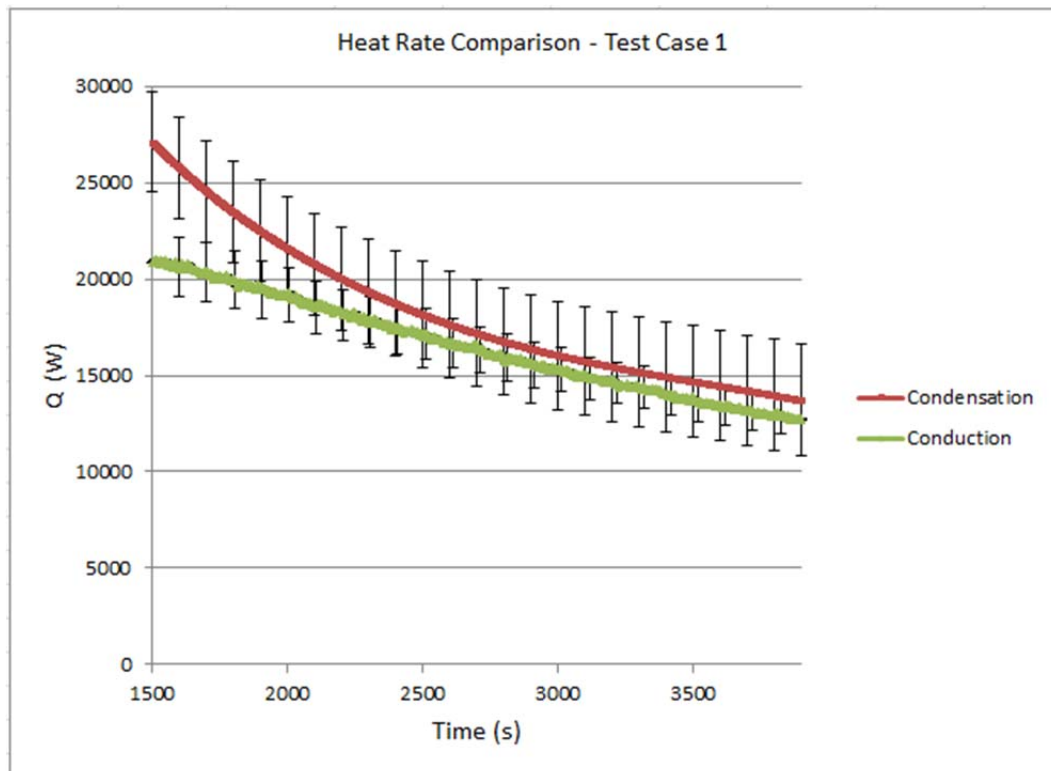


Figure 6.1-6: Conduction-convection heat flow comparison for test case 1.

It's clear that in the pressurized case the condensation accounts for nearly the entirety of the heat transfer. The convection current developed from the steam inlet point are not sufficient enough to generate a large portion of heat removal. The convection heat transfer in this region is thus assumed to be negligible for the region after the pressure peak. The condensation HTC was determined from the heat rate data using the temperature difference between the average of the film thermocouple readings and the saturation temperature of the vessel. Figure

6.1-7 shows the HTC for the entirety of the experimental data. The first and second regions however are not applicable for previously discussed reasons.

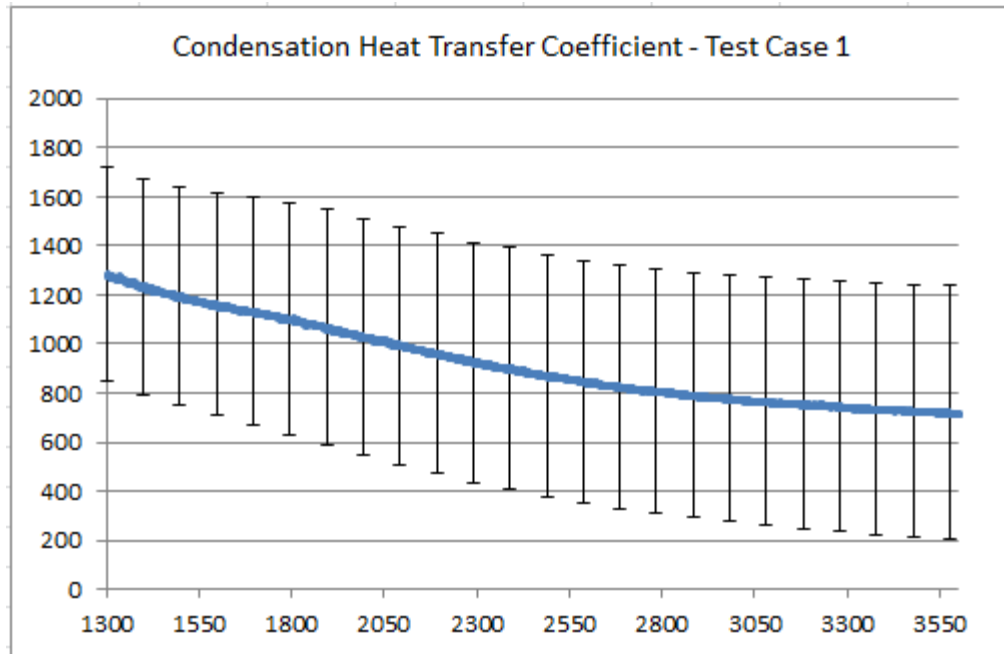


Figure 6.1-7: Condensation heat transfer coefficient calculated from test case 1 experimental data.

The HTC over the region of applicability is fairly constant as expected with the initially high value still showing signs of system warm-up. As this effect lessens the HTC levels out to a value of approximately 1490 W/m<sup>2</sup> K. With respect to temperature difference between the condensate film the HTC displays a more distinct constant trend which is shown in Figure 6.1-8.

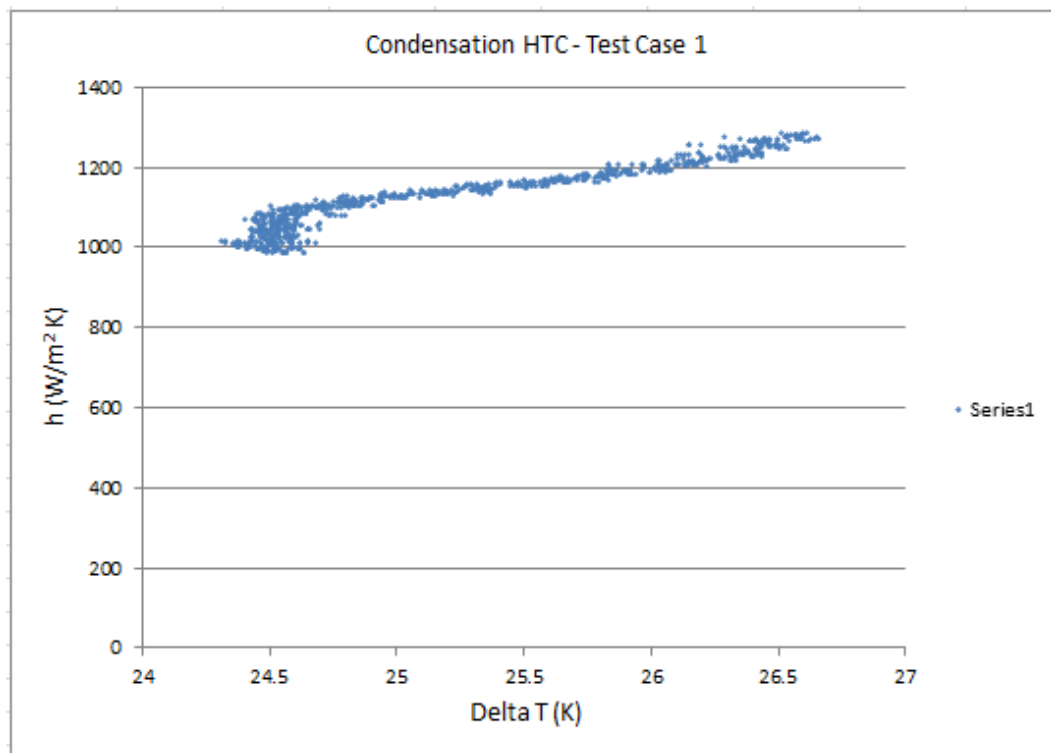


Figure 6.1-8: Condensation heat transfer coefficient vs. temperature difference for test case 1.

The region with the greatest HTC in the experiment was in fact during the portion with the lowest temperature difference near the end of the experiment. The final 15 minutes of the 38 minutes accounted for all of the readings below a 14 degree difference. To compare the results of this experiment with data from the literature the next plot compares the formula developed by Dehbi, et al. (18) and to the Uchida data as correlated by Corradini (29). In order to properly compare the heat transfer coefficient, the air/vapor mass ratio is required. Due to the lack of instrumentation in the test facility the vapor temperature must be estimated.

This estimation is done through the assumption that at the critical point of the temperature transient the vapor temperature is equal to the insulated wall temperature of the containment vessel. Knowing this, the air/steam mass ratio may be calculated for this point only and then will be assumed to be constant throughout the experiment. The same value, 0.25, is used in all three data sets shown.

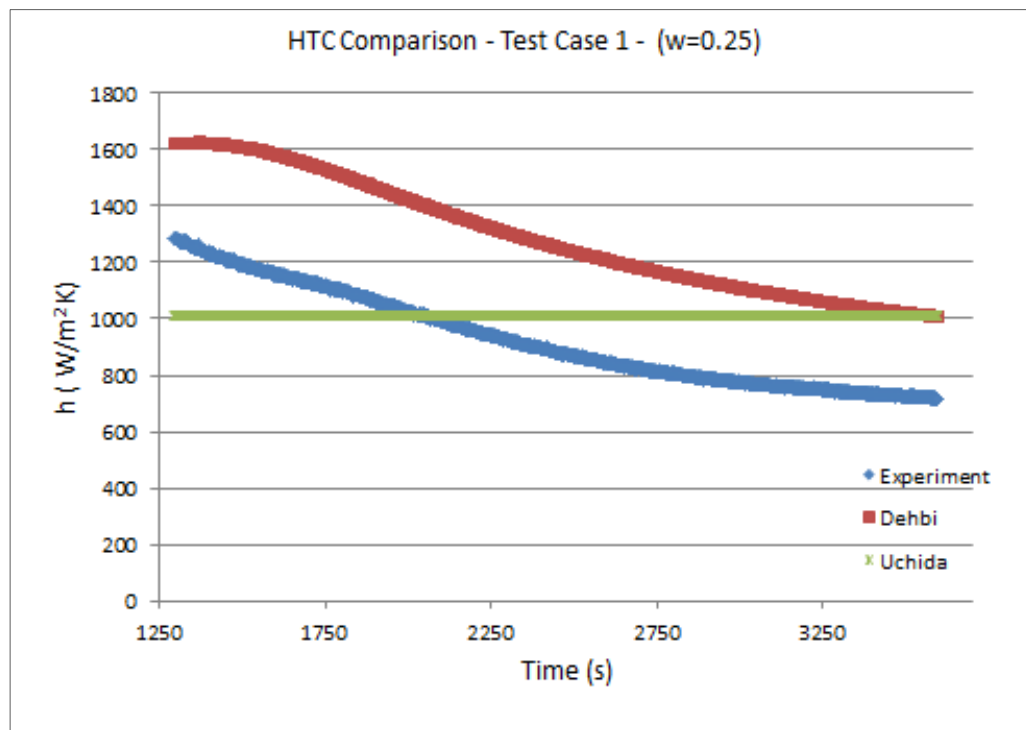


Figure 6.1-9: Comparison of the calculated condensation HTC to the formulated correlation, eq. 2.2 (18) and the Uchida model, (25).

While the two curves do not follow the exact shape the range is acceptably close. The discrepancy is due to the difference in measurement methods of the bulk steam temperature between this work and that of the cited work. Temperature readings for the bulk steam temperature were taken at each elevation along the vertical wall and then averaged in the work leading up to the correlation, where in this work the saturation temperature was used for lack of the proper instrumentation. This reasoning is supported by the final region of the data where the two begin to meet as the bulk steam temperature truly does approach the saturation temperature. Prior to this region, the steam is superheated which makes the temperature difference used in the Dehbi formula smaller than it is in experiment and the HTC subsequently larger. The smaller temperature difference affects the experimental data as well by decreasing the calculated heat transfer coefficient.

The second experimental set of data incorporated both mass transfers to and from the containment system as well as convection currents along the HTP. This experiment also occurred over a much shorter time period though the maximum pressure attained in the HPC was greater in the second set of data. The data set does not follow the same dynamics, i.e. near-pure condensation under vacuum conditions, as the first but does provide a second measure of the containment performance and will be discussed here. Figures 6.1-10 and Figure 6.1-11 display the condensation heat rate for the second experimental data set and the condensation HTC for the same, respectively.

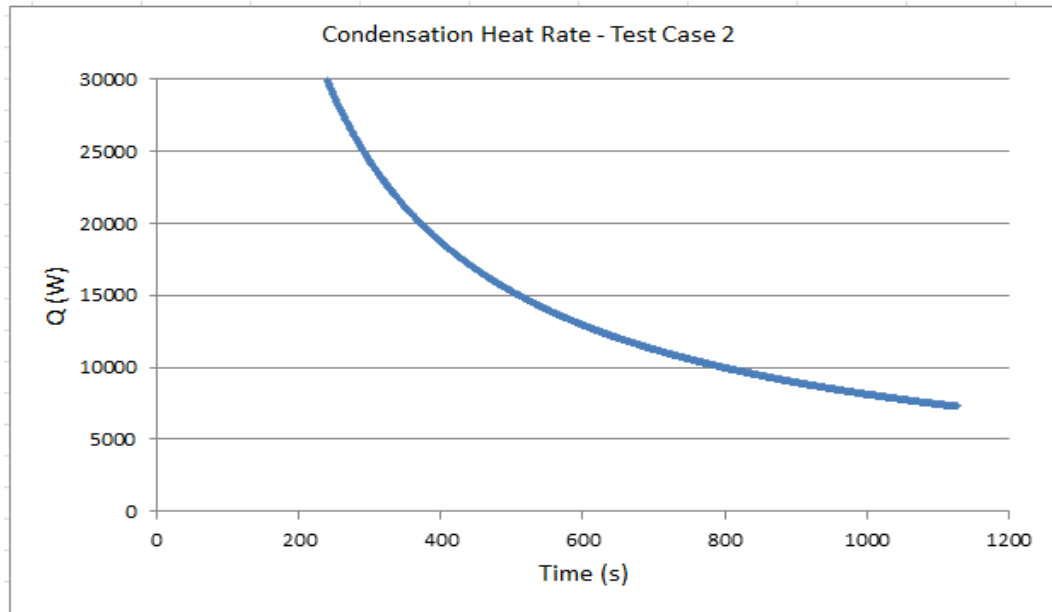


Figure 6.1-10: Calculated condensation heat rate from the second experimental data set.

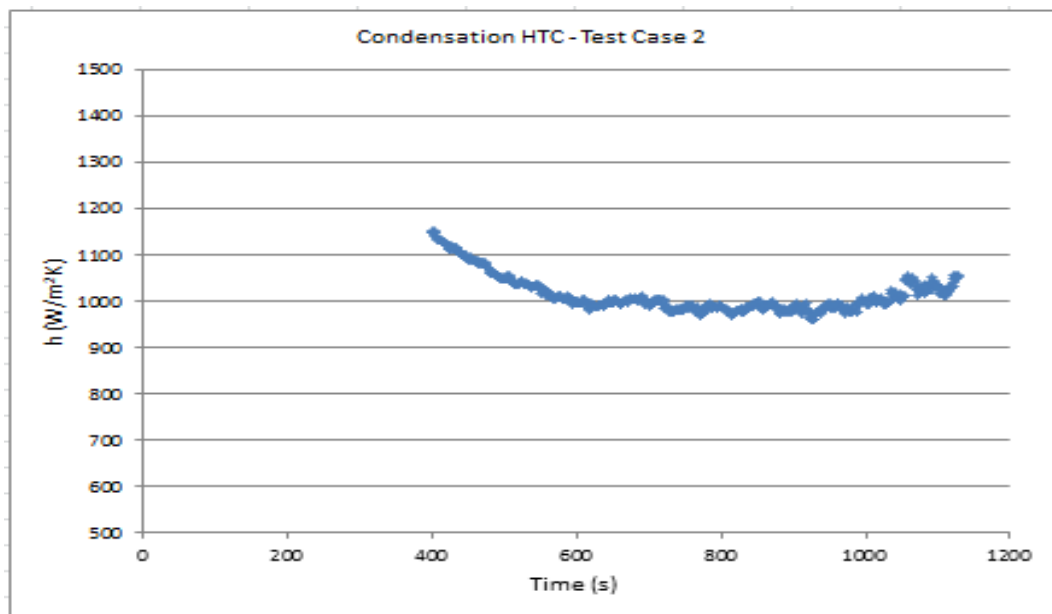


Figure 6.1-11: Calculated condensation HTC for the second test case.

The magnitude of both the HTC and the heat rate in this instance is substantially larger due to the changed in test parameters. The walls of the containment vessel were heated prior to this blowdown which removes the influence of extraneous condensation on surfaces other than the HTP to a large degree. The shifting conditions during an event however are shown here to be exceptionally varied making it difficult to concentrate the condensation on one single surface. The condensation heat rate data did not show the marked discontinuity of the previous experiment as the wall temperature never exceeded the saturation temperature and condensation was not interrupted. After a period from the maximum pressure point (390 s) the HTC does settle to a constant value in this experiment of 1000 (W / m<sup>2</sup> K). The final region again shows a slight increase due to the discrepancy in bulk steam temperature measurement.

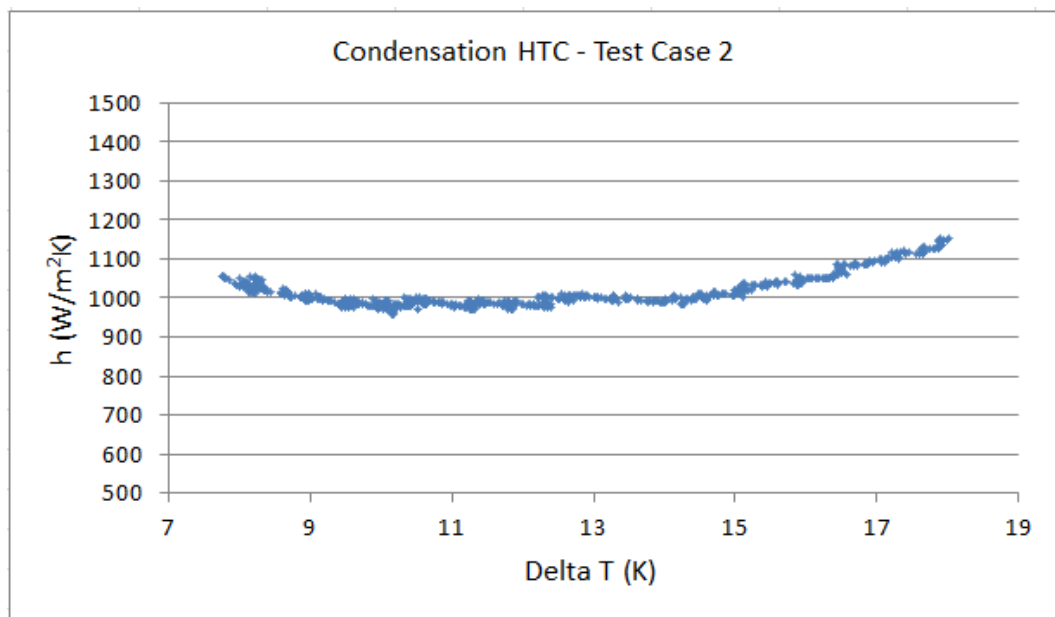


Figure 6.1-12: Condensation HTC for test case 2 vs. temperature difference.

Aside from the qualitative results from this study the facility itself was found to be lacking in the proper capabilities to acquire a complete data set for this area of research. At the time of the stated experiments, the containment vessel was not equipped with a vapor temperature measurement device. A single instrument has since been installed in the upper region of the vessel however the quality of future analyses would be greatly improved by the addition of several vapor temperature instruments along the entire height of the HPC.

These thermocouples would be placed 10-15 cm from the condensation surface to properly evaluate both the condensation and the film heat transfer occurring at each elevation as well as the vertical stratification of the steam vapor. The air-vapor mass ratio is also strongly dependent on temperature. Inaccurate estimations of this property have a strong impact on the average heat transfer coefficient calculation. The temperature variation along the entire length of the HTP wall surface is minimal except for the highest and lowest meter. These regions would benefit the most from further inspection.

Additionally, the condensate pool temperature in the bottom of the HPC is unmeasured currently. The conduction-convection heat transfer occurring between the condensate pool and the lowest portion of the HTP during long experimental testing would significantly affect the total heat removal capability of the system. The density of the condensate would also directly depend on these temperature readings as the change in condensate height is more dependent on the temperature of the entire volume than that of the relatively lower mass and high heat incoming fluid. This measurement could be taken at 1 - 3 points along the centerline of the lower region of the HPC.

The last instrumentation correction would entail the addition of bulk fluid measurements to the cooling pool volume and rigorous verification of the digital conversion modules used in temperature measurement. The manufacturer error bounding of the input-output modules of the thermocouples was found in this work to be insufficient for this analysis. The scaling report addresses the lumped capacitance method of evaluating the thermal response of the cooling pool fluid to preserve similitude. Currently, the facility is not capable of verifying this portion of the system response.

## **6.2 *Condensation Scaling Analysis***

The concern that the condensation heat transfer demonstrated by the MASLWR facility HPC will not conservatively reflect the full scale facility performance is reviewed here. The effect of the 1:3.1 lengths scaling of the containment structure has been evaluated on the condensate film flow and heat transfer. This scaling factor is shown to be of the greatest importance to the relation between experimental and prototypical heat transfer. The effect of the scaling on the Reynolds number of the condensate film is shown to increase the condensation HTC. The results of the condensation heat transfer analysis may then be assumed to be conservatively accurate assessments of the prototypical conditions.

The facility scaling report (29) outlines the geometrical parameters of the test facility containment required to define the relationship to the prototype reactor. The containment geometrical parameters were developed to preserve the isochronicity of the two systems, the temperature response of the cooling pool and finally the fluid property similitude of the containment inventory. The geometrical scaling parameters are summarized in the following tables:

Table 6.2-1: Summary of MASLWR test facility geometric parameters (29).

Parameter Values	Model	Prototype	Units
Containment Wall Thickness	3.81	3.81	cm
Containment Active Heat Transfer Area	0.951	242.2	m <sup>2</sup>
Containment Volume	0.523	133.37	m <sup>3</sup>
Cooling Pool Volume	3.17	808.3	m <sup>3</sup>

Table 6.2-2: Summary of parameter scaling ratios (29).

Scaling Ratio	Ratio
Length Ratio	1:3.09
Cross-sectional Area Ratio	1:82.2
Volume Ratio	1:254.7
Time Ratio	1:1
Power Ratio	1:254.7
Active Heat Transfer Area Ratio	1:254.7
Active Heat Transfer Wall Thickness Ratio	1:1

The length ratio of 1:3.09 will be shown to primarily determine the Reynolds number scaling in this section. This effect of this scaling on the Reynolds number will also be illustrated for the first test case. In order to quantify the condensation relationship based on the scaling relationship, the equation 5.6 will be used to equate the dimensional dependence.

$$q_{condensation} = A \cdot \dot{m}_{cond} \cdot \Delta h_{fg} \quad (\text{eq. 5.6})$$

As shown in the following figure the condensation mass flow is equal to the rate of mass leaving the condensate wall layer.

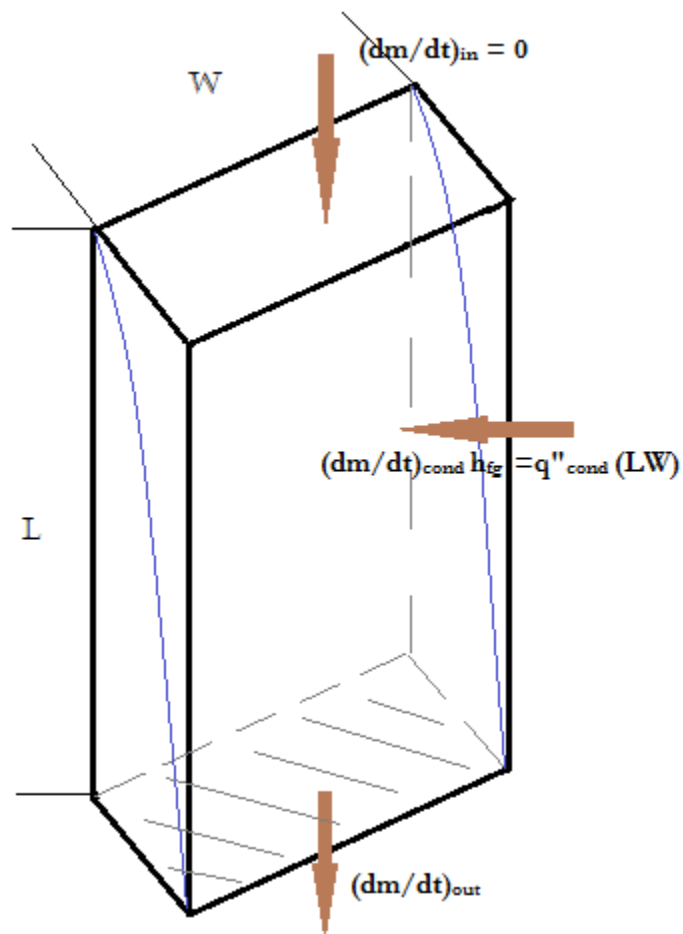


Figure 6.2-1: Condensate mass transfer diagram displaying film heat transfer.

The condensate mass flow entering the film at the vapor-film interface must equal the mass flow leaving the bottom control surface. This flow may be described in terms of the film parameters,

$$\dot{m}_{condensation} = \dot{m}_{out} = (\delta_{film} \cdot W) \cdot \rho \cdot V_{film} \quad (\text{eq. 6.1})$$

Where  $V_{film}$  is the velocity of the film along the heat transfer surface.

The density of the condensate film is dictated by the temperature at which the process is undertaken. The facility scaling has taken this parameter into account via temperature and property similarity has been ensured. The film thickness however is a function of height along the HTP. As the condensate collects on the plate the film develops from top to bottom, increasing with distance. Additionally, the film velocity increases in a similar manner to that of the film thickness.

Scaling the two of these parameters directly would require a complete understanding of the condensation rate as a function of height. As this is not possible with the data collected in experiments conducted on this facility an value of the product of these two parameters has been characterized. Note that the width of the plate drops out of these equations in the process.

Substituting back into equation 5.6 and solving for the mass flow rate,

$$\dot{m}_{out} = \left( \frac{q''_{cond}}{\Delta h_{fg}} \right) \cdot (L \cdot W) \quad (\text{eq. 6.2})$$

$$(\delta_{film} \cdot W) \cdot V_{film} = \left( \frac{q''_{cond}}{\Delta h_{fg} \cdot \rho} \right) \cdot (L \cdot W) \quad (\text{eq. 6.3})$$

$$(\delta_{film} \cdot V_{film}) = \left( \frac{q''_{cond}}{\Delta h_{fg} \cdot \rho} \right) \cdot L \quad (\text{eq. 6.4})$$

The condensate film thickness present in the test facility will not represent that of the full scale design due to the length scaling of the HTP wall. Taking just the length of the plate into account and picturing only a 3 times height prototype, this dimension would thicken due to the increase in mass flowing along the surface. Similarly, the velocity of the same fluid would also increase accordingly.

In order to describe the scale relationship of these parameters the right hand side is examined.

The temperature difference observed in the containment during these experiments has been scaled to match that expected in the design prototype to preserve property similitude of the steam and condensate (29). The condensation heat flux term, being independent of the area, is also representative of the same full scale facility phenomena. Thus, eq. 6.3 may be applied to both scales and compared:

$$\frac{\left[ (\delta_{film} \cdot V_{film}) = \left( \frac{q''_{cond}}{\Delta h_{fg} \cdot \rho} \right) \cdot L \right]_{model}}{\left[ (\delta_{film} \cdot V_{film}) = \left( \frac{q''_{cond}}{\Delta h_{fg} \cdot \rho} \right) \cdot L \right]_{prototype}} = \gamma \quad (\text{eq. 6.5})$$

$$\frac{[(\delta_{film} \cdot V_{film}) = (1) \cdot L]_{model}}{[(\delta_{film} \cdot V_{film}) = (1) \cdot L]_{prototype}} = \gamma \quad (\text{eq. 6.6})$$

$$(\delta_{film} \cdot V_{film})_R = (L)_R \quad (\text{eq. 6.7})$$

This conclusion equates the ratio of products of the film thicknesses and the velocities to the length ratio of the facility scaling. This comparison can be quantified from the length ratio value given in table 6.2-2 of 1:3.09.

$$(\delta_{film} \cdot V_{film})_R = \frac{1}{3.09} \quad (\text{eq. 6.8})$$

The Reynolds number is directly dependent on this term. The quantification of that dependence will dictate the fluid characteristics and heat transfer

properties of the condensate. The Reynolds number for a fluid on a flat vertical surface employs a hydraulic diameter and is equated below.

$$Re_{\delta} = \frac{4 \cdot \rho \cdot (\delta_{film} \cdot V_{film})}{\mu_{film}} \quad (\text{eq. 6.9})$$

As we have already established property similarity, we may take the ratio of the model and prototype Reynolds numbers to quantify their relationship,

$$(Re_{\delta})_R = (\delta_{film} \cdot V_{film})_R = \frac{1}{3.09} \quad (\text{eq. 6.10})$$

Where  $(Re_{\delta})_R$  is the ratio of test facility to prototype properties.

Since the Reynolds number relationship is directly dependent on the length scaling parameter of the facility containment, the relationship between the two scales can be explicitly characterized. This is done through the use of experimental relationships produced in prior work by Labuntsov (32). This work directly related the film heat transfer coefficient as a function of both Prandtl and Reynolds numbers from experimental data.

The conditions experienced during experimentation in the test facility are at the lower boundary of the applicability of this correlation ( $Re_{\delta} \sim 1800$ ) and may require analysis under transition region relations (31) for low-pressure blowdown scenarios as in the data presented in this work. However, under full operating conditions, extended blowdowns should maintain turbulent conditions in the condensate film for the majority of the tests. It should though be noted that the effect of this discrepancy would be to lower the observed heat transfer

coefficient in the facility, preserving conservatism of the experimental results previously reported. The Labuntsov correlation is presented below:

$$\frac{\bar{h}_L(v^2/g)^{1/3}}{k_l} = \frac{Re_\delta}{8750 + 58 \cdot Pr^{-0.5} \cdot (Re_\delta^{0.75} - 253)} \quad (\text{eq.6.11})$$

The correlation was used to predict the ratio of model to prototype average heat transfer coefficient over an applicable region of the Reynolds number. The Prandtl number for these experiments is that of liquid water under the test conditions and is very nearly equal to unity. A constant value of the Prandtl number at this value was used in the calculation. Since we know the relationship of the Reynolds number between the two facilities, the equation was used first to calculate the left hand side for a set of Reynolds numbers. Next, it was used on the same set scaled by the length parameter. The two results were compared and plotted against the experimental Reynolds number set.

Table 6.2-3: Condensate film Reynolds number observations, predictions and plotted region.

Reynolds Number Values	Lower Limit	Upper Limit
Model Observations	800	2200
Prototype Prediction	2400	6600
Plotted Region	1000	5000

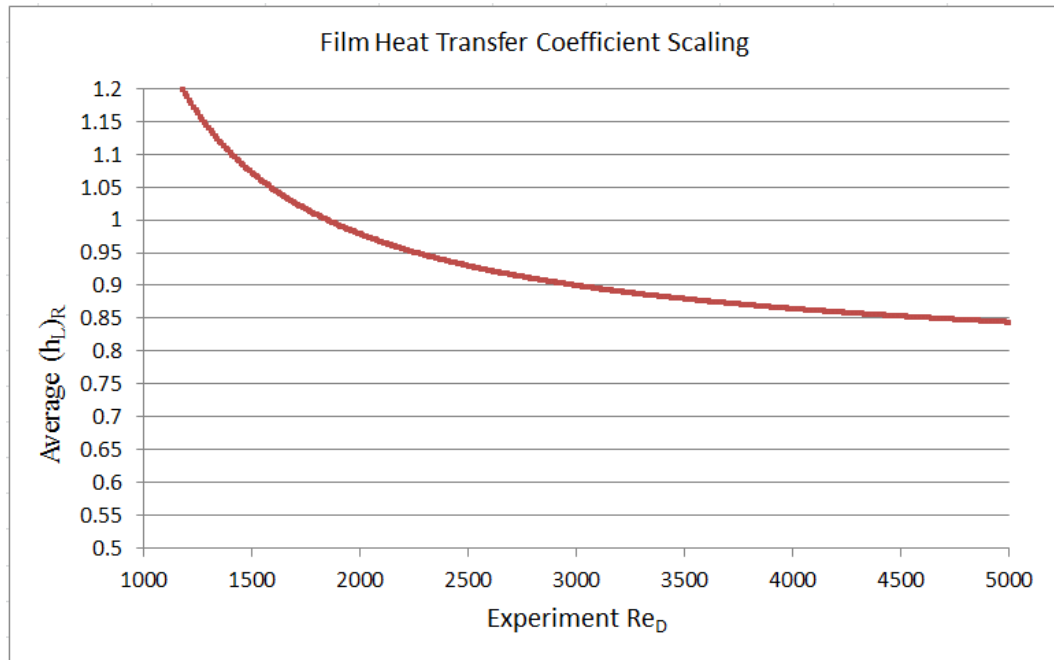


Figure 6.2-2: Calculated film heat transfer coefficient scaling ratio.

The observed region in experimentation spanned a portion of the transition region up to lower turbulent numbers. These observations however were not from full pressure or temperature initial conditions. In future tests utilizing the full capacity of the facility these parameters will increase. The condensation rate will likewise increase and subsequently the Reynolds number will rise fully into the turbulent region.

The comparison plot shows that the average HTC is nearly equal in value at the experimental value turbulent boundary for the two containment scales. At higher Reynolds numbers in the experimental facility the ratio of model to prototype parameters diverges from equality. The expected prototype HTC increases more rapidly than the experimental HTC. The divergence is rapid at first but settles at very high Reynolds number to a value of 0.8.

## **7 Conclusions and Future Work**

### **7.1 *Research Conclusions***

The results of this study have shown that the MASLWR test facility containment structure is capable of removing heat from the primary at exceptional rates. Despite the removal of two additional experiments due to system repairs, funding and ongoing commercial dedication effort, two integral system experiments have been produced under different conditions. The effect of pressurization on condensation has been illustrated and the condensation heat transfer coefficient has been characterized. Furthermore, the experimental data has been compared to academic standards. The facility itself has also been evaluated for the purpose of obtaining quality data for this type of research and several improvements have been recommended.

The correlation used to evaluate the experimental data predicted a much higher heat transfer coefficient than obtained. It is important to note that the experimental parameter in question was estimated conservatively given the data collection capabilities of the facility at the time. These results would likely converge given both a series of containment vapor temperature readings and an improvement to the instrumentation accuracy. The discrepancies between the Dehbi experiments and this study were present largely due to this measurement inaccuracy and an inability to accurately evaluate the air-vapor mass ratio.

The most important result of this study has been the assessment of the data produced from the containment system in relation to the prototypical system performance. The film heat transfer ratio between the model and prototype has been proven to be less than one. Reynolds numbers in this study were

calculated to span the transition region and into the turbulent region. It is important to note however that these experiments were not at full primary pressure. The pressure limitations of the current containment restrict the intensity of testing at this time. The applicability of the reasoning used to obtain the experimental film heat transfer coefficient ratio is weak over the region displayed in this data of this study. Normally addressed conditions, even with the current facility, are at much higher pressures and under purely turbulent wall conditions making this reasoning very sound.

In general, the results gathered during future testing may be considered conservative estimates of the full scale facility performance due to the film heat transfer coefficient relationship. That relationship is dependent on the length scaling's effect increasing the Reynolds number of the condensate film in the prototypical containment vessel and independent of the additional area scaling required by the scaling analysis. This one parameter dependence directly relates the test data in a conservative manner to the full scale design. Additionally, the similarity parameters preserved in the construction of this containment are sufficient to ensure the model-prototype relationship is understood and should be maintained in the next model containment. Finally, it is important to note that the convection heat transfer that was expected to account for a significant portion of the HPC heat transfer was insignificant in the closed system test. This finding should allow researchers to assume that the condensation rate measured through liquid level is representative of the total system heat transfer provided the condensation area is quantifiable, i.e. restricted to the HTP.

## **7.2 Future Work**

In order to fully understand the full scale facility performance these tests should be run from full primary operating pressure. This will simulate the containment response most accurately and will show how high the condensation rate can reach. In addition, pre-heating of the containment walls should be done for all tests. Even heating the walls to 100 °C is sufficient to dramatically reduce the condensation area transient. Assuming future tests will have proper vapor temperature instrumentation the conduction transient will not restrict the region of applicability of this method as stringently.

The condensation heat transfer quantified in this analysis was lacking in depth due to a low amount of sample data sets. Only two tests were conducted successfully and did not have comparable test conditions. The single most useful improvement to this study would be to increase this sample data set size. This may be done on the new containment structure currently planned or on the current facility at higher primary pressure initial conditions. A large sample size of experimental data will be required for the benchmarking efforts planned in the design of this reactor.

Furthermore, accurate readings of the vapor temperature and air-mass ratio will improve the findings of this work immensely and should be included in all future experiments. The addition of comprehensive vapor temperature instrumentation will directly affect the calculation of condensation heat transfer via the temperature difference between wall and vapor. The air-mass ratio will also be defined by these measurements. Future studies should not neglect this contribution to the facility performance.

## Bibliography

1. Nusselt, W.A., The Surface Condensation of Water Vapor, *Zeitschrift Ver. Deut. Ing.* 60, 1916, 541-546.
2. Bromley, L.A., Effect of Heat Capacity of Condensate. *Industrial and Engineering Chemistry.* 44, 1952, 2966.
3. Seban, R.A., Remarks on Film Condensation with Turbulent Flow. *Transactions of ASME.* 76, 1954, 299.
4. Sparrow, E.M., J.L. Gregg, Laminar Condensation Heat Transfer on a Horizontal Cylinder. *ASME Journal of Heat Transfer.* 81, 1959, 13-18.
5. Gerstmann, J., P. Griffith, Laminar Condensation on the Underside of Horizontal and Inclined Surfaces. *International Journal of Heat and Mass Transfer.* 10, 1967, 567-680.
6. Mayhew, Y.R., J.K. Aggarwal, Laminar Film Condensation with Vapor Drag on a Flat Surface. *International Journal of Heat and Mass Transfer.* 16, 1973, 1944-1949.
7. Goodykoontz, J.H., R.G. Dosch, Local Heat Transfer Coefficients for Condensation of Steam in Vertical Down Flow within a 5/8 Inch Tube. National Aeronautics and Space Agency, 1966. NASA TN D-3326.
8. Asano, K., Y. Nakano, Forced Convection Film Condensation of Vapors in the Presence of Non-condensable Gas on a Small Vertical Flat Plate. *Journal of Chemical Engineering of Japan.* 1978.
9. Rose, J.W., Approximate Equations for Forced-Convection Condensation in the Presence of a Noncondensing Gas on a Flat Plate and Horizontal Tube. *International Journal of Heat and Mass Transfer.* 23, 1980, 539-546.
10. Kutsuna, H., K. Inoue, S. Nakanishi, Filmwise Condensation of Vapor Containing Non-condensable Gas in a Horizontal Duct. *International Symposium on Heat Transfer, Beijing.* 1968.
11. Mori, Y., Y. Uchida, Forced Convective Heat Transfer between Horizontal Flat Plates. *International Journal of Heat and Mass Transfer.* 9, 1966, 803-807.

12. Elafify, M.M., M.L. Corradini, Condensation of Vapor in the Presence of a Noncondensable Gas at Low Pressures. *Nuclear Engineering and Design*. 121, 1990, 103-111.
13. Bannwart, A.C., A. Bontemps, Condensation of a Vapour with Incondensables: An Improved Gas Phase Film Model Accounting for the Effect of Mass Transfer on Film Thickness. *International Journal of Heat and Mass Transfer*. 33, No. 7, 1990, 1465-1474.
14. Legay-Desesquelles, F., B. Prunet-Foch, Dynamic Behaviour of Boundary Layer with Condensation along a Flat Plate: Comparison with Suction. *International Journal of Heat and mass Transfer*. 28, No. 12, 1985, 2363-2370.
15. Slegers, L., R.A. Seban, Laminar Film Condensation of Steam Containing Small Concentrations of Air. *International Journal of Heat and Mass Transfer*. 13, 1970, 1941-1947.
16. Cho, D.C., R.P. Stein, Steam Condensation on the Underside of a Horizontal Surface. *Proceedings of Third International Topical Meeting on Nuclear Power Plant Thermal Hydraulics and Operations*. Nov. 1988.
17. Robinson, J.A., S.R. Windebank, Measurement of Condensation Heat Transfer Coefficients in a Steam Chamber Using a Variable Conductance Heat Pipe. *Proceedings 2<sup>nd</sup> UK National Conference on Heat Transfer*, 1, Sep. 1988, 617-637.
18. Dehbi, A.A., M.W. Golay, M.S. Kazimi, Condensation Experiments in Steam-Air Steam-Air Helium Mixtures under Turbulent Natural Convection. *National Conference of Heat Transfer, AIChE Symposium*. Series 87. 283, 1991, 19-21.
19. Tong, L.S., J. Weisman, *Thermal Analysis of Pressurized Water Reactors Third Edition*. Illinois, American Nuclear Society, 1996. 0-89448-038-3.
20. Modro, S.M., J.E. Fisher, K.D. Weaver et al., *Multi-Application Small Light Water Reactor Final Report*. DOE Nuclear Energy Research Initiative Final Report. Idaho National Engineering and Environmental Laboratory, December 2003.

21. Slaughterbeck, D.C., *Review of Heat Transfer Coefficients for Condensing Steam in a Containment Building Following a Loss of Coolant Accident*. Idaho Nuclear Corp., 1970, IN-1388
22. Whitley, R.H., *Condensation Heat Transfer in a Pressurized Water Reactor Dry Containment following a Loss of Coolant Accident*. MS Thesis, University of California at Los Angeles, 1976.
23. Huhtiniemi, I.K., M.L. Corradini, Condensation in the Presence of Noncondensable Gases. *Nuclear Engineering and Design*. 141, 1993, 429-446.
24. Kim, M.H., M.L. Corradini, Modeling of Condensation Heat Transfer in a Reactor Containment. *Nuclear Engineering and Design*. 118, 1990, 193-212.
25. Uchida, H., A. Oyama, Y. Togo, Evaluation of Post-Accident Cooling Systems of LWR's. *Proceedings: International Conference on Peaceful Uses of Atomic Energy*. 13, 1965, 93-102.
26. Tagami, T., *Interim Report on Safety Assessments and Facilities Establishment Project for June 1965*. No.1, Unpublished Work, 1965.
27. Peterson, P.F., Theoretical Basis for the Uchida Correlation for Condensation in Reactor Containments. *Nuclear Engineering and Design*. 162, 1996, 301-306.
28. Herranz, L.E., M.H. Anderson, M.L. Corradini, A Diffusion Layer Model for Steam Condensation within the AP600 Containment. *Nuclear Engineering and Design*. 183, 1998, 133-150.
29. Reyes Jr., J. N., J. King, *Scaling Analysis for the OSU Integral System Test Facility*. Department of Nuclear Engineering Oregon State University 116 Radiation Center Corvallis, OR 97331-5902 NERI Project 99-0129, Prepared For U.S. Department of Energy.
30. Reyes Jr., J.N, Integral System Experiment Scaling Methodology. *Annex 11, Natural Circulation in Water Cooled Nuclear Power Plants Phenomena, Models, and Methodology For System Reliability Assessments*. IAEA TECDOC 1474, November 2005.

31. Kutateladze, S.S., *Fundamentals of Heat Transfer*. Academic Press, New York, 1963.
32. Labuntsov, D.A., Heat Transfer in the Process of Condensation of Pure Vapor on a Vertical Surface and in Horizontal Tubes. *Teploenergetika*. No. 7, 1957, 72-79.
33. Gregorig, R., J. Kern, K. Turek, Improved Correlation of Film Condensation Data Based on a More Rigorous Application of Similarity Parameters. *Wärme Stoffübertrag.* 7, 1974, 1.
34. Incropera, F.P., D.P. DeWitt, T.L. Bergman, A.S. Levine, *Fundamentals of Heat and Mass Transfer Sixth Edition*. John Wiley & Sons, New York, 2007.
35. ASME Boiler and Pressure Vessel Code, Section II, Part D, 1992 ed.
36. Collier, J.G., J.R. Thome, *Convective Boiling and Condensation Third Edition*. Oxford University Press, New York. 1996.
37. Reyes Jr., J.N., J. Groome, B.G. Woods, et al., Testing of the Multi-Application Small Light Water Reactor (MASLWR) Passive Safety Systems. *Nuclear Engineering and Design*. 241 No. 4, 2011, 1137-1144.
38. S. M. Modro, J. E. Fisher, K. D. Weaver et al., *Multi-Application Small Light Water Reactor Final Report. DOE Nuclear Energy Research Initiative Final Report*. Idaho National Engineering and Environmental Laboratory, December 2003.
39. White, F., *Fluid Mechanics Sixth Edition*. McGraw-Hill Engineering, New York. 2007.
40. Mascari, F., G. Vella, B.G. Woods, F.D'Auria, Analyses of the OSU-MASLWR Experimental Test Facility: Review Article. *Science and Technology of Nuclear Installations*. Vol. 2012, 2011, 1-19.
41. Automation Direct. *Automation Direct Analog Modules*. [Online] Automation Direct, 2012 [Cited 9 24, 2012] <http://www.automationdirect.com/static/specs/tioanalog.pdf>
42. B. Wuth, J. Casey, M. Galvin, and Q., Wu, OSU MASLWR drawings. 2011.

## *Appendix*

---

### **OSU MASLWR Test Facility Low Pressure Blowdown and Decay Power Bench Test**

---

#### **OSU-MASLWR-12036 (Revision 2)**

---

Prepared by:

Garret Ascherl

Department of Nuclear Engineering and Radiation Health Physics  
Oregon State University  
116 Radiation Center  
Corvallis, OR 97331-5902

Prepared for:

Internal use

Prepared: \_\_\_\_\_ Date  
Garret Ascherl  
OSU Software Engineer

Reviewed: \_\_\_\_\_ Date  
Ben Bristol  
OSU Facility Manager

Approved: \_\_\_\_\_ Date  
Qiao Wu  
OSU Program Manager

Authorized: \_\_\_\_\_ Date  
Matt Kizerian  
NuScale Representative

**Records of Revisions**

Revision Number	Revision Date	Changes	Approval
0	8/15/2012	Initial release.	Q. Wu
1	8/21/2012	Made edits according to procedural problems found with first run attempt.	Q. Wu
2	9/12/2012	Made further changes according to procedural problems found with first and second run attempts.	Q. Wu

## Contents

Records of Revisions .....	94
Acronyms.....	96
1. Objective .....	97
2. Initial Condition .....	97
3. Tools and Materials.....	97
4. Critical Instrument List .....	98
5. Pre-Test Operations .....	99
6. Procedure .....	100
7. Post Test Operations.....	115
8. Acceptance Criteria .....	116

## Acronyms

CCP	Coolant Charging Pump
CPV	Cooling Pool Vessel
DACS	Data Acquisition and Control System
DP	Differential Pressure meter
FDP	Flow Differential Pressure meter
FCM	Coriolis Flow Meter
FMM	Magnetic Flow Meter
FVM	Vortex Flow Meter
HPC	High Pressure Containment
KW	Power Transducer
LDP	Liquid Differential Pressure meter
MASLWR	Multi-Application Small Light Water Reactor
MFP	Main Feed Pump
OI	Operating Instruction
OP	Operating Procedure
OSU	Oregon State University
PCS	Primary Coolant System
PT	Pressure Transducer
PZR	Pressurizer
RPV	Reactor Pressure Vessel
RV	Root Valve

## **1. Objective**

The objective of this procedure is to operate the facility at steady state conditions of 800 psig and 25 °F subcooled (~495 °F) at the core exit. Upon reaching these conditions, Core Power will be switched to Decay Mode, and a single and continuous blow down into the high pressure containment is to be initiated. The test shall be terminated at the discretion of the OSU Facility Manager once an equilibrium pressure between the RPV and HPC is reached.

This Test is meant to be used as a training for new MASLWR personnel as well as a functionality test of the decay power control function in the DACS.

## **2. Initial Condition**

From cold shutdown conditions with primary side temperature <200°F and the system depressurized.

## **3. Tools and Materials**

No additional tools or material are needed.



## 5. Pre-Test Operations

- STEP 5.1.  Verify facility is in a cold shutdown state with the primary side temperature <200°F and the system depressurized.

## 6. Procedure

- STEP 6.1.  Perform OP-1, Pre-Startup Valve and Switch Lineup.
- STEP 6.2.  Verify that no alarms on the OSU MALSWR DACS are active. If alarms are active make a note in the test log along with actions taken to address the alarm.
- Note in test log

Time of note: \_\_\_\_\_

- STEP 6.3.  Verify and record that feed water conditioning system is supplied with conductivity treatment solution via sampling from MF-509 in the side of the feedwater tank. The water conductivity must be between 15 and 50 microsiemens/cm. If conductivity is outside of required range move on to STEP 6.3.1, otherwise move on to STEP 6.4.

Conductivity Measurement: \_\_\_\_\_

- STEP 6.3.1.  At OSU MASLWR Test Facility Main Power Panel, unlock and close (turn on) Main Power Breaker.
- STEP 6.3.2.  At OSU MASLWR Test Facility 480 V Cabinet, unlock and close (turn on) Power Distribution Panel Knife Switch.

- STEP 6.3.3.  At OSU MASLWR Test Facility 120V Panel, close (turn on) Breaker 4 (chemical feedpump and solenoid).
- STEP 6.3.4.  At OSU MASLWR Test Facility Panel 1, withdraw the emergency stop button.
- STEP 6.3.5.  Check or place MF-504 in AUTO mode.
- STEP 6.3.6.  Enable MFP at 50% speed.
- STEP 6.3.7.  Operate MFP at 100% speed for 5 minutes.
- STEP 6.3.8.  Repeat STEP 6.3.
- STEP 6.4.  Start data acquisition in accordance with OI-2, Start Data Acquisition. Record Root Data Filename.
- Root Data Filename: \_\_\_\_\_
- STEP 6.5.  At the 120 V OSU MASLWR power panel, close (turn on) Breaker 4 (chemical feedpump and solenoid).
- STEP 6.6.  At the OSU MASLWR Test Facility Main Power Panel, unlock and close (turn on) OSU MASLWR Test Facility Main Power Breaker.
- STEP 6.7.  At the OSU MASLWR Test Facility Main Power Panel, unlock and close (turn on) OSU MASLWR Power Distribution Panel Knife Switch.

- STEP 6.8.  At Test Facility Panel 1, withdraw the emergency stop button.
- STEP 6.9.  At the Data Acquisition and Control Console (DACS), perform the following:
- STEP 6.9.1.  Check reset or reset the emergency stop button.
  - STEP 6.9.2.  Verify PCS-103 indicates shut.
  - STEP 6.9.3.  Verify PCS-106A indicates shut.
  - STEP 6.9.4.  Verify PCS-106B indicates shut.
  - STEP 6.9.5.  Verify PCS-108A indicates shut.
  - STEP 6.9.6.  Verify PCS-108B indicates shut.
  - STEP 6.9.7.  Check or place MF-504 in AUTO operation.
  - STEP 6.9.8.  Open or check open MS-503 indicates open.
- STEP 6.10.  If cooling pool vessel (CPV) level indicates  $\geq 255$  inches, perform the following:
- STEP 6.11.  Open CPV Drain Valve DV-901 and drain until level indicates  $< 255$  inches.

STEP 6.12.  If CPV level indicates less than  $250 \pm 5$  inches, perform the following:

STEP 6.12.1.  Connect temporary hose between water supply and CPV fill valve FV-901.

STEP 6.12.2.  Pressurize water supply up to FV-901.

STEP 6.12.3.  Open FV-901 fully.

STEP 6.12.4.  When CPV level indicates  $250 \pm 5$  inches, shut FV-901.

STEP 6.12.5.  Depressurize water supply.

STEP 6.12.6.  Remove temporary hose between water supply and FV-901.

STEP 6.13.  If high pressure containment (HPC) indicates not empty, drain HPC as follows:

STEP 6.13.1.  Open HPC drain valve DV-801.

STEP 6.13.2.  When HPC is empty, shut DV-801.

STEP 6.14.  If pressurizer (PZR) level indicates  $\geq 16$  inches, perform the following at the DACS:

- STEP 6.14.1.  Open reactor pressure vessel (RPV) pneumatically actuated drain valve PCS-103.
- STEP 6.14.2.  When RPV level indicates  $14 \pm 2$  inches, shut PCS-103.
- STEP 6.15.  If PZR level indicates  $\leq 12$  inches, perform the following:
  - STEP 6.15.1.  If RPV is cold and depressurized (TF-111  $\leq 100$  oF and PT-301  $\leq 5$  psig)
    - STEP 6.15.1.1.  Open PZR vent valve PCS-110.
  - STEP 6.15.2.  At the DACS, fill the RPV as follows:
    - STEP 6.15.2.1.  Check or place MF-504 in AUTO operation. Ensure feedwater storage tank (FST) level indicates  $\geq 50\%$  prior to charging.
    - STEP 6.15.2.2.  Set the CCP speed at 10%.
    - STEP 6.15.2.3.  Start the CCP.
    - STEP 6.15.2.4.  Verify flow into the RPV by observing an increase of RPV level from LDP-106 readings on the DACS main screen.

- STEP 6.15.2.5.  Increase CCP speed as desired to establish fill rate.
- STEP 6.15.2.6.  When the PZR level indicates  $14 \pm 2$  inches stop the CCP.
- STEP 6.16.  Once the proper level is achieved in the pressurizer ( $14 \pm 2$  inches), initiate the automatic level control for the pressurizer level (PCS-103 Auto Mode) at the DACS.
- STEP 6.17.  Verify that the secondary side feedwater supply is functional by performing the following:
- STEP 6.17.1.  Open MF-500.
- STEP 6.17.2.  Start MFP in manual mode at 5% speed setting. Verify flow through feedwater system with a reading increase from FMM-501 and audibly confirming feedwater flow exiting into the flow drain beneath the facility.
- STEP 6.17.3.  After confirmation, increase MFP to 50% setting. Observe increase from FMM-501 reading.
- STEP 6.17.4.  After observing increase, increase MFP to 100% setting. Observe increase in FMM-501 reading.

- STEP 6.17.5.  After confirming feedwater control, stop MFP.
  - STEP 6.17.6.  Wait approximately two minutes for the MFP to coast down.
  - STEP 6.17.7.  Close MF-500. Closing this valve will prevent unnecessary drainage of the feed storage tank.
- STEP 6.18.  Close or check closed SV-800.
- STEP 6.19.  Draw a vacuum in containment as follows:
- STEP 6.19.1.  At OCC navigate to the containment screen and enable the vacuum pump, the button will simultaneously open PCS-801 and engage vacuum pump.
  - STEP 6.19.2.  Monitor PT-801 (HPC pressure), when -13.7 psig is achieved, disable vacuum pump.
  - STEP 6.19.3.  If RPV is cold and depressurized, draw a bubble in the PZR and raise primary pressure to 250 psig as follows:

## WARNING

***PCS-111 Provides a path for steam to enter the Advanced Thermal Hydraulic Research Laboratory (ATHRL) Building when PCS-110 or PCS-109 is open. Do not open PCS-111 if PZR temperature is above 200 °F or personnel may be injured when steam is discharged into the ATHRL Building.***

- STEP 6.19.4.       Open PZR vent valve PCS-110.
  
- STEP 6.19.5.       Open PZR vent line valve PCS-111.
  
- STEP 6.19.6.       At the DACS, energize PZR heaters to 100% in manual control mode. Adjust percentage as necessary to not exceed a 250 °F/hr heatup rate. Record heat up rate in Test Log at 15 minute intervals.
  
- STEP 6.19.7.       When the PZR temperature as indicated by TF-301 reaches the saturation temperature corresponding to the PZR pressure indicated by PT-301, or when steam issues from downstream of PCS-111, wait approximately 3 minutes to flush non-steam gasses from the vessel. Perform the following:
  - STEP 6.19.7.1.     Shut PCS-110.
  
  - STEP 6.19.7.2.     Shut PCS-111.

STEP 6.19.7.3.  Record TF-301 reading:

\_\_\_\_\_

STEP 6.19.7.4.  Record PT-301 reading:

\_\_\_\_\_

STEP 6.19.7.5.  Record RPV saturation temperature as indicated on the DACS main screen:

\_\_\_\_\_

STEP 6.19.7.6.  Record Time:

\_\_\_\_\_

STEP 6.19.8.  Operated the PZR heaters as necessary to raise primary pressure to 250 psig. Do not exceed a 250 °F/hr heatup rate. Verify Proper function of PCS-103 in maintaining PZR level at  $14 \pm 2$  inches during PZR heatup. Continue to record heat up rate in Test Log.

STEP 6.19.9.  When PZR pressure reaches 250 psig, place PZR heaters in automatic pressure control mode with a 250 psig set point.

STEP 6.19.10.  Inspect Test Facility mechanical joints for leaks.

STEP 6.19.11.  Close PCS-104B.

STEP 6.20.  Operate PZR heaters as necessary in manual pressure control mode to raise primary pressure to 800 psig. After reaching 800 psig set pressurizer heaters in auto mode at 800 psig. Do not exceed a 250<sup>o</sup> F/hr heatup rate. Verify proper function of PCS-103 in maintaining PZR level at 14±2 inches during PZR heatup. Continue to record heatup rate in Test Log.

***NOTE: In order to reduce the time needed to get to Hot Standby, STEP 6.20 may be performed at the same time as STEP 6.21-STEP 6.22***

STEP 6.21.  Initialize feedwater flow as follows:

STEP 6.21.1.  At the DAS, open MF-500.

STEP 6.21.2.  Enable the MFP in manual mode, at 20% speed.

STEP 6.22.  Raise primary coolant temperature using core heaters until hot leg temperature (TF-106) remains at 495±5 °F and maintain steady operation as follows:

## WARNING

***DO NOT LET TF-106 EXCEED 505 °F TO ALLOW A MINIMUM 15 °F SUBCOOLED MARGIN AT THE CORE EXIT.***

STEP 6.22.1.  Energize core heaters and set core power to 10%. Adjust core power as necessary to maintain hot leg subcooled margin > 20 °F. Allow for natural circulation flow to build up before increasing power further. Do not exceed 25% core power at any time.

STEP 6.22.2.  Adjust main feed pump and core heaters as necessary to control primary conditions.

***NOTE: MAINTAIN STEADY STATE UNTIL READY TO INITIATE LOW PRESSURE BLOWDOWN.***

STEP 6.23.  Increase Core Power to 50% by repeating STEP 6.23.1 through STEP 6.23.2.

STEP 6.23.1.  Increase core power at 10% increments.

STEP 6.23.2.  Adjust main feed pump as necessary to maintain TF-106 at  $495 \pm 5^\circ\text{F}$ .

STEP 6.23.3.  The core power increase will take approximately 2 minutes, during this time adjust main feed pump as necessary to maintain TF-106 at  $495 \pm 5^\circ\text{F}$ . Wait approximately 2 more minutes before repeating STEP 6.23.1 and STEP 6.23.2

STEP 6.24.  At the DACs, perform the following:

STEP 6.24.1.  Navigate to the All Data Screen.

STEP 6.24.2.  Perform OI-3, Stop Data Acquisition System.

STEP 6.24.3. Stop Time: \_\_\_\_\_

STEP 6.24.4.  Perform OI-2, Start Data Acquisition.

STEP 6.24.5. Test Name:  
\_\_\_\_\_

STEP 6.24.6. Root Filename:  
\_\_\_\_\_

STEP 6.24.7. Start Time:  
\_\_\_\_\_

STEP 6.24.8.  Enter the following decay power values:

$P_o = 39.27$

$T_o = 0$

$A = 0.2325$

$B = 0.2317$

STEP 6.25.  Notify personnel in Advanced Thermal Hydraulic Research Laboratory (ATHRL) of test facility blowdown.

STEP 6.26.  Ensure HPC vent valve SV-800 is closed.

STEP 6.27.  Ensure the following conditions are all met before continuing

- PT-801 reads  $-13.7 \pm 3$  psig, if not then repeat STEP 6.19.
- TF-106 reads  $495 \pm 5$  °F, if not then adjust MFP speed until reached.
- PT-301 reads  $800 \pm 5$  psig.

STEP 6.28.  Ensure steady state data has been recorded for at least 10 minutes at 50% core power.

***NOTE: The following steps are the blowdown sequence and should be performed in order and quickly.***

STEP 6.29.  At the DACS enable Decay Power Mode for the core heaters.

STEP 6.30.  Terminate feedwater as follows:

STEP 6.30.1.  Disable the MFP.

STEP 6.30.2.  Shut MF-500.

STEP 6.31.  At the DACS de-energize PZR heaters.

STEP 6.32.  At the DACS, depressurize the RPV by blowdown to the HPC as follows:

CAUTION

***Do not pressurize the HPC to greater than 300 psig or HPC rupture could occur.***

STEP 6.32.1.  Initialize automatic depressurization system (ADS) by opening vent valves PCS-106A to reduce RPV pressure while maintaining HPC pressure below 300 psig.

STEP 6.32.2.  At the discretion of Lead Test Engineer or Facility Manager, initiate opening of the recirculation line as follows:

STEP 6.32.2.1.  De-energize core power.

STEP 6.32.2.2.  Open PCS-108A.

STEP 6.32.3.  At the discretion of the Lead Test Engineer or Facility Manager, initiate system shutdown by performing OP-5, Test Facility Depressurization and Cooldown.

## 7. Post Test Operations

STEP 7.1.  Perform OI-3, Stop Data Acquisition System.

Stop Time:

---

STEP 7.2.  Perform OI-4, Acquired Data Transfer.

STEP 7.3.  Perform OI-5, Data Acquisition and Control System Shutdown.

## 8. Acceptance Criteria

STEP 8.1.  All critical instruments function throughout the test.

STEP 8.2.  All STEPS were performed as written. Any deviations have been properly documented.

STEP 8.3.  All known discrepancies have been logged for further action.

### Acceptance Criteria Met

---

Lead Test Engineer Name

---

Lead Test Engineer Signature

---

Date

Comments:

---

---

---

---

---

## TEST LOG

Procedure Number:	OSU-MASLWR-12036
Procedure Name:	Low Pressure Blowdown with Decay Power Test
OSU Lead Test Engineer:	Garret Ascherl
Test Start Date:	9/12/12

Time	Remarks
11:40	Safety Security and Operations Brief performed. Following personnel present: Kyle Hooper, Garret Ascherl, Ben Bristol, Bradyn Wuth, Don Buenaventura
12:03	PZR level high, will be drained
12:13	PCS-103 won't open
12:20	PCS-109 won't close, PCS-105 was opened to begin draining
12:25	PCS-105 closed
12:32	Air pressure check: MS-504, 503 & PCS-103 toggled; PCS-109 still not responding
12:55	PCS-109 attempted to toggle; did not work
1:04	PCS-109 appears to be working, loose wire
1:06	PCS-109 stopped working again; PZR activated at 80%, TF-301 reads 179°F
1:11	Pressurizer stopped working, relay did not trip. PCS-109 appears to be working
1:14	Knife switch opened, main power breaker opened, checking fuses in 480 cabinet
1:16	Kyle Hooper takes over for Garret Ascherl as operator. Fuses in main power cabinet (480) are fine
1:20	PZR heater relay closed; still no power
1:27	Main power breaker and knife switch closed
1:33	Main power breaker and knife switch opened
1:42	Installing replacement relay for PZR heaters
1:50	DACS shut off to avoid strange readings due to no power

Page 1 of 26 GA 9/12/12

Page 24 of 27

Test Engineer:  Date: 9/12/12

## OSU MASLWR Low Pressure Blowdown and Decay Power OSU-MASLWR-12036-R2

Procedure Number:	OSU-MASLWR-12036
Procedure Name:	Low Pressure Blowdown with Decay Power Test
OSU Lead Test Engineer:	Garret Ascherl
Test Start Date:	9/12/12

Time	Remarks
2:43	Transducer for CR-301 (KW-301) replaced. Shunting required replacement for 2 relays (for pressurizer & MS-504). Fuses for sensing instruments replaced.
2:52	Confirming Facility Functionality
2:52	CCP enabled & confirmed working
2:53	MFP enabled & confirmed working
2:54	VP enabled & confirmed working
2:54	PCS-103 confirmed working
2:56	CR-102 & 101 enabled w/ manual power at 1%.
3:00	Knife switch opened; main breaker opened.
3:01	Breaker 4 opened; emergency stop depressed
3:02	DABs turned off; facility locked.
8:40	Started procedure again with O.I-2
8:45	Data acquisition started.
8:47	PCS-105 opened
8:49	PCS-109 activated successfully
8:53	Vacuum pump activated
8:55	Pressurizer activated at 80%. TF-301 reads 158°F
9:03	Vacuum pump deactivated
9:10	TF-301 reads 213°F
9:12	Steam issuing from PCS-111
9:14	PCS-111 shut
9:16 p.m.	Small air leak noticed near MS-504, proceeding with test

Page 2 of 6  
 6A 7/13/12

Test Engineer: Stan Buehner Date: 9-12-12

## OSU MASLWR Low Pressure Blowdown and Decay Power OSU-MASLWR-12036-R2

Procedure Number:	OSU-MASLWR-12036
Procedure Name:	Low Pressure Blowdown with Decay Power Test
OSU Lead Test Engineer:	Garret Ascherl
Test Start Date:	9/13/12

Time	Remarks
9:19 a.m.	Air leak at MS-504 confirmed to be air supply line to MS-504
9:25	TF-301 reads 259°F
9:40	TF-301 reads 307°F
9:56	TF-301 reads 365°F
10:08	250 psi reached, PZR set to auto mode
10:10	TF-301 reads 405°F
10:14	Leak found in PCS-109, working to seal it. Also PZR PID having trouble maintaining 250 psi. Manual adjustments will be made accordingly
10:21	PZR heater relay turned off
10:24	MFP activated at 20%
10:25	MFP turned itself off, but after being restarted, appears to be working
10:26	Core relays activated at 10%, took a bit of time to ramp up to 10%
10:28	Core reached 10% power
10:29	TF-301 reads 432°F
10:30	Core power increased to 15%
10:31	Core power set to 20%
10:32	Core power set to 25%
10:34	MFP set to 10%
10:41	MFP set to 7%
10:45	TF-301 reads 470°F
10:45	MFP set to 8%

10:29  
887-13-12

Page 3 of 6

Test Engineer:

Garret Ascherl

Date:

9-13-12

## OSU MASLWR Low Pressure Blowdown and Decay Power OSU-MASLWR-12036-R2

Procedure Number:	OSU-MASLWR-12036
Procedure Name:	Low Pressure Blowdown with Decay Power Test
OSU Lead Test Engineer:	Garret Ascherl
Test Start Date:	9/13/12

Time	Remarks
10:46	MFP set to 7%
10:51	MFP set to 5%
10:54	MFP set to 3%
10:56	MFP set to 2%
10:59	TF-301 reads 480°F
11:01	MFP set to 1%
11:02	MS-504 set to 0% open
11:03	MS-504 set to 25% open
11:06	MS-504 set to 100% open, MS-503 closed
11:06	MS-504 set to 70%
11:07	MS-504 set to 50%
11:07	MS-504 set to 40%
11:08	MFP set to auto mode @ 1 GPM
11:09	MS-504 set to 25% 30%
11:10	MFP PID - prop set to 0.6500
11:11	MS-504 set to 25%
11:13	MS-504 set to 20%
11:14	MS-504 set to 15%; TF-301 reads 494°F
11:23	MFP set to 0.75 GPM
11:28	MS-504 set to 20%
11:29	TF-301 reads 516°F
11:31	PER set to auto mode @ 800 PSI
11:32	MS-504 set to 50%
11:35	<del>MS-504</del> MFP set to 0.60 GPM
11:40	<del>MS-504</del> MFP set to 0.3 GPM 0.25 GPM;

Page 4 of 6

Test Engineer:

Garret Ascherl

Date:

9-13-12

## OSU MASLWR Low Pressure Blowdown and Decay Power OSU-MASLWR-12036-R2

Procedure Number:	OSU-MASLWR-12036
Procedure Name:	Low Pressure Blowdown with Decay Power Test
OSU Lead Test Engineer:	Garret Ascherl
Test Start Date:	9/13/12

Time	Remarks
	MS-504 set to 40%.
11:41	MS-504 set to 25%.
11:42	PZR relay turned off; attempting to return to 800 psi set point
11:46	PZR relay turned on; PT-301 reads 797 psi
11:46	TF-301 reads 519°F
11:58	PZR relay turned off; attempting to return to 800 psi set point
11:59	PZR relay turned on; TF-301 reads 519°F
11:59	MFP set to 0.25 GPM from 0.2 GPM
12:02	PZR relay turned off
12:05	PZR relay turned on; PT-301 reads 796 psi
12:07	PZR relay turned off
12:11	PZR relay turned on; set to auto @ 800 psi
12:13	PZR relay turned off
12:14	TF-301 reads 519°F
12:14	MFP set to 0.5 GPM
12:15	MS-504 set to 35%.
12:16	PZR relay turned on
12:17	core set to 30% power; MFP set to 0.75 GPM
12:19	MS-504 set to 40%.
12:20	core set to 40% power; MFP set to 0.9 GPM
12:22	MFP set to 1 GPM
12:24	MS-504 set to 50%.
12:25	core set to 50% power; MFP set to 1.1 GPM

Page 5 of 6

Test Engineer:

Jon  
Bromventry

Date:

9-13-12

## OSU MASLWR Low Pressure Blowdown and Decay Power OSU-MASLWR-12036-R2

Procedure Number:	OSU-MASLWR-12036
Procedure Name:	Low Pressure Blowdown with Decay Power Test
OSU Lead Test Engineer:	Garret Ascherl
Test Start Date:	9/13/12

Time	Remarks
12:29	TF-301 reads 519°F
12:33	PZR relay turned off; vacuum pump turned on
12:33	PZR relay turned on
12:34	vacuum pump turned off
12:38	PZR relay turned off
12:39	PZR relay turned on
12:40	commenced blowdown
12:40	PCS-103 auto mode disabled
12:45	TF-301 reads 449°F
1:00	TF-301 reads 424°F
1:02	Kyle Hoover relieves Garret Ascherl as operator; Brodyn with supervising
1:45	Opening recirculation line PCS-108A after de-energizing the core
2:44	Began shutdown procedure CP-5
2:48	started forced shutdown, ended test - TF-301 is 374
2:50	CCP speed set to 25%
2:52	CCP speed set to 100%
3:04	TF-301 reads 364°F
3:12	DV-301 opened, CCP stopped
3:24	PR level dropped below 12", CCP reactivated at 10%

Page 6 of 6

Test Engineer: GA Date: 9/13/12